Micro-scale definition of the engineering properties of complex biological materials

Thesis submitted to the University of London
for the degree of
Doctor of Philosophy in Biochemical Engineering

by

Ioannis Papantoniou

The Advanced Centre for Biochemical Engineering
Department of Biochemical Engineering
University College London

September 2007

ProQuest LLC
789 East Eisenhower Parkway
P.O. Box 1346
Ann Arbor, MI 48106-1346

To my parents Vassilis and Vassoula

Acknowledgments

First and foremost, my gratitude goes out to my supervisor, Prof. Mike Hoare, for his encouragement, continuous support and positive energy.

My thanks also to my colleagues and friends Spyros Gerontas and Alfred (Capuccino) Ding for never ending discussions on weather, politics, mass transfer, basketball, fluid dynamics, greek-chinese relations etc, and for making the office a 'place to be'.

Special appreciation should go to my parents Vassilis and Vassoula and to my beloved sisters Georgia, Kyriaki and Andreana for being always there in every possible psychoanalytical and not only aspect, my grandmother Georgia for asking me on a never ending basis the question "How are you, when are you coming back?" from the first day I set my foot on this island to date, and for their endless love.

Finally I should not forget to mention people that have shared with me small and big moments in different periods of this four year adventure sharing our 'immigrant' experiences. So George Papamarkos, Yiannis Pontikis, Marinos Manolessos, Loanna Karavangeli, Chryssi Kotretsou, Vangelis Bellonias, Lillian Glava thank you I am really happy to have met you!

Abstract

Shear is present in almost all bioprocesses and high shear is associated with processes involving agitation, pumping and separation. The capability of predicting parameters such as the effect of shear on the processed material, from a small scale experiment to large scale processes is of importance in the successful development of bioprocesses especially in cases were the process material is scarce.

The target of this work was to conduct experiments at the ultra scale-down level using a rotating disc device requiring quantities of processed material in the range of a few tens of millilitres and then moving down to even smaller volumes using an alternative capillary based design. For the experiments two ultra scale-down devices were designed, capable of producing high levels of shear rate ($>10^5\ s^{-1}$). The flow field within the two devices was mapped and a profile of shear rate was established using computational fluid dynamic simulations (CFD).

The effect of shear on two aggregate biological systems was examined. Microbial protein precipitate was chosen to be studied as a material which could be prepared reproducibly and was of relevance to the bio-processing area where the final scale of operation can be many thousands of litres. Mouse embryoid bodies (EBs) are representative of another class of aggregated biological material where the final scale of operation volume will be small due to its limited availability.

The translation between rotating disc and capillary devices was studied using the larger quantities of the protein precipitate available. The break-up of protein precipitates was demonstrated to be a function of the exposure time to high shear fields whereas the final size was related to the extent of shear in the capillary. It was possible to correlate between the results of the rotating disc and the capillary by using the energy dissipation rate as a connecting parameter.

The capillary system was further used for the controlled processing of the embryoid bodies since only small quantities were available for experimentation. It was of interest not only to study the break-up of the embryoid bodies and their final size distribution, but also the viability of the released cells. It was seen that the break-up was a function of both the amount of shear as well as of the exposure time of the particle in high shear regions. Total breakage of the embryoid bodies was observed when material was exposed to sufficiently high flow intensities.

Table of Contents

List of figures

Chapter 1

Chapter 2

Chapter 3

Chapter 4

List of tables

Chapter 1

Chapter 3

Chapter 4

CHAPTER 1

Introduction

1. Introduction

The ability to predict the performance of large scale processes is central to the rapid development of successful operations at the pilot and industrial scale. This is especially useful in cases where the product is expensive and scarce, thus making large scale experimental procedures to establish new industrial processes and applications rather difficult. Companies need to take products to market as quickly as possible in order to maximise the return because of limited patent life and other licensing issues. To achieve this transition from the research level and scientific discovery to actual production new methods must be developed. The development process is often expensive due to the problems of scale up for the transfer from laboratory to large manufacturing scale (Datar, 1986). The gap between these two extremes of scale is usually spanned by the pilot plant. With the use of this stage, process equipment tends to operate in a similar fashion to the industrial scale in terms of product quality, and reproducibility (Fahrner, 1993). New methods of mimicking the actual industrial downstream process of bio-pharmaceutical production will have to be developed if the expensive studies of the pilot plant scale are to be avoided. In this way time and funds will be spared especially if this development and new methods will be achieved down to a level where small amounts of scarce material for the execution of experiments will be needed. Furthermore, in small-scale experiments the number of results that can be obtained is far greater thus allowing a greater understanding of the process.

It is unavoidable that biopharmaceutical materials experience shear when exposed to various interfaces during the wide range of bio-processing operations from cell culture to product formulation. Shear is common in many unit operations such as centrifugation, filtration, separation, purification and

even during pumping and passage through pipes and tubing. From the above we can conclude that the study of the behaviour of biomaterials during their flow through high shear fields and the impact on their physical properties and characteristics is of great interest and importance in the improvement of bioprocess design. The processing of biological aggregates is studied in the current thesis. Two examples of biological aggregate systems were chosen; a protein precipitate and an embryoid body solution. Experimentation was undertaken to understand the behaviour of these biomaterials in dedicated shear devices, while at the same time seeking to define the flow conditions in such a way as to correlate them with the actual industrial process.

In the first part of this work a study was made on the development of a novel ultra scale-down device, capable of simulating the damage caused by stress to bio-materials in the high speed centrifugation operation during the stage of separation in the downstream processing of the bio-pharmaceuticals. Additionally the translation between a rotating disc and capillary devices and the effect of the different flow fields developed within the devices on protein precipitates was studied.

In the case of regenerative medicines, bio-processing is still an area under development. Soon, discoveries that have been made in the laboratory will have to be evaluated and translated into industrial application via scale-out or scale-up procedures. Furthermore methods in this field have been based on manual skills and specialisation of particular staff, some of whom have developed sophisticated techniques to achieve successful outcomes (Mason and Hoare, 2006). Translation into robust reliable processes requires a great deal of fundamental understanding of the effect of the process engineering environment of the cellular material.

The formation of embryoid body systems in order to produce differentiated stem cells for use in cell therapy applications is a promising new process. The effect of a controlled shear field in a dedicated capillary device in order to break down and dissociate embryoid bodies provides one option for cell release. It is of great importance to establish bioprocess methods that will guarantee a yield to

satisfy the demand and a consistent outcome with more units of material. Finally, a fundamental understanding of the effect of shear on material such as EBs and cells is necessary in order to progress the creation of these bioprocess methods.

1.1 Process scaling issues

1.1.1 'Scale up' and 'scale out'

Scale-up is a procedure for designing and building large scale systems on the basis of the results of experiments with small scale models. Ideally, the small scale system should produce the same results as the large scale setup. In practice differences in performance often occur and allowances must be made. Problems often associated with the small scale model approach are that conditions employed at small scale are often not transferable to large scale and hence disparities in process performance occur. These can be very costly, particularly if they appear only in the later stages of design. A method for solving the problems of scale up is that of scale-down. This involves the simulation of full scale conditions at small scale. Such an approach as scale-up in a single bioreactor is thus applicable in the use of allogeneic cells where the cells are destined for a number of patients.

Most of the procedures in cell therapy are currently conducted manually. Automated bioprocessing is not yet well developed. A connection between manual and automated processes should be established for the expansion of the scale of production. In the case though of regenerative medicines, this jump in scale is more likely to be achieved in a scale-out, rather than in a scale-up approach. This means that the expansion will happen in a greater number of small volume parallel operations rather than a single large volume one. The handling of such bioprocesses, where cells must be cultured and harvested in parallel operations under sterile conditions in order to be reintroduced to the patient, should be consistent and safe. In order to achieve successful automated processes the use of robotic devices controlling the processing,

seems like the next step forward. Such an approach could find application in autologous cell therapies where cells are harvested, grown and reintroduced to a specific patient.

1.1.2 Role of scale down on biotechnology

Bioprocess development and optimisation is traditionally performed at pilot scale since operating characteristics are more similar to large scale and hence successful transfer into production is more likely. However, pilot-scale development is expensive and hence any useful process data that can be obtained at a small scale with scale down procedures will provide considerable savings. Additionally, scale down operation is particularly important in the early stages of development when often there are only small fermentation volumes available for study. The ability to obtain useful design data at this stage will help to accelerate the development process.

The ultra scale-down methodology combines the use of very small volumes of process fluid in dedicated devices to predict accurately the behaviour of process scale biotechnological unit operations. In effect the use of volumes of a few millilitres will be sufficient to predict what will happen in the pilot-scale process and furthermore, what will happen in the actual industrial scale. Furthermore, in the ultra scale-down methodology the design of the miniature devices often changes significantly ceasing to have proportions with the large scale processes. The important factor in this methodology is to obtain the same behaviour with the manipulation of the same experimental parameters and then be able to translate between the scales of operation.

1.2 Protein precipitates

Protein precipitates and the subsequent recovery of the precipitates from the mother liquor represent one of the most important operations for the laboratory and industrial scale recovery and purification of proteins. Precipitation is a key process operation in the industrial production of a wide range of proteins from

human, animal and vegetable sources and furthermore from genetically engineered sources (Bell et al., 1983; Hoare and Dunnill, 1986a,b, 1989). In most applications the intention is to recover the protein in either an unchanged molecular form or one which is readily returned to that form.

1.2.1 Methods of protein precipitation

One important aim of the precipitation operation, is to create a physical and chemical environment in which the primary particles can combine. In this way relatively large particles and dense aggregates are formed without loss of structural integrity or risk of protein denaturation. The formation and recovery of protein precipitates are important operations widely used in industrial scale purifications (Stavrinides et al., 1993).

The methods by which proteins are precipitated can be divided into two groups. In the first, protein solubility is reduced by the addition of high concentrations of reagent which change the nature of the solvent environment in a major way. This category includes organic solvents such as ethanol, acetone and ether and neutral salts such as ammonium sulphate. In the second group, which includes acids, bases and some metal ions, low concentrations of reagent are effective by direct interaction with the protein. Aggregation and densification greatly improve precipitate properties for subsequent downstream processing operations including their separation from the mother liquor (Devereux et al., 1984; Titchener-Hooker et al.,1990).

The precipitation methods to be described can be summarized as follows:

a) the addition of high concentrations of neutral salts generally decreases protein solubility an effect known as 'salting out'
b) the ionization of the weakly acidic and basic amino side chains of proteins is influenced strongly by pH. Solubility is a function of the net charge on these groups and proteins have zero net charge at some pH known as the isoelectric point, where they will tend to precipitate from solution

c) if the dielectric constant of aqueous medium is reduced, for example by the addition of miscible organic solvents, electrostatic interaction between protein molecules is enhanced and precipitation will result.
d) proteins are precipitated by non ionic polymers probably as a result of a reduction in the amount of available water for their salvation
e) a number of charged poly-electrolytes are capable of precipitating proteins, probably by acting as flocculating agents under appropriate pH conditions.
f) several poly-valent metal ions which interact directly with proteins have proved valuable in reversibly precipitating proteins.

Protein precipitation in a stirred vessel involves the following basic steps. First the protein environment is altered by the addition of the precipitation agent, causing the solution to become unstable. Second a solid phase appears as small spherical 'primary' particles of solid protein which grow by diffusional transport of protein molecules to the solid surface. Third, primary particles aggregate as a result of convective transport. In the meantime, the aggregate particle size is limited by the hydrodynamic forces in the flow field where the process is taking place (Vold, 1963). Furthermore in a study examining the kinetics of protein precipitation using a set of different agents, Chan et al (1986) observed that during protein precipitation, a rapid initial growth of precipitate particles was followed by a slower approach to a final size, the value of which depended on the precipitating agent used.

It has been shown from studies with several precipitants that protein solids probably constitute a protein rich phase rather than a pure solid phase complicating many times the analysis of precipitation (Kunz and Kauzmann, 1974).

1.2.2 Characteristics of protein precipitates

The structure of proteins is of central importance in appreciating how precipitating reagents function. The polypeptide chain of water soluble proteins will be folded in such a way that the majority of polar hydrophilic amino acid

side-chain groups will be on the exterior and the hydrophobic ones buried. This division can never be complete so that changes in the exterior environment brought about by the reagent will affect both types of group as well as the backbone. The overall effect on the protein results from the sum of individual effects which will often be opposed to one another. The situation is complicated by the fact that a protein structure prior to precipitation will not generally be much more stable than a large number of related but undesirable structures. Given the complexity of chain folding it will be impractical under industrial conditions to refold the protein to the original conditions. The molecular weights of globular proteins can range from a few thousand to over a million giving equivalent spherical diameters up to several nanometers. Most globular proteins are ellipsoidal to various degrees.

As previously seen, under the appropriate environment and physicochemical conditions, proteins will form precipitates of much larger sizes than the original protein particles with their own particular properties. These particles are held together by weak intra-particle forces. The strength of the aggregate is dependant on the number of bonds per area between the proteins that have precipitated as well as on the force of each of these bonds (Firth and Hunter, 1976). An increase in the aggregate density is probably accompanies by a rise in the strength of the aggregate due to the reduction in the distance over which the short range intra-particle bonding forces holding the aggregate sub-units act (Titchener-Hooker and McIntosh, 1992). The aggregates tend to be open in nature with voidages of the order of 0.8 μm for a 10 μm diameter aggregate not being uncommon (Bell et al. 1982). Different sets of size distributions have been reported in a number of experimental works ranging from maximum diameters of 10 μm to less than 50μm according to the precipitation method followed (Virkar et al., 1982; Hoare, 1982a,b; Chan et al. 1986; Fisher and Glatz, 1988a,b). Protein precipitates are also associated with varying levels of tightly or loosely bound water which forms a hydration shell around the molecule. The density difference between protein precipitates and the liquid is always small. This combined with the relatively small particle sizes which can be achieved and the significant enhancement of viscosity which may be used by proteins and some reagents, leads to problems of recovery. Moreover with an aggregate

density typically less than 10% higher than that of the mother liquor protein precipitates can be difficult to recover by conventional means of separation such as high speed centrifugation (Bell et al., 1983). The solids volume fraction of soya protein precipitates has for example been calculated to lie in the range of 0.75-0.90 (Bell et al., 1982). They are made more severe by the hydration and compressibility of the precipitate particles. The distribution of constituent particles within individual aggregates is non uniform and it is expected that the density of an aggregate decrease continuously as the aggregate diameter rises (Bell and Dunnill, 1982a; Devereux et al., 1984; Titchener Hooker et al., 1990).

1.2.3 Effect of precipitation process on aggregate properties

The properties of the protein precipitates might be affected by the way that they are formed. By manipulating certain parameters during the precipitation process the properties of the resulting aggregates are influenced. It has been seen that acid addition rate has an impact on precipitate size as well as on the strength of the particle. Rapid acid addition gives primary particles that are larger and a particle size distribution showing a larger, stronger aggregate, having a greater fraction of its bonding sites attached on the precipitator. On the other hand the aggregate prepared by slow addition of acid does have a lower volume fraction of solids (higher porosity) is a weaker aggregate under shear, and may therefore be expected to be more deformable (Fisher et al., 1985). The concentration of the precipitating agent used (Fisher et al., 1986), the initial protein concentration and nature and the extent of mixing and residence time in the reactor (Fisher and Glatz, 1988; Glatz et al., 1986; Rothstein, 1994) have also an impact on the precipitates formed. Spiegel (1999) found that whey protein aggregates formed at different temperatures have not only different size but different strength, and that the presence of a shear flow modified the size and strength of the aggregates formed at the same temperature. Furthermore, the impeller speed during the addition of the acid in the solution has been seen to have a strong influence on the particle size of the aggregates formed (Zumaeta et al., 2006; Ayazi Shamlou et al., 1996; Petenate and Glatz, 1983; Serra et al., 1997). In fact Byrne et al. (2002) reported that (smaller) aggregate particles formed under high impeller speeds could withstand breakage to a

greater degree when exposed to a turbulent flow field than aggregates formed under lower impeller speeds. The previous study showed that the size of the initially smaller aggregates resulted in larger size particles after breakage. The density of the aggregates has been also manipulated with the use of continuous low frequency conditioning. The levels of hydrodynamic stress under which the particles where exposed during conditioning was correlated with the density increase of the new aggregate population. The fine particles of the less dense outer area of the aggregate would re-aggregate after breakage in a re-orientated denser structure (Titchener-Hooker and McIntosh, 1992).

The physical properties of the aggregates further depend on more general factors such as the type of precipitation reactor choice (Foster et al., 1976). Previously the effect of certain parameters of the precipitation process in a stirred bioreactor, were extensively presented. It has been reported though, that the use of a continuous flow tubular reactor results in large irregularly shaped particles of low density that are more prone to shear damage than precipitates formed in a batch stirred-tank reactor, with the high flow stresses in the impeller region leading to smaller denser and consequently less shear sensitive particles (Bell and Dunnil, 1982).

1.3 Aggregates of mouse embryonic stem cells

Aggregates of stem cells are a complex biological material composed from living stem cells attached together with extra-cellular matrix molecules produced by them. These aggregates have their own properties as a separate entity, while the properties of the cells retain their importance and should be taken into consideration in the downstream processing. In the experimentation process mouse embryonic stem cells were used as a model mammalian stem cell material.

1.3.1 Mouse embryonic stem cells

Mouse embryonic stem (ES) cells are continuously growing cell lines isolated from the undifferentiated inner cell mass of mouse blastocysts and have a pluripotent ability to differentiate into various cell lineages in vitro, including neurons (Evans and Kauffman, 1981; Martin, 1981). It was observed that leukaemia inhibitory factor (LIF) was a feeder-cell derived molecule of significant importance in the maintenance of these cells (Smith et al. 1988; Williams et al. 1988; Stewart et al.1992). Recombinant LIF can, in the presence appropriate batches of fetal calf serum (FCS), replace the feeder cell function and support the growth of undifferentiated ES cells (Smith et al. 1988; Williams et al., 1988). In a recent work (Ying et al. 2003a), it was demonstrated that Bmp4 (mouse protein), in the presence of LIF, can replace the requirement for serum. This means that, it is now possible to grow ES cells with defined factors without having to use feeder cells or animal serum. Because of the property of the ES cells to be maintained and expanded in an undifferentiated state under defined culture conditions, and while retaining their capacity to differentiate into functional cell types in vitro, these cells hold promise as a cell source for multiple clinical and biotechnological applications. Studies up to now have led to the development of appropriate culture conditions and protocols for the generation of a broad spectrum of lineages. Understanding and controlling cell fate determination remains though a major challenge (Smith, 2001). The use of mouse embryonic stem cells is widely exploited as a model for conducting in vitro and in vivo studies to gain insight into different aspects of developmental biology and regenerative medicine that may eventually benefit humans.

1.3.2 Differentiation of embryonic stem cells

Directing ES cell differentiation towards specific lineages is a great challenge. It has been attempted mainly by the use of growth factors to promote differentiation, proliferation and survival of the specific cell type of interest.

1.3.2.1 Culture systems for differentiation of embryonic stem cells

After withdrawal of LIF and when transferred to a non adherent surface, ES cells will spontaneously differentiate forming three-dimensional aggregates. Their differentiation can be controlled though to a certain extent with the use of certain growth factors such as retinoic acid (RA). Stem cells of all three germ layers have been obtained by following different protocols in order to induce differentiation. Haematopoietic cells and cardiomyocytes were among the first specific cell types to be characterized from differentiating EBs formed from mouse ESCs. In the mouse system a purity of 99% of differentiated cardiomyocytes has been achieved (Zweigerdt et al., 2003). High percentages (>50%) of cells expressing neural progenitor markers (ectodermal cell types) can be obtained as well. Schuldiner (2001) cultivated EBs for 21days in serum replacement media with retinoic acid treatment and subsequently plated them into collagen coated dishes. Fifty per cent of the cells expressed neuronal markers. A number of research works (Zhang et al., 2001; Carpenter et al., 2001; Reubinoff et al., 2001) further demonstrate a high percentage of neuron precursor stem cells even in the case of human embryonic stem cells. In the case of production of endodermal cell types such as hepatocytes and pancreatic beta cells, directed differentiation is a challenging issue. The use of growth factors, as seen in this chapter does enrich the desired population, however a mixed population of differentiated cells in other lineages, will still be present posing a further challenge for the isolation and purification of the desired cell types.

1.3.2.2 Differentiation of in the neuronal pathway

Since the differentiation pathway that was followed in this research work aimed in the formation of neuron progenitor cells within the EB, in this chapter different methods and protocols that are used to derive neuron stem cells from ES cells are examined and presented.

Extensive effort in order to develop protocols that will successfully promote neuro-ectoderm differentiation on mouse embryonic stem cells has been made

up to date. Several protocols have evolved including treatment of serum stimulated embryoid bodies induced with retinoic acid (Bain et al, 1995), sequential culture of embryoid bodies in serum followed by serum-free medium (Okabe et al, 1996), differentiation of ES cells as a mono-layer in serum free medium (Tropepe et al, 2001; Ying et al, 2003b) and differentiation of ES cells directly on stromal cells in the absence of serum (Kawasaki et al, 2000; Barberi et al, 2003). It has been observed that the majority of the cells that develop in these cultures appear to have the characteristics if a neural cell (Okabe et al, 1996; Kawasaki et al, 2000; Barberi et al, 2003). In a study by Li et al (1998), a highly enriched neural population was achieved with (>90% of the population) using the retinoic acid differentiation induction protocol.

The differentiation of the embryonic stem cells towards the neuronal direction has as a result the possible generation of all of the cell types of the central nervous system; this means that neurons, astrocytes and oligodendrocytes can be generated in relatively pure populations each, and can be isolated when cultured under appropriate conditions (Okabe et al, 1996; Barberi et al, 2003). Furthermore, conditions have been established for the development of different subtypes of neurons such as midbrain dopaminergic neurons (Kim et al, 2002), cholinergic, serotonergic neurons (Barberi et al, 2003) and also cells that demonstrated characteristics of motor neurons (Wichterle et al, 2003).

Cell type	Reference
Yolk sac endoderm	Doetschman et al. 1985
Yolk sac mesoderm	Doetschman et al. 1985
Primitive hematopoietic	Doetschman et. al. 1985, Nakano et al. 1996
Definitive hematopoietic	Nakano et al. 1996, Nishikawa et al. 1998, Wiles & Keller 1991
Lymphoid precursor	Potocnik et al. 1994
Mast cell	Tsai et al. 2000
Dendritic cell	Fairchild et al. 2000
Endothelial cell	Risau et al. 1988, Yamashita et al. 2000
Cardiomyocyte	Doetschman et al. 1985, Maltsev et al. 1993
Striated muscle	Rohwedel 1994
Smooth muscle	Yamashita et al. 2000
Adipocyte	Dani et al. 1999
Osteoblast	Buttery et al. 2001
Chondrocyte	Kramer et al. 2000
Keratinocyte	Bagutti et al.1996,Yamashita et al. 2000
Neuron	Bain 1995, Strubing et al. 1995
Astrocyte	Fraichard et al. 1995
Oligodendrocyte	Brustle et al. 1999, Liu et al. 2000

Table 1.1: Differentiated cell types produced from mouse ES cells in vitro

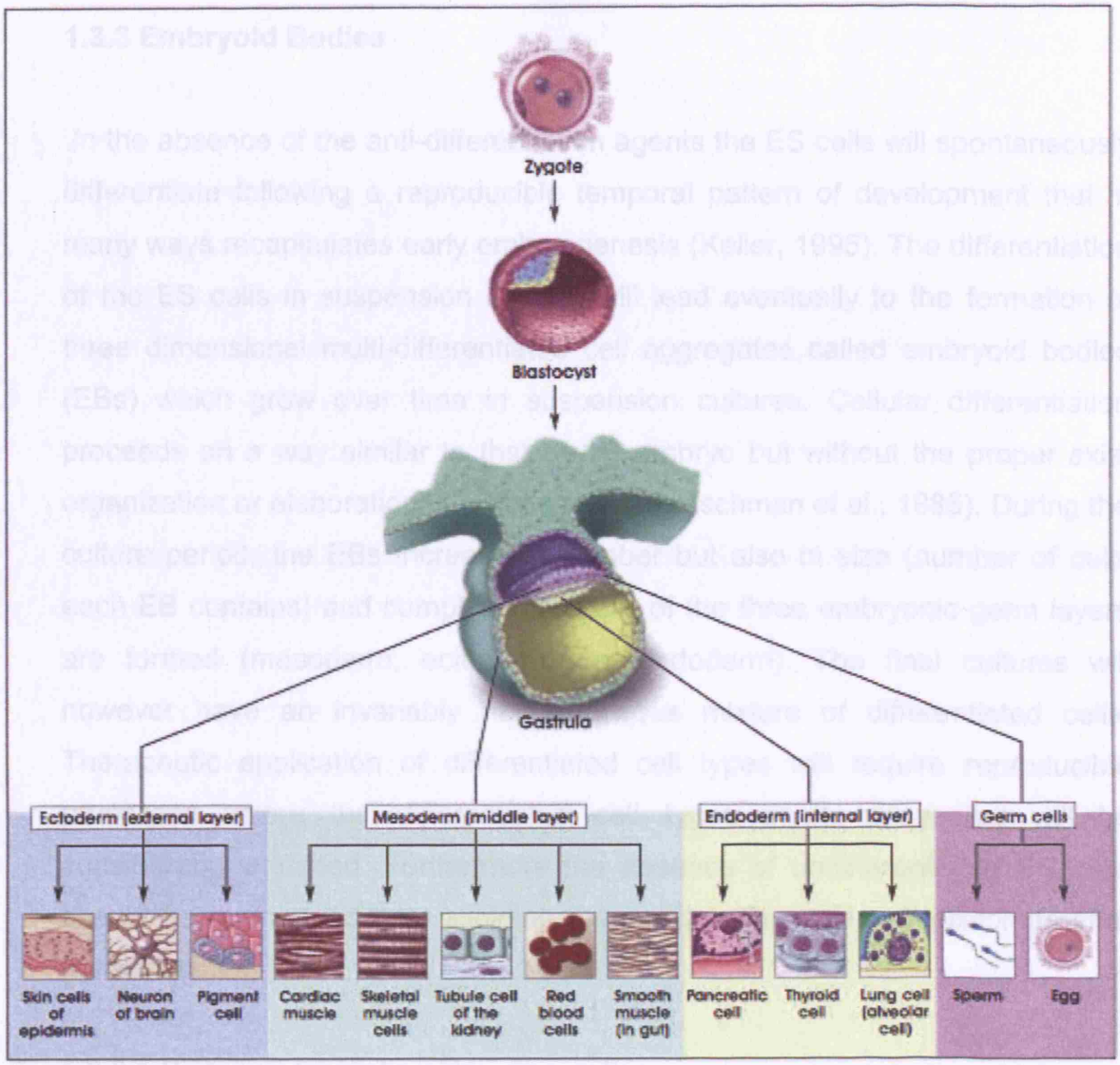

Figure 1.1: Differentiation pathways of mouse embryonic stem cells. Image taken from the National Center for Biotechnology Information (NCBI) website.

1.3.3 Embryoid Bodies

In the absence of the anti-differentiation agents the ES cells will spontaneously differentiate following a reproducible temporal pattern of development that in many ways recapitulates early embryogenesis (Keller, 1995). The differentiation of the ES cells in suspension culture, will lead eventually to the formation of three dimensional multi-differentiated cell aggregates called embryoid bodies (EBs) which grow over time in suspension cultures. Cellular differentiation proceeds on a way similar to that of the embryo but without the proper axial organization or elaboration of a body plan (Doetschman et al., 1985). During the culture period, the EBs increase in number but also in size (number of cells each EB contains) and complexity as cells of the three embryonic germ layers are formed (mesoderm, ectoderm and endoderm). The final cultures will however have an invariably heterogeneous mixture of differentiated cells. Therapeutic application of differentiated cell types will require reproducible processes where the differentiated cell types or its progenitor will be considerably enriched. Furthermore the absence of undifferentiated ES cells should be guaranteed thus avoiding the possible formation of teratomas after transplantation.

1.3.3.1 Protocols for embryoid body creation

Up to date numerous lab scale protocols for EB induction have been published. For example, the hanging drop technique permitted the formation of EBs with highly uniform size and cell content (Maltsev et al., 1993) since the use of this particular method prevents embryoid body agglomeration. In each drop, a single cell is placed and the differentiation process that leads to aggregate formation is only due to the growth of the initial cell with which the drop was seeded. In addition to this method, bulk EB induction on Petri dishes (with or without semisolid media) can be used leading to a wider variety of EBs in terms of size distribution. This method lies on a totally spontaneous EB formation in static a static culture without using any sort of technique in order to manipulate the characteristics of the EB. Lastly, culturing of ES cell suspensions on rotation

devices have been shown to give rise to controlled EB formation (Dang et al., 2002; Wobus et al., 1997; Zandstra et al., 2003).

1.3.3.2 Growth of Embryoid Bodies

During the culture of ESCs and after the removal of the LIF factor the creation of the EBs starts taking place as we have pre-mentioned, each being formed by hundreds or thousands of cells. In the early stages dispersed cells migrate on surface and move towards each other. The initial cluster of cells subsequently becomes a focus for further agglomeration engulfing more cells which come in contact. In a suspension of cells the initial clusters are formed by collision of particles. It must be pointed out that EBs are not a simple agglomeration of cell but a mass of cells with a regular shape and semi organised structure. The result of this process is a random, in terms of aggregate size, formation of EBs depending always on the culture method followed (stationary, stirred, hanging drop). The size of the aggregate might have an impact on the viability of the cells lying in the inner part of the entity, due to the limitations in nutrient and oxygen delivery to them. Cells at the outer edge of the aggregate will be exposed to higher nutrient, oxygen, and growth factor concentrations than those cells that lie a few layers underneath the surface of the aggregate. A concentration gradient from the edge to the centre of the aggregate is formed and it has been observed that in large aggregates (>300 μm) a necrotic centre starts being formed due to these limitations (Sen et al., 2001). The size of the aggregates formed during ES culture should be expected to be in the scale of several hundred microns. Murine embryonic stem cell aggregates that have been cultured for 9 days in stirred tanks, have been reported to reach sizes of 1000 μm (Fok and Zandstra, 2005). It has been observed that regardless of the method of cell culture, the embryoid bodies will eventually grow to a similar maximum cell number of 28,000 ± 9,000 per EB, after 10 days of culture (Dang et al., 2002). The process of EB creation and formation has not been studied extensively.

1.3.3.3 Bioreactors for stem cell differentiation

Stirred culture systems have been well characterised and have been extensively used for microbial and mammalian cell culture. An ideal culture and differentiation system should be suitable to scale up and allow control of certain parameters such as pH, oxygen tension, cytokines, nutrient concentration. There have been successful attempts of stirred tank cultivation for mouse but also for human ES cells (Sharon Gerecht-Nir et al., 2003) in an effort to scale-up and produce sufficiently large numbers of differentiated cells that could be used for novel clinical applications (in the case of human ES cells). By using observations of mass transfer and shear stress effects on the development of mouse ES-cell derived neural precursor cell aggregates in optimised small scale systems, scaled up production was achieved in a controlled manner in computer controlled 500 mL suspension stirred bioreactors (Gilbertson et al., 2006). Spinner flask culture systems have been used as well to differentiate mouse embryonic stem cells to cardiomyocytes (Zandstra et al. 2005) and hematopoietic cells (Dang et al., 2002)

1.3.4 Medical significance of neural stem cells

Experiments have been carried out to control the differentiation of ES cells into neurons to realize potential applications in neuroscience and regenerative medicine. Research up to now has highlighted the possible use of (ES) cells as sources of neurons with unlimited resource potential (Keller, 2005). More specifically, in 1992 scientists discovered that the adult central nervous system (CNS) contained neural stem cells (NSCs) and therefore had the potential for regeneration, raising the possibility of cell-based therapies (Reynolds and Weiss, 1992, 1996). Lately neural stem cells (NSC) are gaining importance as potential therapeutic agents to treat diseases such as Parkinson's and multiple sclerosis and cell therapy has been seen as an exciting potential new avenue for the treatment of human ailments, especially in the central nervous system (Weissman et al, 2001; Svendsen and Smith, 1999; Weiss S, 2000). Using a rat model for Parkinson's disease, Kim et al. (2002) demonstrated that ES-cell derived dopamine neurons that had been transplanted in these animals

survived and displayed electro-physiologic properties characteristic of the midbrain neurons. These animals showed some recovery suggesting that the transplanted cells were functional. Furthermore, in the case of human patients, recent evidence from post-mortem analyses of brains of Parkinson's patients transplanted with fetal cell suspension grafts, indicated that cell suspension transplants integrated seamlessly and were not rejected by the host (Mendez et al, 2005).

1.3.5 Commercial perspective of regenerative therapies

In 2002, of the four F.D.A approved products, three were living skin equivalents for diabetic or venous ulcers (Apligraf, Organogenesis; Dermagraft, Advanced Tissue Sciences) or burns (OrCel, Ortec), and one autologous cell cartilage repair treatment (Carticell, Genzyme Biosurgery). Between 2000 and 2002 there was a substantial shift within industry from structural applications towards cellular therapies, largely driven the collapse of large firms in skin equivalents (Organogenesis, Advanced Tissue Sciences) and a growth in small stem cell based firms (Lysaght and Hazlehurst, 2004). The demise of these pioneering firms was reported in the media as being due to a variety of reasons, including high product price, poor sales due to slow product uptake, high costs associated with delays achieving regulatory and reimbursement approval, a generalised collapse of private sector funding (Stone, 2003), a lack of automation and scaleability and poor manufacturing efficiency resulting in high production costs and small profit margins (Moore SK, 2002). These developments in the tissue engineering industry have underlined the need for a shift in approach to product development, making a realistic appraisal during early research and development of issues such as product functional requirement, scaleable manufacturing, clarifying and meeting regulatory requirements, and ensuring cost effectiveness, reimbursement and commercial viability of a product and the manufacturing process. A central issue in establishing future successful regenerative bioprocesses is that of processing without major intervals from manual operations to automated methods.

1.4 Effect of shear during bioprocessing on biomaterials

While biological materials have a wide range of forms such as polymers, mammalian cells, viruses etc, this thesis will primarily focus on the effect of shear on biological aggregates. Protein precipitates and embryoid body solutions were the materials that where studied in the current thesis. As side projects the effect of shear on plasmid DNA and single progenitor stem cells of which the EBs consisted, was investigated.

1.4.1 Deformation of protein precipitate particles

1.4.1.1 Effect of down stream processing on protein precipitates

In many industrial applications it is desirable to avoid particle breakage as much as possible. For example, in water treatment it is desirable to have larger flocs so as to obtain faster settling (Kobayashi, 2004); in crystallization the agitation must be controlled to increase the crystal size (Biscans et al., 1996); in protein precipitation and separation the breakage must be reduced to improve precipitate separation efficiency (Ayazi Shamlou et al., 1994; Byrne et al., 2002). However it has been shown that protein precipitates can break up during exposure to fluid induced stresses in mechanically stirred vessels (Bell and Dunhill, 1982a; Pentnenate and Glatz, 1983; Glatz et al., 1986), in centrifuges (Bell and Dunhill, 1982b), in pipeline transportation (Hoare et al. 1982) and in different types of pumps (mono, centrifugal and gear pump) (Hoare et al., 1982, 1984).

More specifically, it has been seen that in the case if the pumps, exposure to shear in the Mono and gear positive displacement pumps follow a similar break up pattern , the Mono pump causing the lesser precipitate breakage. For the centrifugal pump there is a similar final particle size reached as with the mono pump. No precipitate breakage was observed for the peristaltic pump (Hoare et al., 1982). During agitation in stirred tanks turbulent flow is usually the prevalent flow. In that case, protein precipitate breakage is caused by the turbulent fluid induced shear stresses occuring in the viscous dissipation sub-range and the

final particle size is determined by the intensity of agitation and the impeller tip speed. However, the effect of these stresses on protein precipitates during processing in a mechanically stirred vessel is not well understood since there is a possibility that different mechanisms may take place during breakage, such as fluid shear, collisions between aggregates and impact between aggregates and inserts in the reactor (Shamlou et al., 1994). Furthermore in many liquid solid separators, such as centrifuges, the particles are exposed to high levels of turbulence thus resulting in particle breakage. It is known that in specific areas of the devices, where sharp transitions in flow are expected, such as the feed/inlet and outlet zones, highly turbulent areas flow regions are formed leading to particle breakage. A grade efficiency analysis of a precipitate suspension processed through a disc stack centrifuge, concluded that breakage of aggregates occurred primarily in the feed zone (Manweiler and Hoare, 1992). This has also been shown also for a multi chamber– bowl centrifuge (Boychyn et al., 2000). Concerning the flow of protein precipitates through pipes, models describing the breakage have been established in the case of turbulent flow and laminar flow throughout the piping (Zumaeta et al., 2005). As previously seen, according to the flow field to which the material is exposed in each bioprocess, a relevant effect on the breakage of the precipitate can be observed. Excessive breakage of the protein precipitates can severely limit the size and density of the precipitates and can thus hinder downstream processing of the protein products.

1.4.1.2 Mechanism of precipitate particle breakage

There are many definitions of breakage ranging from claiming that breakage is the separation of fragments from a whole, to saying that breakage is the destruction of the integrity of a whole entity by a force. There are three mechanisms that can, in a broad sense, classify the meaning of breakage depending on the energy input in a system and the way it is applied. These are: 1) abrasion, 2) cleavage 3) shattering (Redber, 1990). In abrasion, the mechanism is applied specifically on the surface and the energy intensity is sufficiently small that only small particles are removed from the surface of the parent particle. In cleavage, the energy is sufficient to cleave the parent particle

into a small number of daughter particles that are of the same order in size as the original particle. Brown et al. (1996) showed that cleavage failure exists at low energy impacts and the particle is broken into 2 or 3 daughter particles. In shattering, much higher energy intensity is imparted to the parent so that many regions of the particle are stressed beyond breaking point. This leads to a wide range of fragment sizes being produced, most having smaller size than the original particle (Biscans et al., 1996). Suggestions have been made that aggregates are composed of a compact and strong core surrounded by a weaker loose layer of particles attached to the core in a fractal manner (Byrne et al., 2002; Ayazi-Shamlou et al., 1994, 1996). Luo and Svendsen (1996) and Hagesaether et al. (2002) proposed that the formation of two daughter particles of the same size is the most improbable event in a breakage process. It is more likely that precipitates break into uneven sizes and into more than one daughter particles (Galinat et al., 2005). Austin (2002) performed a study in which he modelled the breakage of a single particle in a single impact process. The extent of breakage was associated with the energy of impact and the particle size and a description of the way the impact energy was dissipated in the breakage event was made.

1.4.2 Effect of shear on cell aggregates and cells

Shear is encountered in routine lab-work relevant to cell culture so both the aggregate and the cells are often exposed to stresses. It is also believed that in bioprocesses that will be developed shear will have an important role in the design of bioreactors for ESC expansion and differentiation, as well as for other units of operation in the downstream processing. The embryoid bodies is a material composed of live cells thus the effect of shear on both the EBs and the cells is of particular interest. The size and the cell density of an embryoid body as well as the viability of single cells are expected to be affected by shear.

1.4.2.1 Effect of shear on cell aggregates

Most of the experimental work done on this field up to now has to do with the effect of shear stress due to impeller and stirrer rotation in culture systems and

bioreactors. In experiments with baby hamster kidney (BHK) cell aggregates, it was seen that impeller-associated shear effects have an effect on aggregate characteristics are quite dependent upon hydrodynamics: When agitation rate is increased, a larger number of smaller and more dense aggregates are formed (Moreira et al, 1995). Furthermore an experimental correlation between maximum aggregate diameter and power dissipation per unit of volume was established (close to *-0.25),* similar to the dependence of Kolmogoroff's eddy scale upon power dissipation per unit of volume. In the case of cell aggregates of mouse embryonic stem cells, stirrers where used to control the final size of the aggregates in cell culture experiments. Agglomeration between the embryoid bodies formed during the culture was prevented due to hydrodynamic shear stress developed within the bioreactor (Fok and Zandstra, 2005). In a different type experimental work Sen et al. (2004) dissociated mechanically aggregates of neuronal stem cells (neurospheres), by drawing the neurospheres repeatedly into a pipette tip and then expelling them while holding the tip against the bottom surface of a test tube with only a small gap for the passage of the spheres. Shear generated throughout this process had as a result to dissociate the spheres into single cells. This procedure creates fluid shear that results in the death of approximately 20–30% of the cells, and damages the remaining viable cells (Kallos et al., 1999).

However a well defined, in terms of shear stress and flow field characterization study, has not been recorded up to now for embryoid body systems. A further understanding of the mechanism of breakage of the EB's as well as a monitoring of the fate of the single stem cells under stress conditions should be established.

1.4.2.2 Effect of shear on mammalian cells

Shear stress is known to cause a wide variety of effects on cell populations, including cell death by lysis (i.e severe mechanical damage), trans-membrane ion leakage, physiological and metabolic changes (e.g cell morphology, gene expression levels), apoptosis or necrosis (Chisti, 2001) and loss in cell number (Born et al, 1992). Biochemical changes induced by shear are not immediately

obvious; it takes a time scale of the order of a cell-generation before changes can be measured, whereas severe mechanical damage is immediately detectable (Mardikar and Niranjan, 2000). As a result shear damage studies use often assays that probe cell membrane integrity permeability, such as trypan blue (Born et al., 1992) lactate dehydrogenase (LDH) release (McQueen et al., 1987) and flow cytometric assays (Al Rubeai et al., 1995).

In different processes cells will be eventually exposed in various flow fields and stresses. Turbulent flow is encountered in most bioprocesses and cells being exposed in such a flow field have been observed to be damaged. The damage is due to the interaction between turbulent eddies (in the order of the size of the cell) and the cells. If a cell is being exposed to stress due to a collision with an eddy and the energy that is exposed to is higher than the membrane surface bursting energy, cell disruption will occur (Zhang et al., 1992). In case of turbulent flow in a capillary system cell death has been correlated with the power dissipation within the capillary (Chisti, 2001). Cell damage may occur under elongational or extensional flow (e.g flow through a sudden contraction, capillary entrance). In this case cells experience deformation under elongational flow or stable laminar flow, will rupture if elongational forces exceed the critical bursting tension of the cell membrane (Born et al., 1992; Chisti, 2001). As turbulent hydrodynamic conditions are generally accepted as being more damaging than laminar conditions (Chisti, 2001), it is assumed that the optimum conditions for cell survival and processing will be consequently in a laminar flow environment.

Several studies have been carried out to investigate the effect of shear forces on animal cells in different processes. Some researchers have used a standard impeller operating at different speeds (Al-Rubeai et al., 1995; Lakhotia et al., 1992; Zhang et al., 1995) whereas others have used flow apparatus forcing the culture through narrow tubes (McQueen et al., 1987). The principal cause of damage to suspended cells in sparged bioreactors has been identified the very high shear forces that are generated locally, during bubble burst at the fluid surface (Chisti, 2000). In the case of cells exposed in laminar flows it has been observed that damage has been induced throughout a range of shear stresses

varying from $19*10^{-3}$ Pa to 100 Pa, with exposure times between 10 minutes and 24 hours (Born et al.,1992). One report has highlighted an effect where cell loss or damage at low shear causing damage to the cells at low shear stress (~1 Pa) and high shear stress (~100 Pa) is greater than intermediate values of shear stress (~10 Pa) (Mardikar and Niranjan, 2000). This big variation in the values of shear forces could be due to the effect of different breakage mechanisms in each case.

It must be stressed that in the shear studies that have been done up to date, the exposure time of the aggregates to shear conditions has never been in the range of seconds but rather consisted in cells being exposed to stress conditions for minutes, even hours. Taking into consideration the fact that typical cell transfer steps such as aspiration, dispension and pipe flow all involve flows where the cells are exposed for short time periods (sub-second), but may be repeated many times during processing, there is importance for the understanding of such conditions in cell functionality.

1.4.3 Effect of shear on plasmid DNA

An analysis of experimental data on the effect of flow of a plasmid DNA solution through a capillary was made as part of the understanding of the effect of shear stress on biomaterials which is the scope of this thesis. A brief overview of the literature covering the issue of plasmid DNA de-naturation (scission or damage to supercoiled form) follows.

Plasmid DNA molecules are exposed to highs shear environments and different flows during separation and purification processes. Plasmid DNA molecules have been observed to degrade under elongational flow, shear flow and turbulent flow. The physical structure and biological activity of DNA in solution is detrimentally affected by flow induced stress fields. There are several early studies demonstrating DNA degradation due to shear forces in laminar flow fields (Bowman et al., 1972; North et al., 1974; Adam et al., 1977). On the other hand there is evidence that simple shear flows may only be capable of inducing scission in the presence of intra-molecular entanglements or turbulence (Odell

et al., 1994). Furthermore stress induced degradation of DNA molecules has been seen in turbulent flows (Hershey et al., 1960; Burgi et al., 1962) during impeller mixing in stirred vessels. Turbulent flows have a high elongational component and have stagnation points between vortices. Levy et al (1999) subjected plasmid DNA molecules in solution to shear rates of up to 10^6 s^{-1} during turbulent flow in a rotating disc shear device under different conditions. The ionic strength of plasmid DNA solution and the time of shearing strongly affected damage to the plasmids.

1.5 Project aims

The primary aim of this thesis is to develop a micro scale process environment for the study of the effect of shear on biological aggregates. From the processing point of view there will be both scale-up and scale out approaches, having in mind an automated application with the use of robotic technology in the effort to mimic whole bioprocesses in the micro scale. Furthermore an understanding of the breakage mechanisms and the effect of different process parameters on the material studied each time was established.

1.5.1 Applications of ultra scale-down

A rotating disc device has been successfully used for the development of laboratory mimics for the feed zone of continuous centrifuges where maximum damage to protein aggregates was observed to occur (Manweiler and Hoare, 1992). A further use of such a device helped mimic computationally predicted stresses in the critical zone of the centrifuge entrance region where maximum energy dissipation rate was found to be generated (M. Boychyn et al., 2001). An improved prediction of industrial scale continuous centrifugation using ultra scale-down studies was achieved with the aid of the rotating disc device which helped improve the accuracy of mimic of the actual centrifugation process, by mimicking material damage that was occurring in the feed zone of a disc-stack centrifuge (Hutchinson et al., 2006).

As a way forward a capillary device was designed and used in an effort to further minimize working volumes, following a further scale down direction. Such a device had a number of advantages over the rotating disc device that had been used. Issues such as heat generation were avoided since the exposure time within the capillary, which was in the order of a fraction of a second, was not enough for a temperature rise of the solutions processed. Furthermore a larger proportion of material is exposed to the high shear area within the device. Finally in a capillary system and according to the flow rate both laminar and turbulent flows can be developed according to requirements, giving more choice for more accurate analysis and understanding of the flow fields developed.

Microbial protein precipitate was chosen to be studied as a material which was of relevance to the bio-processing area where the final scale of operation can be many thousands of litres. The material used in this experimental work is an example of a biological material that has been used extensively and whose properties were known and could be controlled during preparation. The translation between rotating disc and capillary devices was studied using the large quantities of the protein precipitate available. This would eventually allow the mimicking of an industrial scale operation using a device suitable for adaptation to robotic micro-well systems using small (sub-millilitre) quantities of material. This is demonstrated schematically in Fig 1.1.

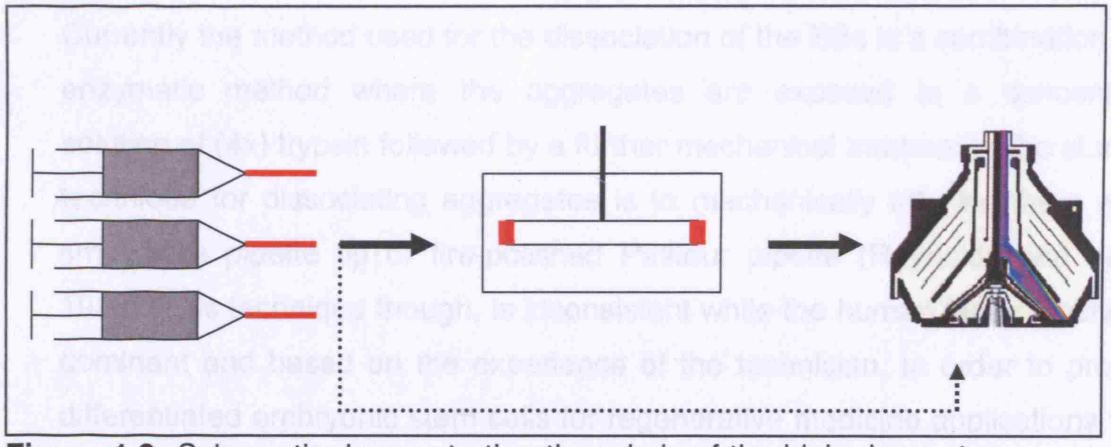

Figure 1.2: Schematic demonstrating the mimic of the high shear stress area of the centrifuge with the use of a rotating disc ultra-scale down device and furthermore with a capillary ultra-scale down device. The high shear areas are indicated in red colour.

1.5.2 Automation and scale-out. Processing of Embryoid Bodies

As regenerative medicine develops in to a broader field with wide potential applications, it will be necessary to progress to bioprocess methods that can yield a consistent outcome with more units of material. The scale out to many parallel small bioreactors rather than scaling up in one big bioreactor is a promising possibility for the expansion of current manual and semi-automated cell culture methods. The shift to fully automatable process operations in the future will eventually have to substitute the ongoing manual methods guaranteeing a reproducible efficacy and safety. This work is a first step towards that direction (Fig 1.2).

The use of the capillary ultra scale-down device which was developed in the first part of the research was chosen as a tool for the processing of EBs. The small working volumes needed for the processing made the capillary device appealing since the particular material was scarce and available in small quantities. Concerning the embryoid body system, a well defined (in terms of shear stress and flow field) characterization study has not been recorded up to now. In most of the experimental works that involved exposure of EB to shear conditions, shear stresses were used in order to control the properties of the EBs during its growth.

Currently the method used for the dissociation of the EBs is a combination of an enzymatic method where the aggregates are exposed to a concentrated solution of (4x) trypsin followed by a further mechanical treatment. The standard technique for dissociating aggregates is to mechanically triturate them with a small-bore pipette tip or fire-polished Pasteur pipette (Reynolds and Weiss, 1992). This technique though, is inconsistent while the human factor involved is dominant and based on the experience of the technician. In order to produce differentiated embryonic stem cells for regenerative medicine applications there is need to process the material and dissociate embryoid body in a consistent manner. Furthermore an insight on the mechanism of breakage of the embryoid body and the understanding of its engineering properties, as well as monitoring

of the fate of the single stem cells under stress conditions, should be established.

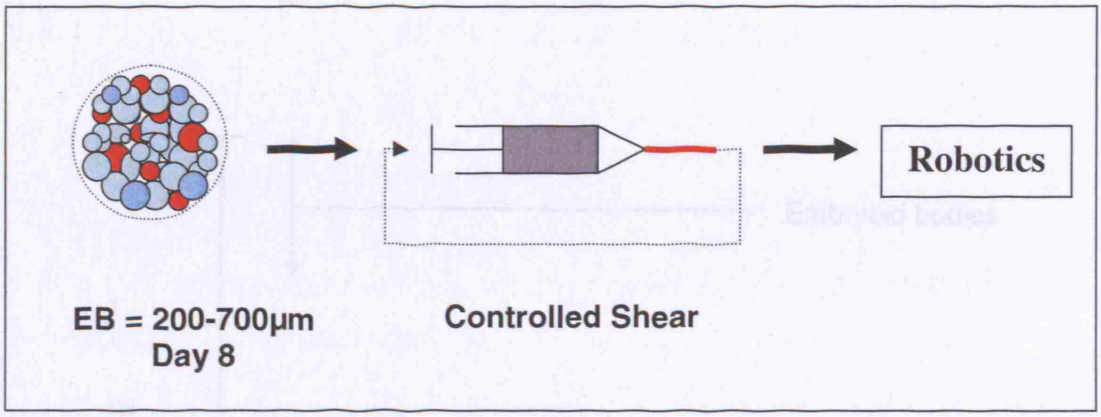

Figure 1.3: Schematic of the use of capillary shear in order to break down embryoid bodies in an effort to develop automated bioprocesses. On day eight the EB contains different types of differentiated stem cells. The differentiation pathway that was followed in this research work aimed in the formation of neuron progenitor cells shown as light coloured spheres within the EB.

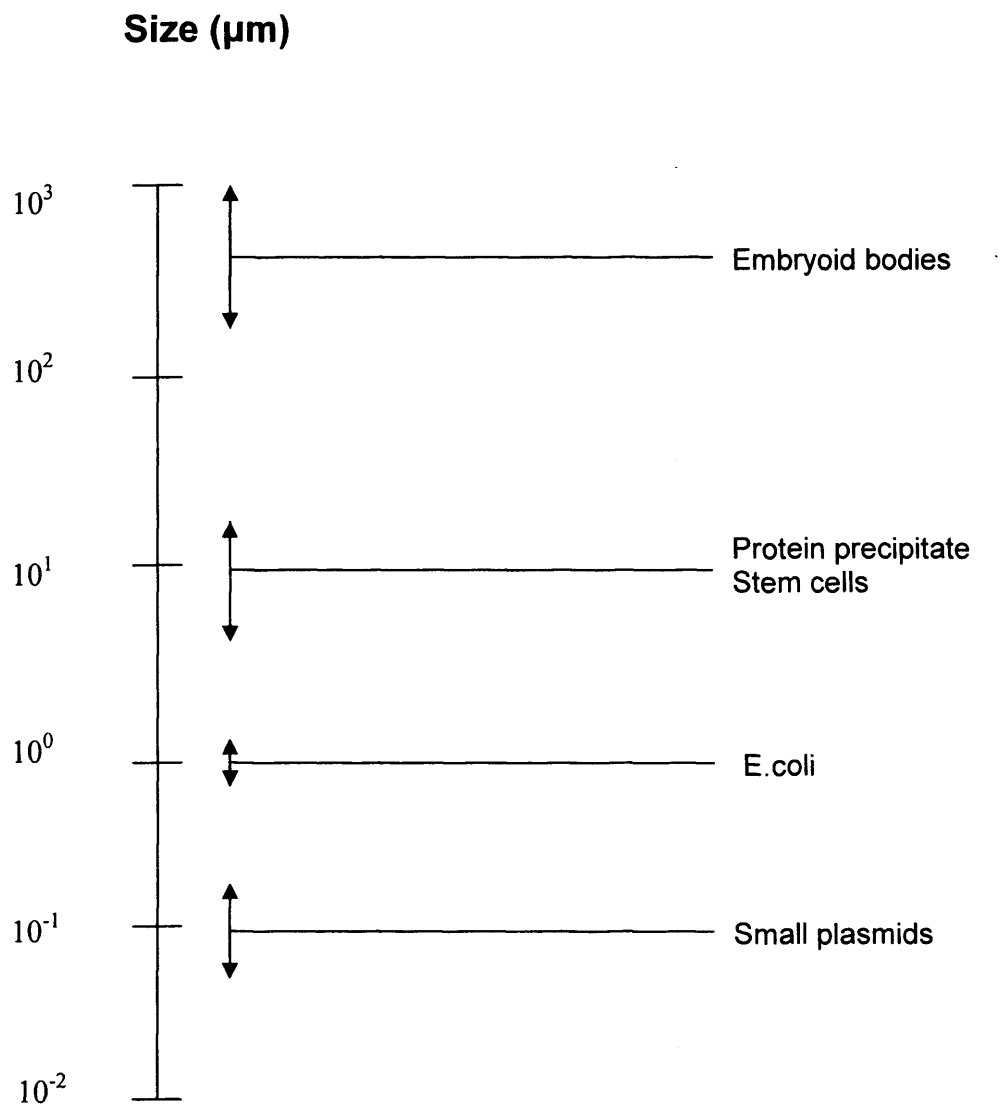

Figure 1.4: Typical size range of biological particles relevant to this study

CHAPTER 2

Materials and Methods

2.1 Methods – procedures followed

In this section the methods for the preparation of the materials used during experiments are presented.

2.1.1 Preparation of yeast protein precipitate suspension

All the protein precipitate solutions used for the experimental analysis, were prepared in the same way as outlined below. High activity baker's yeast (*Saccharomyces cerevisiae*) provided by DCL London (London, UK) was suspended to 28% packed wet weight per volume in phosphate buffer (0.1M KH_2PO_4, adjusted to pH 6.5 using a 4M NaOH). This was then disrupted by five discrete passes at 500 bar pressure through a high-pressure continuous flow homogenizer (Lab 60) and centrifuged in order to remove the cell debris. The centrifugation lasted for 40 minutes at 13.000 rpm in a swing out motor. The clarified homogenate was placed into 50 mL falcon tubes and stored in the freezer (-20°C) as a sample used for every future experimental procedure. Each time before an experiment the clarified homogenate was placed in a water bath (25°C) until the moment when it was totally thawed. Subsequently the solution was placed in an agitated precipitation vessel (Fig 3.1) to which HCl was added in order to achieve a pH of 4.5. The impeller rotational speed was 600 rpm and the time for which the solution was left to precipitate in the vessel was 300 s. The addition rate of the acid was stable throughout all experiments as one drop per second (0.1 mL per sec), the addition was kept constant since the rate of acid addition influences the size and the nature of the aggregates that are under formation (Fisher et al., 1986). The precipitate was aged for 10 minutes at 400 rpm. The container in which the precipitation step took part was a 100 mL glass beaker. Four baffles within the container helped ensure efficient mixing during the time of the precipitation.

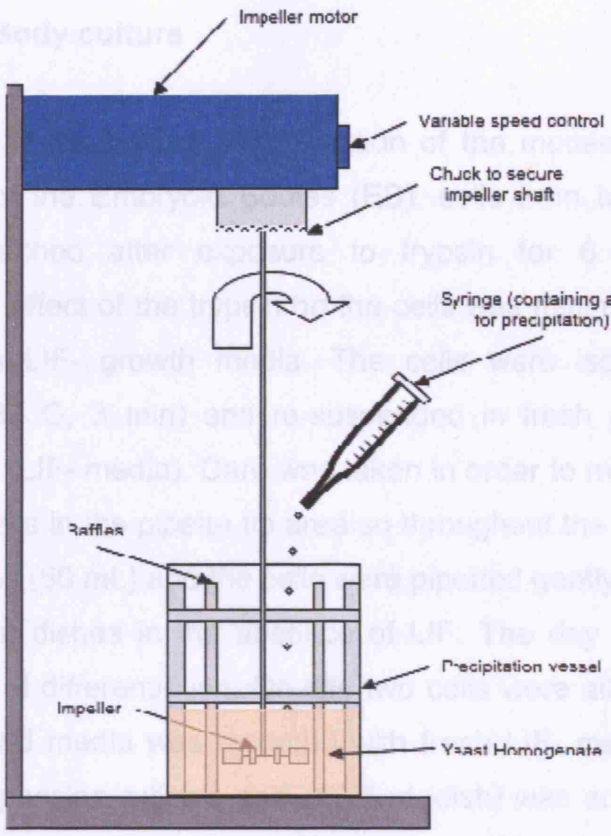

Figure 2.1: Schematic of the precipitation process and experimental apparatus

2.1.2 Embryoid Body culture

For the initiation of the in-vitro differentiation of the mouse ES cells and the further creation of the Embryoid Bodies (EB), cells from two confluent T150 flasks were detached after exposure to trypsin for 6 minutes in 35°C temperature. The effect of the trypsin on the cells was minimised by quenching the solution with LIF- growth media. The cells were isolated after gentle centrifugation (280 G, 3 min) and re-suspended in fresh growth media that didn't contain LIF (LIF- media). Care was taken in order to minimise any effects of shearing the cells in the pipette tip area so throughout the process wide bore pipettes were used (50 mL) and the cells were pipetted gently. Finally cells were inoculated in Petri dishes in the absence of LIF. The day of inoculation was defined as day 0 of differentiation. On day two cells were allowed to settle in a centrifuge tube and media was replaced with fresh LIF- media. On the fourth day of the EB expansion retinoic acid (13.5 μL/dish) was added with the fresh media in order to induce a further differentiation of the cells in the neuronal direction (Ying, 2003). On day six the EBs were re-suspended following the same method in a serum free medium (DMEM/F12 and neurobasal medium at a ratio of 1:1 supplemented with N2, B27 and glutamine) and finally on day eight the EBs produced were ready to be processed in the capillary shear device.

2.1.3 Cell passaging protocol in tissue flasks

Mouse embryonic stem cells derived from a UCL working cell bank were thawed and seeded ino 150 cm^2 tissue flasks (T150) and passaged every 2 days at a split ratio of 1:6 to 1:8 (1 flask into 6 or 8 new flasks). The cells were observed macro and microscopically for cell confluency (density), evidence of mitotic cells, pH/colour of medium, amount of cell debris in medium, and other characteristics of the cells morphology.

During a typical tissue flask passage, the spent medium was removed from the flask using a pipette. Then the cell growth surface of the flask was rinsed with 20 mL (0.13 mL/cm^2) of DPBS to remove residual FBS proteins that reduce

trypsin activity. Next, 6 mL (0.04 mL/cm^2) of 0.25% trypsin/0.02% EDTA was added to each flask and spread evenly over the growth surface. After 5-7 minutes, the mESCs were detached from the growth surface by tapping the flask against the palm of the hand. After completely dislodging the cells, 12 mL (0.08 mL/cm^2) of DPBS was immediately added to quench remaining trypsin activity. The cells were not exposed to trypsin longer than 10 minutes since trypsin will eventually permeate the cell membrane. The cell suspension from all individual flasks was pooled together and a sample was taken to determine cell density by counting the cells using a haemocytometer. Viability was assessed using the trypan blue dye assay. To seed the next passage flasks, the cell suspension was transferred into 50 mL centrifuge tubes and centrifuged at 300 G for 5 minutes. The supernatant was discarded and the cell pellet was re-suspended with 1 mL of medium for each T150 flask planted. The 1 mL of the cell suspension was added to 20 mL of fresh medium into each new T150 flask. Finally, the flasks were incubated at 37°C in a 5% CO_2 humidified incubator. The mESC cultures were also re-fed with fresh medium after 2-3 days to prevent build-up of metabolic intermediates and waste products, and depletion of nutrients and growth factors in the medium.

2.2 Materials

In this section the materials and apparatus used during experimentation are presented.

2.2.1 Rotating disc shear device

The rotating-disc high-speed device, consisted of a single flat disk and shaft assembly, fabricated from an aluminium alloy. The disk was 40 mm in diameter and 1mm in thickness. The addition of a cocentric metal cylinder around the rotational axis (shaft), down to the disc level provided the sealing of the shear chamber. The shaft was extended through the top cover and was connected to a high speed motor. Three different speeds were used for experiments ranging between 6,500 rpm and 15,000 rpm. Speed was controlled and monitored by an in-house built control pack (electronics workshop, UCL). In all experiments care

was taken so as to ensure that there was no air trapped within the chamber that could lead to the formation of an air-liquid interface within the chamber during the experiments. This was made possible with observing the chamber through a transparent Perspex bottom part as well as being careful when liquid sample was inserted in the device. The temperature in the chamber was maintained stable throughout the experiment (20 °C) since a cooling jacket was fitted to the external part of the device circulating cold water on its surface. The temperature was measured with a thermocouple throughout each experimental process, in order to monitor any temperature rise.

A normal experimental run consisted of filling the chamber with the test solution and stirring at a fixed speed for a specified time in the range of 1 to 10 minutes. The chamber was emptied and washed before the start of each time point.

2.2.2 Capillary device

The Instron capillary rheometer (Instron Ltd, High Wycombe, UK) was modified in-house to study a range of stress conditions. The plunger and barrel are constructed from an aluminium alloy i.e. Durrel (Smith Ltd, UK) with a barrel diameter and length of 20 mm and 60 mm respectively. Exact alignment of piston and barrel was not needed, because some freedom of movement was permitted in the attachment of the piston to the crosshead. The plunger speed was controlled by a series of cog combinations and was able to produce flow rates of up to 4 mL/s through the barrel.

The tubing used, was a narrow biocompatible polymer material chemically inert to most solvents. The PEEK bore capillary can be used to replace stainless steel tubing in most liquid analytical equipment systems, and has very high mechanical strength. Unlike stainless steel and titanium tubing, PEEK tubing is flexible and can be easily cut to desired lengths. The inner diameter of the tubing that was used for the experiments was varied according to the biomaterial processed. Four different lengths of capillary tubes were also used, in order to examine the effect of the retention time of the sample within stress

conditions. Experiments were carried out with capillary lengths of 15 mm, 30 mm, 60 mm, 90 mm and inner capillary diameter of (250 μm).

In the experiments where EB processing was involved, a different size of capillary diameter was used. This was due to the fact that the size of the EBs was much bigger (d_{90} = 600 μm) than the size of the precipitate particles (d_{90} = 15 μm). The size of the diameter of the capillaries used for these experiments, was 1 mm. Capillary lengths were varied in order to maintain the retention time within the capillary constant. The lengths of the capillaries used were varied from 5 mm to 200 mm.

In all the experiments an 80 mm piece of silicone tubing (5mm ID) was connected to the outlet of the PEEK capillary in order to constrain the development of a jet of the liquid a phenomenon that is expected in high fluid velocities, giving a possibility for additional causes of degradation of the material. The outlet of the silicone tubing was placed at the bottom of a plastic container, which collected the protein precipitate solution after it was forced through the capillary. The sample was collected and the syringe was refilled after each pass.

2.2.3 Sterile capillary shear device

The Instron capillary rheometer (Instron Ltd, High Wycombe, UK) was modified in-house to study a range of stress conditions. The plunger and barrel were constructed from an aluminium alloy i.e. Durrel (Smith Ltd, UK) with a barrel diameter and length of 20 mm and 60 mm respectively. Exact alignment of piston and barrel was not needed, because some freedom of movement was permitted in the attachment of the piston to the crosshead. The plunger speed was controlled by a series of cog combinations and was able to produce flow rates of up to 4 mL/s through the barrel. A stainless steel capillary was connected to the barrel and through this the embryoid bodies were processed. The inner diameter of the capillary was chosen to be 1 mm so that it would be wider than the biggest EB formed during the culture. The length of the capillary was chosen to be between 50 mm and 200 mm according to the flow rate with

which the material was pushed through it. The outlet of the capillary was connected to a silicone tubing that ended in a container where the sample was collected after each pass through the capillary.

2.2.4 Set of metal capillaries

A set of capillaries with double luer-lock fittings in both ends was devised in order to conduct experiments in a sterile environment. Two syringes were attached on each end of the capillary and the solution was pumped backwards and forwards for as many passes as needed. The capillaries were made of stainless steel having four different lengths and two different diameters. The different lengths were 15mm 30mm 60mm 90mm and were used in order to manipulate the retention time for a set flow rate within a capillary. There were two different sets of capillaries for the pre-mentioned lengths with two different inner diameters of 1mm and 0.5 mm. For all previous capillaries the entrance formed a 90^{o} with the axis of flow. A further set of capillaries for the same lengths and diameters as previously mentioned was devised, having though a smooth entrance of 60^{o} angle with the axis of flow minimising any possible entrance effects. The capillaries were created by Cooper's Needleworks workshop.

2.2.5 Homogeniser

A continuous process Lab60 homogeniser was used in order to disrupt yeast cells for the release of the intracellular contents and in particular the proteins. Solution was re-circulated in high pressure (500 bar) for 5 passes which were considered enough for the total rupture of the cells. Extensive processing was avoided so that any possible damage on the proteins released from the cell would be avoided.

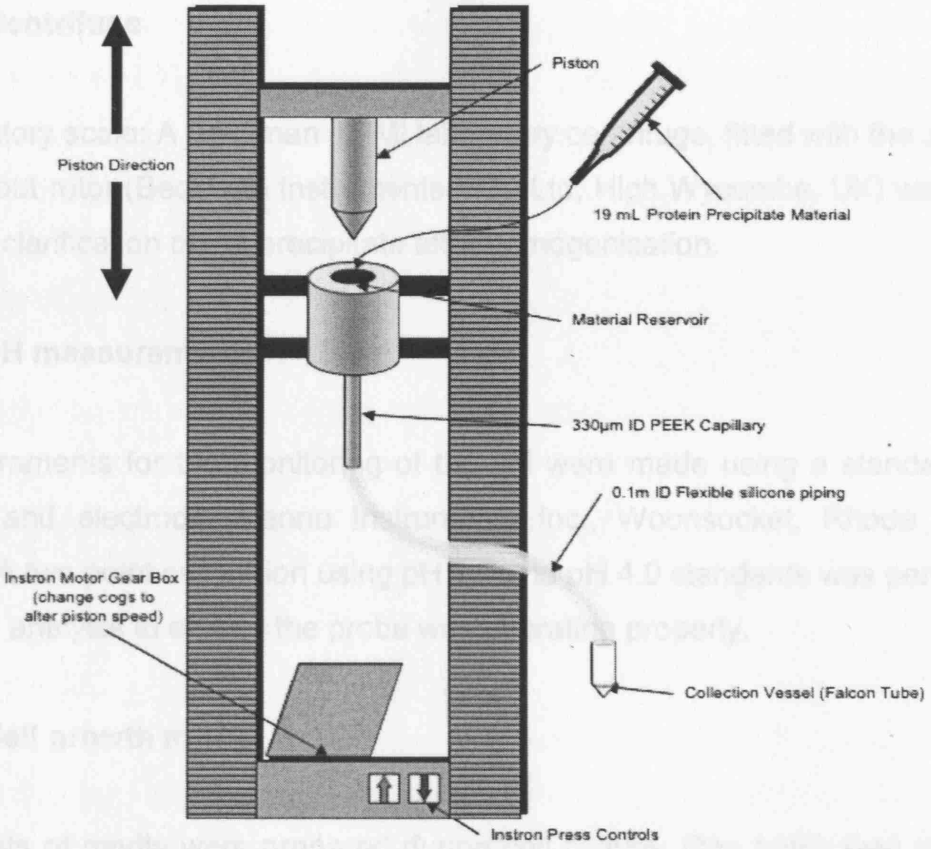

Figure 2.2: Schematic of the Instron press and the incorporated capillary device used during experimentation. The dimensions of the capillary were changed during experiments and different lengths and different diameters were used.

2.2.6 Centrifuge

Laboratory scale: A Beckman J2-MI laboratory centrifuge, fitted with the JS-13.1 swing-out rotor (Beckman Instruments (UK) Ltd, High Wycombe, UK) was used for the clarification of the precipitate after homogenisation.

2.2.7 pH measurements

Measurements for the monitoring of the pH were made using a standard pH-meter and electrode (Hanna Instruments Inc., Woonsocket, Rhode Island, USA). A two point calibration using pH 7.0 and pH 4.0 standards was performed prior to analysis to ensure the probe was operating properly.

2.2.8 Cell growth media

Two sets of media were prepared during cell culture. One batch was used for mESC growth and contained LIF so as to keep cells in the undifferentiated state, while the other was used for the growth of EBs during which differentiation was occurring.

PBS: Phosphate buffer saline (1X) without Ca^{2+} and Mg^{2+} (biowhittaker) (cat. num. : 17-516F)
L – glutamine (200mM) : (Biowhittaker, cat. num. : 17-605E)
0.25% trypsin / 0.02% EDTA (Sigma, cat. num. : T4049)
DMSO: (Sigma, cat. num. : D2650)
2-beta mercaptoethanol 0.1mM : (Gibco, 31350 010)
Glasgow MEM : (Sigma, G15145)
Fetal calf serum FCS (mES serum) : (Invitrogen, 10270-106)
LIF, Serum, PBS.

2.2.9 Mouse embryonic stem cells

Engineered 46C mouse embryonic cells donated by "stem cell sciences" were used for expansion and further differentiation in the presented research activity.

The mouse ES cells were maintained in GMEM supplemented with b-mercaptoethanol, non essential amino-acids, glutamine pyruvate, 10% fetal calf serum (FCS) and 100units/ml LIF (Smith, 1991). Cells were cultured in T75 and T150 gelatinised tissue culture flasks and were passaged every 48 hours.

2.3 Measurements

In this section the methods used for measuring the properties of the materials processed, such as particle size for protein precipitates and Embryoid Bodies and viability for single cells, will be presented.

2.3.1 Particle size analysis

Samples were sized by dynamic light scattering using a Zetasizer 3000 (Malvern Instruments Ltd., Malvern, UK). Size measurements were carried out at a 90° angle (fixed setting) and analyzed using the automatic analysis software supplied by the manufacturer. Measurements were taken from samples in the reservoir and from samples that had passed through the different flow geometries. Every measurement was carried out in three serial measurements with a counting time of 60 s each and at a set temperature of 25°C.

In experiments where protein precipitates were processed, measurements were taken from samples that had been exposed to different shear conditions through the different flow geometries from within the reservoir at the exit of the latex tubing. Prior to analysis, samples were diluted 200-fold in water while the stirrer was set to a rotational speed of 1000 rpm. Every measurement was carried out in three serial measurements with a counting time of 60s each and at a set temperature of 25°C. All samples were analyzed in duplicate. In experimental work that involved processing of Embryoid Bodies and their size distribution measurement after processing, samples were diluted in PBS in a 1:10 ratio and analyzed in duplicates. Particular care was taken that the stirrer speed would remain in low rotation speeds (400 rpm) so as to avoid any further possible damage to the embryoid bodies and the single cells due to the stirrer rotation. It

was seen that there was no effect for this rotational speed on the size distribution of the cell aggregates even for prolonged exposure times (more than a measurement would require).

2.3.2 Visualization of cell growth using light microscopy

Cells grown in tissue flasks were observed using 100-400X magnification on an inverted light microscope. The cells were observed for degree of confluency (cell density), presence of mitotic cells which indicated cultures were in exponential growth phase, and amount of cellular debris in the spent medium which indicated cell death. As the age of the culture increased, the cells became more densely packed in the flask. For optimal detachment as single cells, the cultures were trypsinized when ca. 80-90% confluent. In addition the pH of the spent medium indicated a healthy culture if it was orange/red in colour due to release of CO_2 from respiring cells and build-up of metabolic waste products such as ammonia. Cultures that were red/purple indicated lower cell density or possibly poor cell growth. The medium from cultures that were contaminated with micro-organisms was turbid or more yellow (acidic) in colour.

Cells seeded onto the surface or within the alginate or collagen constructs were also observed in this same manner. In addition the morphology of the cells could be observed to determine whether the cells were rounded, or elongated and networked together.

2.3.3 Cell enumeration using haemocytometer

The density of the cell suspension was determined using a haemacytometer. After trypsinization and quenching with complete medium, a small sample ca. 0.5 mL was removed to determine the cell density. 100 µL of cell suspension was typically added to 100 µL of trypan blue dye (Biowhittaker) and mixed to homogeneity using a micro-pipette. Then ca. 20 µL of sample was injected onto the haemocytometer under a cover slip. Cells were counted in the grid that was etched onto the surface of the haemocytometer. The cell count was repeated

for a total of 3-4 replicates and averaged. The total number of cells/mL was determined by multiplying the total cells counted in 10 squares by 1000 times the trypan blue dilution factor (usually 2) as shown below. The multiplication factor of 1000 was obtained from the volume of 1μL contained in the counting grid (10 squares x 1 mm x 1 mm x 0.1 mm) and converted to mL for the original sample.

Avg. no. of cells in 10 squares x 1000 x Dilution factor (2) = Number of cells/mL

equation3.1

The accuracy of the cell count was dependent upon the homogeneity of the cell suspension. Suspensions that were aggregated produced lower results than actual numbers. Therefore this operation was dependent upon the age of the culture, effective trypsinization and the operator's technique. If possible between 100 and 300 cells were counted for each replicate so that the numbers were not prone to increased statistical error due to the small sample size used.

2.3.4 Cell viability using trypan blue dye exclusion

Viability was assessed using the trypan blue dye exclusion assay. Trypan blue is a small molecular weight dye that stains the cytoplasm of cells. Equal volumes of trypan blue stain and cell suspension were added together. Live cells had an intact cell membrane which excluded the dye. Dead cells had a permeable membrane that allowed the dye to enter the cell, thus dead cells appeared blue. Viable cell concentration and viability were assessed by cell counting in an improved Neubauer haemocytometer under phase contrast microscopy. 100 μL of cells were diluted 1:1 with 0.4% (w/v) trypan blue in water (Sigma, Poole, UK). Cells from 4 grids per slide were counted and the cell death calculated based on a single grid volume of 1 μL. Therefore, cells that excluded trypan blue were counted as viable and those that did not were considered as dead. The microscopic evaluation was completed within 15 minutes after dye addition because trypan blue dye will eventually permeate live cells. The viability of the cell suspension was determined by the equation:

$$\text{Percentage of viable cells} = \frac{\text{Number of live cells (unstained)}}{\text{Total number of cells (unstained + stained)}} x100$$

equation3.2

2.4 CFD modelling

The flow engineering environment in the rotational disk USD device and the capillary device was characterised by solving the Navier-Stoke equations with specified boundary conditions. The numerical solution was carried out by using a commercial CFD package, Ansys CFX 5.7.1 (ANSYS, PA, USA, 2003). The geometry for both devices was drawn on Workbench 9.0 and the unstructured mesh was generated from CFX-Mesh. The CFX Solver was used to solve the mass and momentum equations simultaneously to obtain local information for velocity and turbulence. The *k*-ε based Shear-Stress-Transport (SST) model by Menter was employed in this study as it was designed to give a highly accurate prediction of the onset and the amount of flow separation under adverse pressure gradients by the inclusion of transport effects into the formulation of the eddy-viscosity (Menter, 1996), which results in a major improvement in terms of flow separation predictions compared to the general k– ε turbulence model. Cartesian coordinates were used in the case of the capillary model whereas cylindrical coordinates were used for the rotating disc device.

2.4.1 Navier-Stokes equations

The basic set of equations solved by the CFD program for laminar flows comprise equations for conservation of mass and momentum; these equations are the continuity equation and momentum equation, respectively:

$$\partial\rho / \partial t + \nabla \bullet (\rho \upsilon) = 0$$

$$\partial(\rho\upsilon)/\partial t + \nabla \bullet (\rho\upsilon \otimes \upsilon) = B + \nabla \bullet \sigma$$

Where ρ is the fluid density, U is the fluid velocity vector, p is the pressure, t is the time and σ is the stress tensor. The relationship between the strains and stresses in a particular substance are given by a constitutive equation for that substance. For a Newtonian fluid the viscous stresses are directly proportional to the rates of strain, and the 3-dimensional stress tensor is given by:

$$\sigma = -\rho\delta + (\lambda - \frac{2}{3}\mu)\nabla \bullet \upsilon\delta + \mu(\nabla\upsilon + (\nabla\upsilon)^{\mathrm{T}})$$

the previous three equations are known as the Navier-Stokes equations. On the discretised flow domain, the Navier-Stokes equations take the form of a large system of nonlinear equations. Except for special cases, no closed-form solutions exist to the Navier-Stokes equations. The system of non-linear equations is typically solved by an iterative, Newton-like method, which in turn requires solving a large, sparse system of equations on each iterative step. That is, the values of all the variables (velocity, pressure, energy dissipation, etc.) are initially guessed. These values are then updated by feeding them back into the equations that one is trying to solve. If the updated values are the same as previous values (to a desired tolerance) the solution is said to have 'converged'. Otherwise, the iterative process is repeated, until convergence is achieved.

The biological materials in the both devices may subject to both tangential (shear) and normal stress. To represent the real flow intensity, the shear rate in this thesis was defined as the following, including the normal and tangential velocity gradients.

$$sstrnr = \left[2\left\{\left(\frac{\partial U_x}{\partial x}\right)^2 + \left(\frac{\partial U_y}{\partial y}\right)^2 + \left(\frac{\partial U_z}{\partial z}\right)^2\right\} + \left(\frac{\partial U_x}{\partial y} + \frac{\partial U_y}{\partial x}\right)^2 + \left(\frac{\partial U_x}{\partial z} - \frac{\partial U_z}{\partial x}\right)^2 + \left(\frac{\partial U_y}{\partial z} + \frac{\partial U_z}{\partial y}\right)^2\right]^{\frac{1}{2}}$$

Within the rotating disc device breakage is considered to happen within the area of the boundary layer. The energy dissipation rate within the boundary layer can be calculated by:

$$\varepsilon = sstrnr^2 \times \frac{\mu}{\rho}$$

2.4.2 Boundary conditions

Flow boundaries

At flow boundaries in the model, the fluid enters and leaves the flow domain. At inlets, the velocity, turbulent energy and turbulent energy dissipation are specified, and the pressure is extrapolated from downstream. Generally, the inlet velocity is known but the turbulent energy and energy dissipation are not known at the inlets.

Pressure boundaries

The constant pressure condition is used in situations where exact details of the flow distribution are unknown but the boundary values of pressure are known. At a pressure boundary, the fluid pressure is specified, and the velocity and turbulent scalars are extrapolated from upstream. The pressure at the outlet of the capillary was set to be the atmospheric pressure. In the rotating disc pressure on the wall was set at 0.

Wall Boundaries

The wall is the most common boundary encountered in confined fluid flow problems. The no slip condition (velocities perpendicular and normal to the wall are zero) is the appropriate condition for the velocity components at solid walls.

This condition was used both capillary and rotating disc device modelling for the liquid solid (wall) interfaces.

Density and viscosity

The density and viscosity of the protein solution was assumed to be the same as water. All capillary simulations were run using one liquid phase.

Initial conditions

The entire model geometry was initially set full of stagnant liquid. At the inlet boundary, the fluid velocity of the entering liquid was specified. The pressure was set to atmospheric pressure at the pressure boundary. For the rotating disc the rotational speed was set for three values 6500, 10000 and 15000 rpm.

CHAPTER 3

Protein Precipitate Breakage

3.1 Introduction

One of the objectives of this thesis is to understand the effect of different flow fields on a range of biomaterials, in scale down devices with working volumes of few millilitres or even less. In this chapter the break-up of microbial protein precipitate due to shear, when processed in two dedicated shear devices, was studied under conditions of controlled fluid stress. The goal was to translate the experimental results gained between two ultra scale-down shear generating devices, a rotating disc and a capillary one. In past studies flow conditions similar with the turbulent flow fields generated in processes such as the feed zone of industrial centrifuges (Boychyn et al., 2000; Manweiler and Hoare, 1992) have been successfully mimicked with the use of rotating disc ultra scale-down devices (in terms of local energy dissipation rate values). The first sections of this chapter where based on computational flow dynamics (CFD) simulations that were used in order to calculate the values of parameters such as energy dissipation rate in turbulent flow fields. Moreover a mapping of the flow field within the shear devices could be obtained giving a better insight in the understanding of the breakage of the protein precipitates. The need for experimentation with smaller material volumes led to the use of capillary devices in this study. Eventually the mimicking of an industrial scale operation using a device of very small working volume that will also be suitable for adaptation to robotic micro-well systems should be established. Microbial protein precipitate was chosen to be studied as a material which is of relevance to the bio-processing area, where the final scale of operation can be many thousands of litres. Furthermore, protein precipitate is a biological material that has been used extensively in a range of bioprocesses and whose properties are known and can be controlled during its preparation.

3.2 CFD calculations

CFD has many advantages over more traditional, experimentally based, design methods. The use of CFD can provide the designer with information about the physics of the problem to be solved, giving a complete and clear picture of the flow fields. From an experimental point of view, it is typically neither feasible, nor cost effective, to determine all the fluid flow parameters to the same detail provided by CFD. In addition a running CFD model can easily be manipulated. Improvements and changes concerning the geometry of a device and the manipulation of parameters such as flowrate and pressure can be made. Moreover the use of computational simulations can calculate values of flow induced parameters (such as shear stress, shear rates energy dissipation rates) that otherwise would be difficult to obtain in process (industrial) scale equipment. Mapping of flow fields can be made both for entire units or for more specified (local) areas of a process equipment i.e entrance zone of centrifuges. The ability to examine various hypothetical scenarios and cases, carrying out at the same time calculations on that base, makes CFD a powerful design tool.

The model used for the solution of the Navier-Stokes equations and the boundary conditions used in both geometries have been described in chapter 2. CFD was used so as to calculate certain parameters associated with high flow within our experimental devices. Maximum shear rate values were calculated for the whole domain of the devices.

3.2.1 Grid size convergence

A grid size convergence study was performed for the capillary model consisting of a 10 mm diameter upper chamber constricting to a 250 μm capillary. The k−ε turbulence model was used for all simulations in the capillary system due to the sharp restriction in the entrance area. The piston speed was termed as the inlet speed for the simulation and was set at 0.0242 m/s. Initial simulations were run using coarse grids, followed by simulations with progressively finer grids. Because the simulations were being run so as to determine wall shear strain

rates and turbulent energy dissipation rate, the convergence of these two parameters was monitored as the grid size was reduced. The flow properties converged to constant values using 10 micron grids or smaller. The 10 micron grids were used for all subsequent simulations since the speed chosen for the convergence was the highest used in experimentation followed.

3.2.2 CFD simulations for the capillary device

The capillary geometry that was modelled was chosen to be identical to the geometry of the laboratory shear device. All capillary systems consisted of a 1 mm diameter wide bore contracting into a 250 μm capillary where protein precipitate breakage was happening. Details of the capillary geometry are described in chapter 2.

In order ensure that the CFD simulations were giving meaningful results, the CFD predictions for the model were compared to analytical predictions. Analytical expressions were available for the pressure drops and strain rates within the system. Comparison of these predictions with the CFD results, are shown in Table 3.1. The simulated results matched the analytical results closely, showing that the CFD simulations were converging to realistic results. Furthermore, calculations of the Reynolds number using the average velocity values used during the experiments can be seen in Table 3.1.

The development of the boundary layer around the inner wall of the capillary can be observed by the simulation shown in figure 3.1 as well as 3.2. With increase of speed and thus Reynolds number, the thickness of the layer decreases. The boundary layer thickness measured via simulations (defined as the distance from the capillary wall at which the flow velocity is 99% of the freestream velocity) was 20, 18 and 15 μm for an increase of average flow speed from 18.4 to 24 and 36.8 m/s respectively. Other flow associated parameters used in the analysis of this chapter are shown in Table 3.1. Consequently the high shear volumes developed in the capillary will be 0.11, 0.22, 0.44 and 0.66 μL for an average flow velocity of 18.4 ms^{-1} and for increasing capillary lengths of 15, 30, 60, 90 mm respectively. For an average

flow velocity of 24 ms^{-1} the high shear volumes developed are 0.1, 0.2, 0.4.and 0.6 µL whereas for 36.8 ms^{-1} the corresponding high shear volumes are 0.086, 0.17, 0.33 and 0.52 µL.

Average flow velocity (m/s)	Reynolds number	Wall shear strain rate simulation (max) (s^{-1})
18.4	5170	$1.15*10^6$
24	6740	$1.53*10^6$
36.8	10300	$2.6*10^6$

Table 3.1: *Flow associated parameters calculated analytically and with the use of simulations. The parameters correspond with the flow experiments done with the use of the capillary ultra scale down devices.*

Validation of the results gained via simulations and the ones gained from using corresponding analytical equations was done by comparing the pressure drop values during flow in the capillary system as follows. The pressure drop can be divided between pressure drop in the entrance region and within the actual capillary. The entrance pressure drop was calculated by the following equation:

$$\Delta P_{entr} = 1/(C_D^2)\ (0.5\ \rho\ u^2)$$

C_D: Coefficient of discharge depending on Reynolds number and entrance geometry.

For a capillary with d=250 µm and Re = 5170 (u=18.4 m/s), the coefficient is C_D=0.7, and the calculated pressure drop is:

$$\Delta P_{entrance} = 365000\ Pa$$

In the case of turbulent flow the pressure drop within a capillary is given by:

$$\Delta P_{turb} = 2 f L \rho (u^2)/d$$

where $f = 0.0792 Re^{-1/4}$

In the following table the values gained via CFD simulation and analytical equations concerning pressure drop within the capillary matched to a satisfying degree.

Turbulent flow	**Pressure drop (Pa)**			
	Length			
Speed (m/s)	15mm	30mm	60mm	90mm
18.4	391000	781000	1560000	2340000
24	622000	1240000	2480000	3730000
36.8	1310000	2630000	5260000	
Simulation	Length			
Speed	15mm	30mm	60mm	90mm
18.4	382000	741000	1560000	2290000
24	612000	1180000	2320000	3670000
36.8	1280000	2570000	5150000	

Table 3.2: *Pressure drops occurring during flow in a 250 μm diameter capillary. These values were calculated both analytically and with simulation for the case of turbulent flows. The pressure drops for the different lengths of capillaries used are demonstrated.*

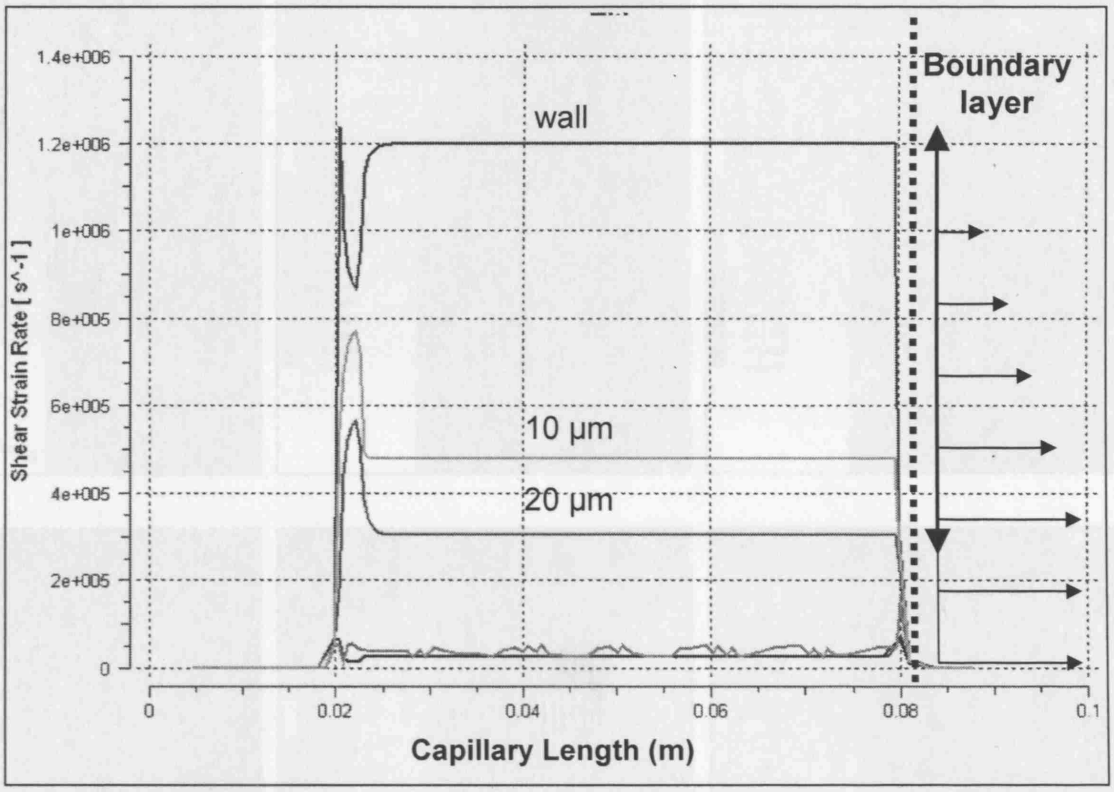

Figure 3.1: CFD Shear strain rate values calculated within the capillary, starting from the entrance until the outlet of the capillary. The local values of shear rate when moving from the capillary wall towards the centre radially, with a step of 10 µm are also shown in the graph. According to this simulation the boundary layer can be considered as having a thickness of 20 µm for the specific flow conditions. After that distance from the wall, there was a significant drop (>100 fold). The shear rate values shown in this simulation were gained for a 60 mm long capillary when water was flown with a velocity of the 18.4 m/s.

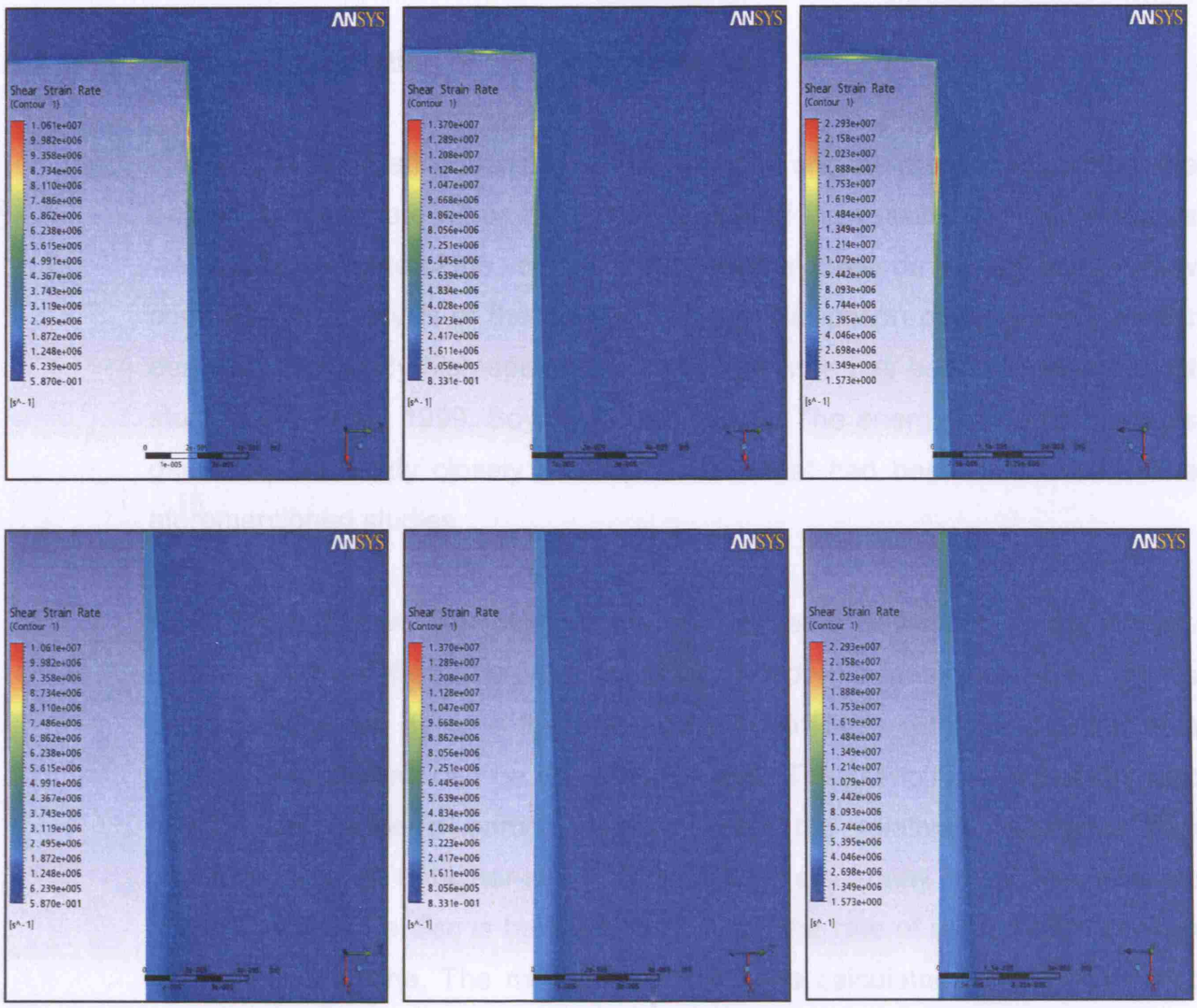

Figure 3.2: CFD simulations of the distribution of shear strain rate at the capillary entrance (first line of simulations) for the three flow speeds used in the experiments. There was a sharp contraction from a capillary with a diameter of 1 mm tubing to a 250 μm diameter capillary. The analytically calculated average flow speeds represented in these simulations are: 18.4, 24 and 36.8 m/s (from left to right). The second line of simulations shows the distribution of shear strain rates further downstream in the capillary from the capillary wall moving radially to its centre. The development of the different thickness boundary layers of the flows can be also observed (note the different scale bars on the simulations).

3.2.2 CFD simulation of rotating disc device

Flow within the rotating disc device was mapped and the energy dissipation rate and shear strain rate within the whole domain of the vessel were calculated as well as the estimate of the volume of the boundary layer developed in each flow condition. An analysis of the flow and energy dissipation patterns for a similar design to this study high-speed rotating-disc device has been reported in past study (Levy et al., 1999, Boychyn et al., 2001). The energy dissipation results gained in this study closely match the ones that had been calculated in the aforementioned studies.

From figure 3.3 we can observe the flow patterns developed in the device. Liquid is pumped from the tip of the disc towards the inner wall of the device being recirculated back to the disc again. A similarity with the function of a centrifuge feed zone can be observed as well. The pumping effect of the disc rotation will cause a particle to pass from the relatively low-shear bulk conditions through to higher-shear volume of the disc many times. The increase of the speed of the disc is believed to increase the rate of recirculation through the high-shear zone. The maximum shear rates calculated for the three disc speed used for the experimentation as well as the corresponding boundary layer thickness are shown in Table 3.2. Figure 3.4 shows the high shear area developed around the tip of the disc where we expect to have maximum energy dissipation, when the disc is rotated at 15,000 rpm (tip speed of 31.5 m/s). This area is calculated from the simulations and extended 120 μm from the disc surface. From the disc tip moving inwards towards the disc centre the high shear area was measured to be 200 μm. The total high shear volume consists of a volume of 0.235 ml. This measurement suggests that only 1.2 % of the total volume of the vessel can be considered as at high shear for such a disc speed. The values gained from the simulations correspond well with other boundary layer calculations for rotating discs done at the same disc speeds (Boychyn et al., 2001). Similarly the boundary layers for the rest of the rotating speeds were seen to be in the same range and match closely with the results gained from the CFD simulations. The high shear volume measured in the case of 6,500 and 10,000 rpm were 0.30 and 0.26 ml respectively.

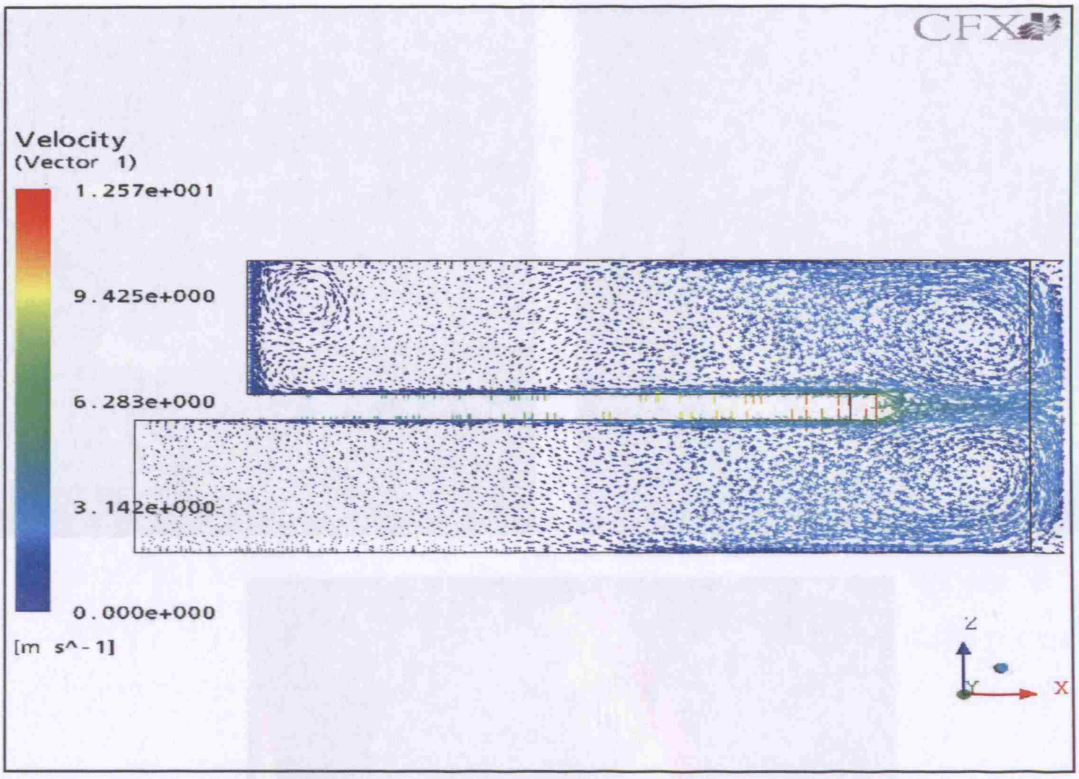

Figure 3.3: Mapping of the flow field and demonstration of the velocity vector distribution within the rotating disc shear device used for the experiments. This simulation image was gained for a rotating speed of 6.500 rpm.

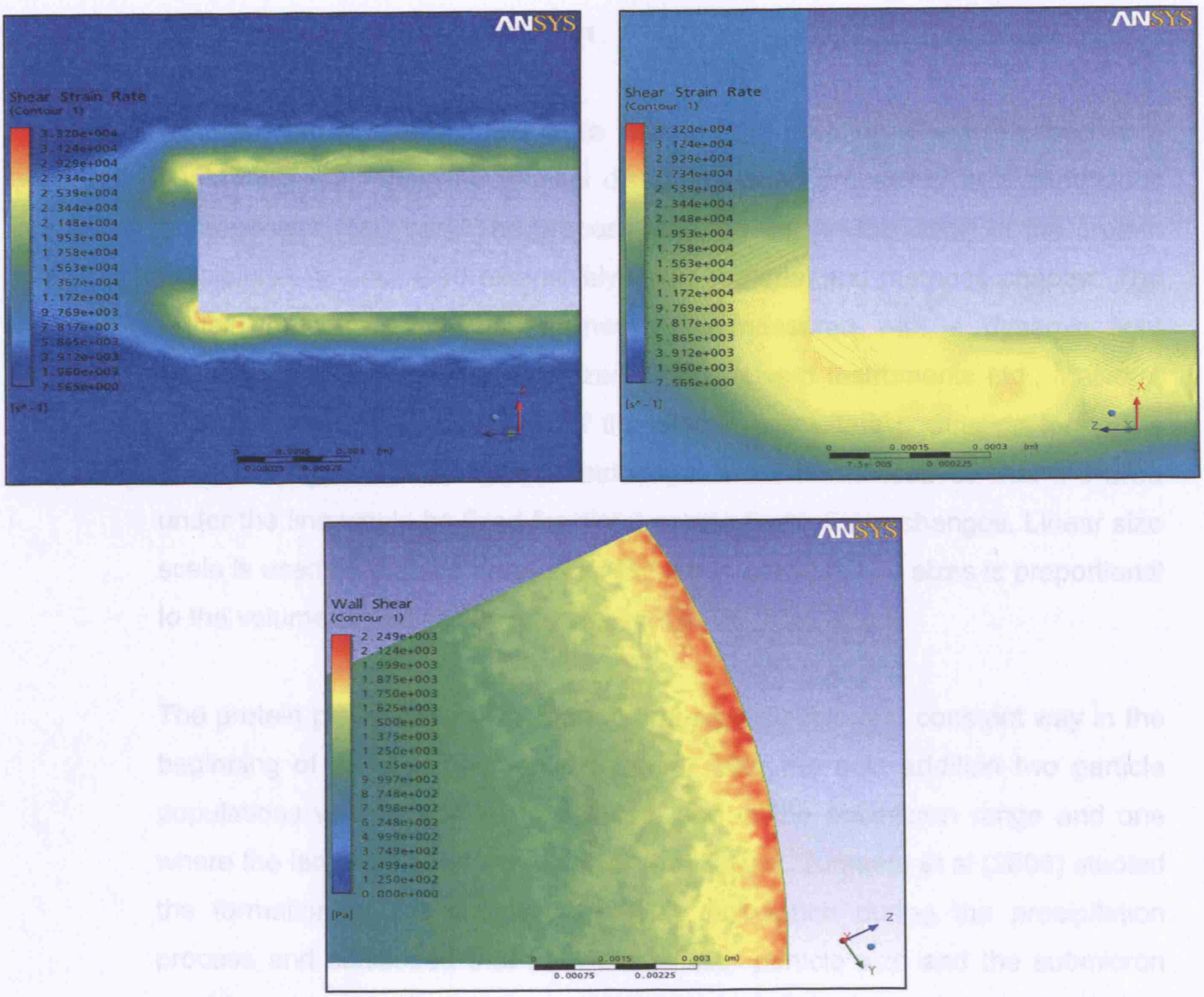

Figure 3.4: CFD simulation of the distribution of high shear strain rates around the tip of the disc of the rotating disc. The high shear strain rate area where energy is expected to be dissipated occupies ~ 1.5 % of the total volume of the vessel. The distribution around the disc is seen as part of the overall vessel volume (a) and in a more magnified case in (b). In (c) the distribution on the wall of the disc can be seen. These simulations will help in the determination of the volume which will be considered as 'high sheared volume'.

3.3 Protein precipitate formation

Microbial protein precipitates were formed from proteins which released from yeast cells after their mechanical disruption when processed in a continuous homogeniser (500 bar). The process followed for the formation of the protein precipitates is described extensively in the material and methods chapter. The protein precipitate particles formed were measured with a dynamic light scattering method using a Zetasizer 3000 (Malvern Instruments Ltd., Malvern, UK). A typical size distribution of the protein precipitate population formed is shown in figure 3.5. The size distributions were normalised so that the area under the line would be fixed for direct comparison of size changes. Linear size scale is used so that the area under the curve between two sizes is proportional to the volume of particles in that size range.

The protein precipitates were formed in a reproducible and constant way in the beginning of every experimental session. After the acid addition two particle populations were observed to develop, one in the submicron range and one where the larger particles ranged from 1 to 14 μm. Zumaeta et al (2006) studied the formation of the submicron particle population during the precipitation process and concluded that both the smaller particle size and the submicron particle production were due to the presence of hydrodynamic disruptive forces in the precipitation tank during the acid addition process. In fact, the higher the impeller speed during the precipitation process the bigger the population of submicron particles. The size distribution of the protein precipitates formed was measured to have a d_{10}=2.2 μm, d_{50}=4.7 μm, d_{90}=9.1 μm. These values correspond well with other experimental works were protein precipitates were formed with acid addition in stirred vessel (Zumaeta et al., 2005, 2006). The precipitate was left in the vessel for an ageing period of 10 minutes. During ageing, substantial particle size reduction usually occurs, but only when precipitates are subjected to shear-rates higher than those experienced during their initial formation. In any case most of the breakage that occurs during the ageing stage happens during the first 10 minutes of this process step (Brown and Glatz, 1987; Ayazi Shamlou et al., 1994, 1996 a,b). The precipitates formed for this experimental work were left exposed to shear conditions for 10 minutes.

The level of shear during the ageing period was smaller than the one during acid addition.

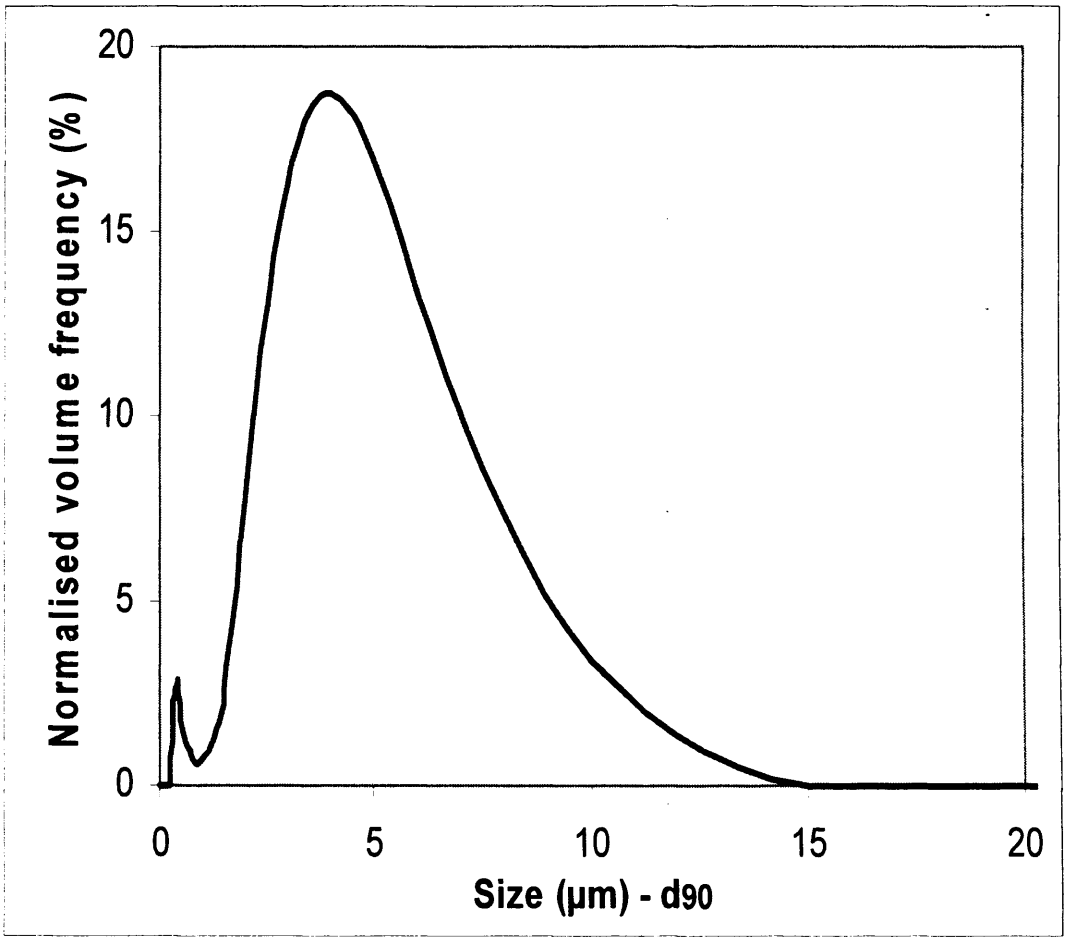

Figure 3.5: Normalised particle size distribution of the initial protein precipitate population that was used in shear experiments. The distribution of precipitates ranged between 1 and 14.5 µm. A minor population of submicron particles developed as well in the submicron size range, probably as a result of the ageing process. The protein precipitate population was aged for 10 minutes in the precipitation vessel.

3.4 Capillary experiments

Following the precipitation process, the aggregates formed were exposed to shear in order to study their breakage process. A capillary device was used for the processing of the precipitate suspension. The inner diameter of the capillary used was 250 μm. For the flow velocities used in the experiments through such a diameter it was possible to generate high shear rates (~10^6 s^{-1}) for the piston speed available. The shear rates generated in the experimental procedure were in the range of the shear rates that have been seen to develop in parts of bio-processing equipment. The effect of flow intensity and exposure time were investigated by recycling the particle solution for an increasing number of passes through a capillary for a range of flow speeds. Different lengths of capillaries were used for the experimental process. The lengths that were used in these experiments were 15, 30, 60 and 90 mm respectively. The sudden contraction was from a 1000 μm to a 250 μm capillary giving a contraction ratio of 0.25. The effect of shear conditions was determined by measuring the change of the particle size distributions as well as the change of the d_{90} value. The d_{90} value was chosen as a parameter to monitor the breakage since big particles in the population are expected to be more susceptible to shear and can be monitored better.

3.4.1 Effect of flow intensity

It was anticipated that the exposure of protein precipitates to shear stress would have an effect on the size of the initial population, with the magnitude of the effect being greatest at the higher shear rates. All flows were turbulent (Re > 5000) as shown previously in Table 3.3 and the precipitates were flown through the capillary with average speeds of 18.4 m/s, 24 m/s and 36.8 m/s. As expected, increased flow speed resulted in more extensive particle breakage. Breakage of the particles of the initial population produced smaller particles while at the same time an increase in the population of the submicron 'fine' particles was observed indicating another breakage phenomenon. The increase of flow rate had an increasing effect on the population of fine particles developed. The shift of the particle size distribution of the precipitate

populations to smaller sizes with increasing shear is demonstrated in figure 3.2. Figures 3.3a, 3.3b, 3.3c show the effect of increasing shear on the d_{90} value of the precipitate population when processed through different capillary lengths. It can be seen that for every flow condition and for a prolonged exposure a critical final particle size is reached, after which no further breakage occurs under the specific flow rate. The critical size reached depends on the magnitude of flow intensity. For increasing levels of shear, lower critical particle sizes and d_{90} values were reached. The breakage of particles during flow through pipes and capillaries, has been related to various parameters. For instance, Zumaeta et al (2005) correlated the breakage of whey protein precipitates with the turbulent energy dissipation rate (ε) found within a pipe, whereas shear rate and shear stresses have also been correlated with aggregate breakage.

3.4.2 Effect of exposure time

Particles were exposed to shear conditions within the capillary for a range of different time periods. In figure 3.7 the effect of increasing number of passes through a 60 mm long capillary on the particle size distribution of the unsheared population can be seen (for a velocity of 36.8 m/s). A shift towards smaller size particles as well as an increase of the 'fine' particle population can be seen. Major breakage is occurring in the first couple of passes through the capillary, with a reduction to the extent of breakage occurring as the number of passes increases. After eight passes no further breakage was observed for the precipitate particles for all flow conditions used during experimentation. Figures 3.8a, 3.8b illustrate the effect of increasing number of passes on the d_{90} size value when flown through a 30 mm and 60 mm long capillary. It can be clearly seen in all cases that after a certain exposure time to shear, in all experiments particle populations attain a critical d_{90} value after which no further breakage occurs for a specific flow intensity. When the flow velocity is increased, the time needed to reach the critical size is smaller. Similar concepts, of critical size reached after prolonged exposure to shear conditions, have been made for a range of different aggregate and floc systems. Zumaeta et al (2006) observed a 'threshold' size value for whey protein precipitate system after it was recirculated for a number of cycles through a 100 mm pipe.

3.4.3 Effect of length – continuous exposure time

An observation that can be made from the previous graphs is that the increase of capillary length, leads to a smaller difference between the critical d_{90} values obtained for increasing flow intensities. It can be seen that in the case of a 60 mm capillary (figure 3.8b) the final d_{90} values for the three flow rates are much closer than those in a 30 mm long capillary (figure 3.8a). It can be assumed that as the length of the capillary increases the increase of flow rate has less impact on the critical d_{90} size reached. In addition, figure 3.9 shows a comparison between two passes through a 30 mm and one pass through a 60 mm capillary. In the lower flow speed it seems that when exposed continuously in the longer capillary the breakage reached is higher than when a capillary is processed for the same amount of time in discrete passes. With the increase of flow speed, this difference become smaller until it seizes to exist for the same flow rate. The effect of 'continuous' exposure to shear seems to have an effect on the extent of breakage. For every flow speed it can be assumed that there exists a 'maximum critical size' obtained for a certain continuous amount of exposure time. This maximum critical size is not the same as the one attained when material is flown many equal exposure times through shorter capillaries for discrete passes. The increase of flow speed requires less exposure and thus shorter capillaries. This explains why in the case of the highest flow speed used the breakage was similar between two different length capillaries. One explanation for this behaviour could be the fact that the material re-entering a capillary after processing has a different shear history than one continuing to flow. A different structure rearranged by shear deformation might lead to particles that will be able to withstand more the experience shear fields. It has been shown that ageing of protein precipitate particles has a direct effect on the properties and especially on the stiffness of the formed particles (Bell and Dunnill, 1982; Titchener-Hooker and McIntosh, 1992).

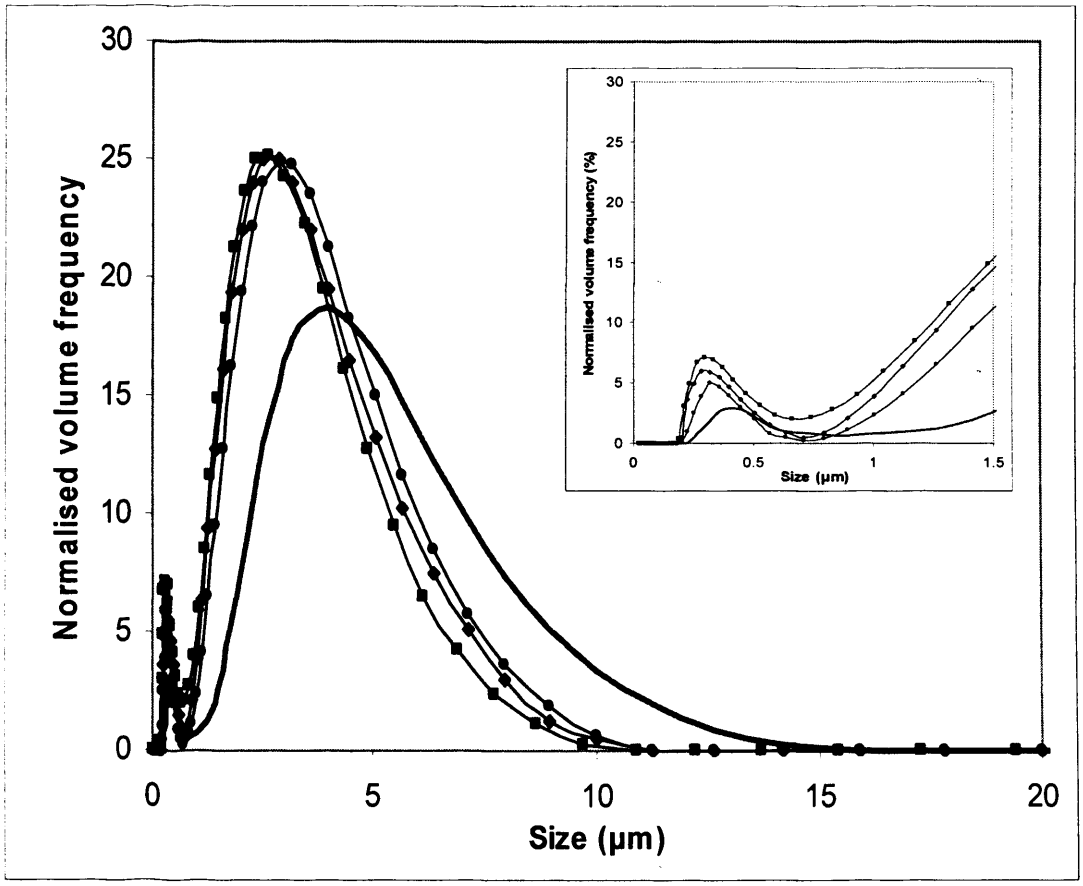

Figure 3.6: Effect of average flow speed on the size distribution of the precipitate population when processed for 1 pass through a 60 mm long capillary. The increase of flow rate is seen to have an effect on the larger precipitate particles. On the small graph on the upper right hand corner the increase of the population of submicron particles for increasing flow speed can be observed. The flow speeds studied were: 18.4m/s (●); 24m/s (♦); 36.8m/s (■).

		d_{10}		d_{50}		d_{90}
l = 1.5 mm						
(m/s)						
18.4		1.6		3.72		7.52
24		1.51		3.55		7.1
36.8		1.47		3.41		6.55
l = 3 mm						
(m/s)						
18.4		1.63		3.58		6.75
24		1.52		3.33		6.25
36.8		1.32		3.135		5.65
l = 6 mm						
(m/s)						
18.4		1.42		3.1		5.86
24		1.36		2.9		5.62
36.8		1.26		2.8		5.3
l = 9 mm						
18.4 m/s, 1 pass		1.3		2.92		5.35
36.8,m/s 1pass		1.23		2.76		5.13
Rotating disc						
(rpm)						
6500		1.51		3.17		5.52
10000		1.42		2.93		5.25
15000		1.39		2.86		5.1

Table 3.3: Critical d_{10}, d_{50}, d_{90} values of protein precipitate population. These values have been obtained after extensive processing through a capillary and rotating disc device. Under the particular flow field no further breakage is induced to the precipitate particles.

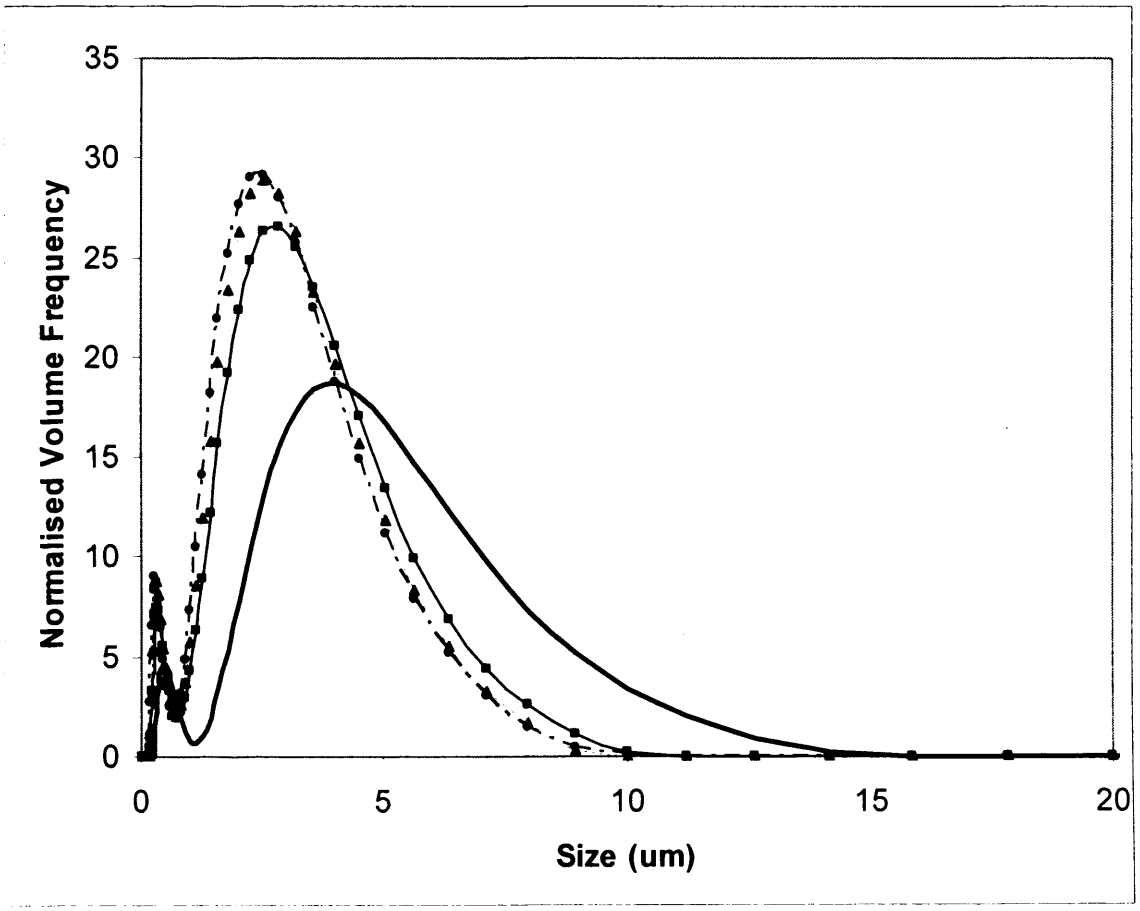

Figure 3.7: Effect of increasing number of passes on the initial size distribution (bold line) when the protein precipitate is processed through a 60 mm long capillary with an average speed of 36.8 m/s. The distributions shown in the graph are for: pass1 (■); pass2 (▲); pass4 (●).

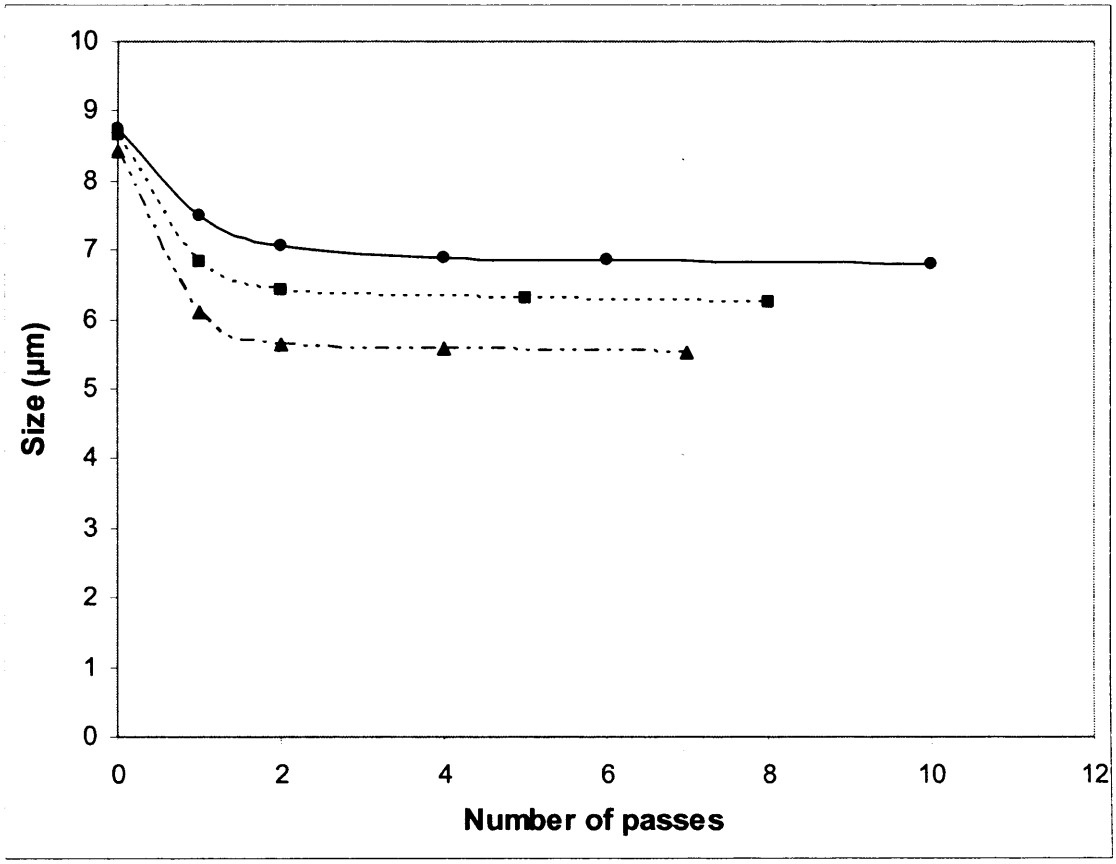

Figure 3.8a: Effect of flow through a 30 mm long capillary on the d_{90} value for three different speeds. The inner diameter of the capillary was 250 µm. After a number of passes no further effect on the d_{90} value of the population can be observed. It is considered that a final (critical) size of the particles under these conditions has been reached after which shear has no further effect on the size of the aggregates (d_{90} ± 0.09 µm). The average speeds with which the precipitate solution flows in the capillary are: 18.4m/s (●); 24m/s (■); 36.8m/s (▲). No considerable breakage is observed after 4 passes through the 250 µm capillary and the size distributions overlap for any further processing under this flow intensity.

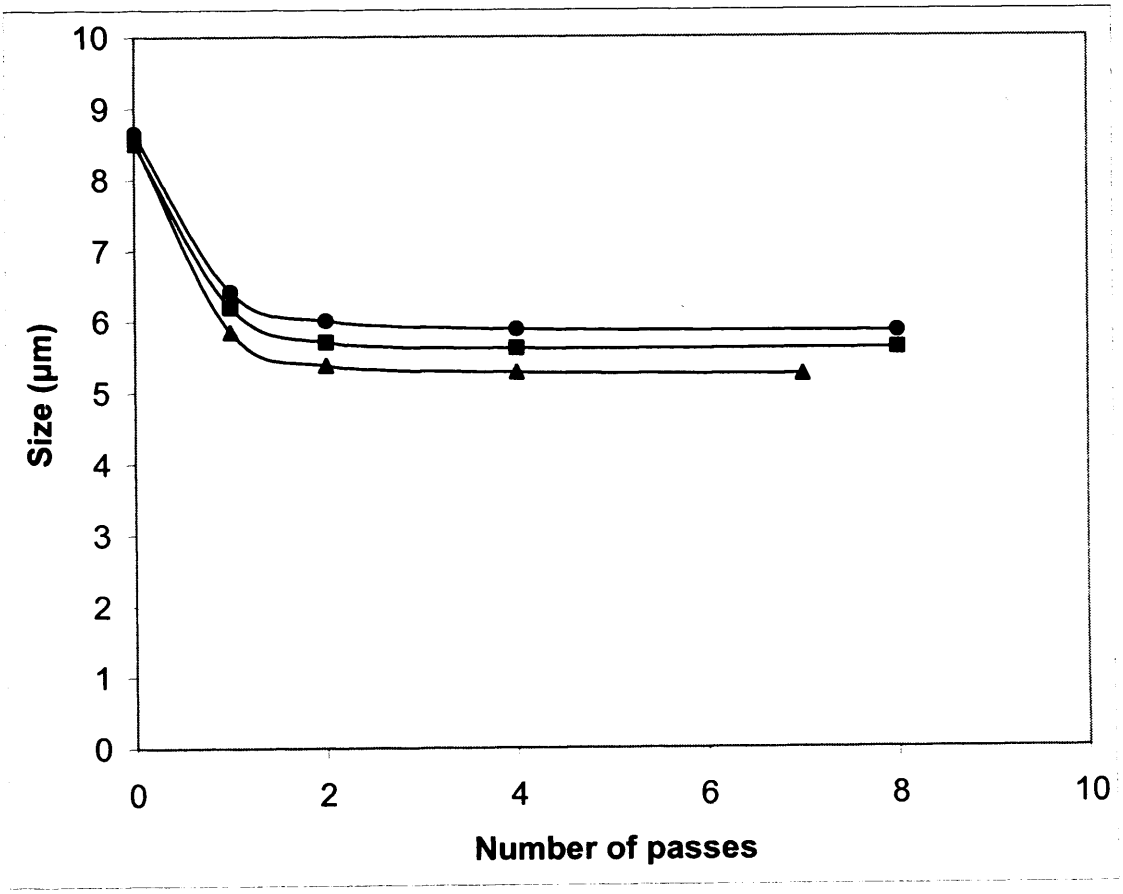

Figure 3.8b: Protein precipitate breakage as a function of number of passes through a 60 mm long capillary, for three different speeds. The average speeds are: 18.4 m/s, (●); 24 m/s, (■); 36.8 m/s, (▲). The inner diameter of the capillary was 250 µm. After a critical number of passes no further effect on the d_{90} can be observed and it is considered that final size of the particles under these conditions has been reached.

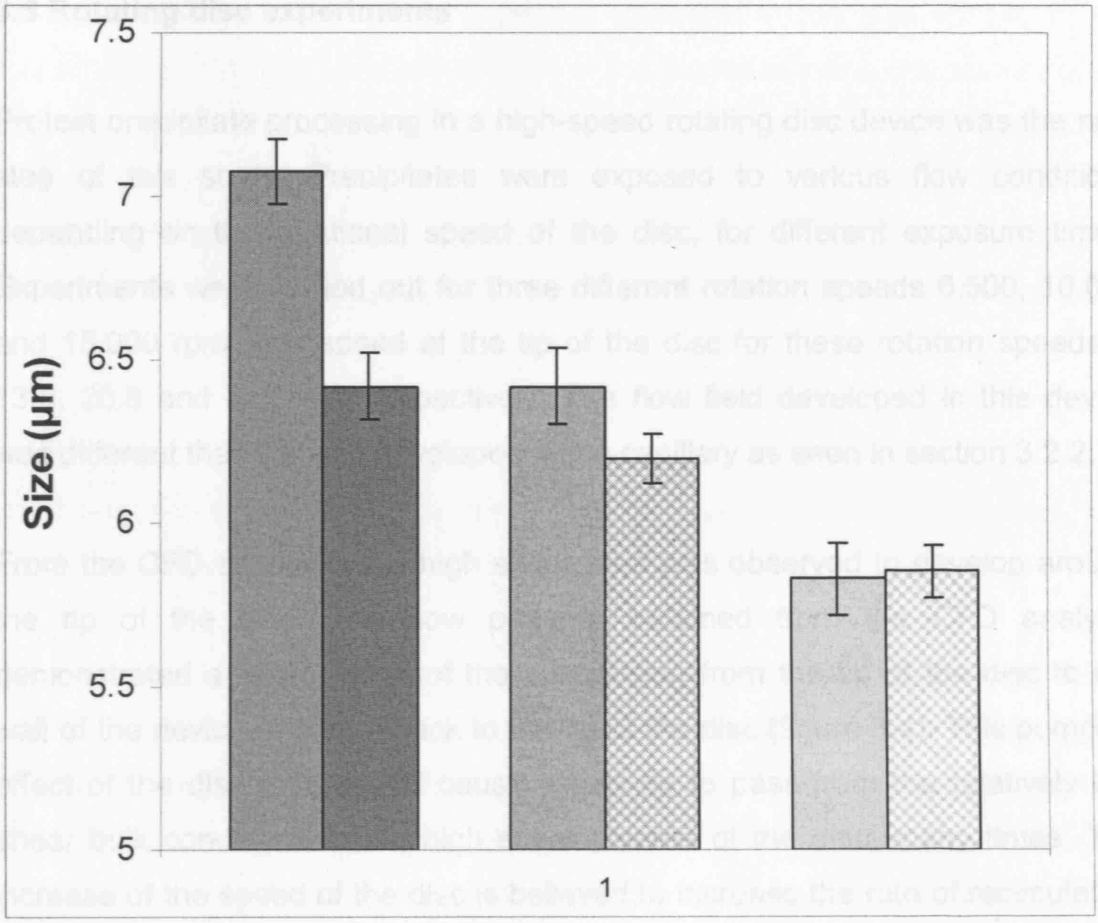

Figure 3.9: Effect of continuous exposure time to shear in capillaries for increasing shear rate, on the d_{90} value of the precipitate solutions. Each couple of columns represents the d_{90} value obtained after processing through a 250 µm capillary, for the same exposure time and flow rate. The sets of columns compare the d_{90} value after 1 pass through a 6cm capillary (dotted grey column) and 2 passes through a 3 cm capillary (solid column) for increasing flow rates. Flow rate increases moving to the right; 18.4 m/s for the first set, 24 m/s for the second set, 36.8 m/s for the last set of columns.

3.5 Rotating disc experiments

Protein precipitate processing in a high-speed rotating disc device was the next step of this study. Precipitates were exposed to various flow conditions depending on the rotational speed of the disc, for different exposure times. Experiments were carried out for three different rotation speeds 6.500, 10.000 and 15.000 rpm. The speed at the tip of the disc for these rotation speeds is 13.6, 20.8 and 31.3 m/s respectively. The flow field developed in this device was different than the one developed in the capillary as seen in section 3.2.2.

From the CFD simulations a high shear area was observed to develop around the tip of the disc. The flow patterns obtained from the CFD analysis demonstrated a recirculation of the suspension from the tip of the disc to the wall of the device and then back to the tip of the disc (figure 3.4). This pumping effect of the disc rotation will cause a particle to pass from the relatively low shear bulk conditions to the high shear volume of the disc, many times. The increase of the speed of the disc is believed to increase the rate of recirculation through the high-shear zone. Calculations of the size of the eddy length scale developed (Kolmogorov's length) due to turbulence and dissipation of energy, showed that particle breakage was due to precipitate–eddy interactions and the subsequent turbulent stresses developed. So it was assumed that all the particle breakage was occurring on the boundary layer developing on the solid-liquid interface around the disc surface and especially around the tip of the disc, where the velocity is expected to be at its highest. Considering that the size of the precipitate particles was of the order of 15 μm and the boundary layer thickness was of the order of 200 μm, it can be assumed in fact that the breakage of the particles occurs only by fluid stresses in the boundary layer.

Figure 3.10 shows the size distribution of the precipitated particles before and after shearing for increasing exposure times when the rotational speed of the disc is 10.000 rpm. The shift in the size distribution towards smaller particles which can be observed in this graph is indicative of particle breakage. Eventually particle breakage stops occurring for a specific rotational speed and a (plateau) critical particle size is reached (figure 3.11). In this graph it can be

seen that the majority of the breakage happens in the first minute of the experimental run. After a sharp decline of the d_{90} value in the first minute of the process, there follows a period where breakage is still occurring but in less intense levels until it stops. The critical size reached is dependant on the flow intensity within the vessel. For all flow intensities within one minute of processing 90% of the breakage had already occurred. The critical sizes reached are shown for all flow conditions in Table 3.2. The effect of retention time in the shear device on the particle size distribution of the protein precipitates can be observed in graph in figure 3.10. Figure 3.11 further demonstrates that when the rotational speed is increased the critical size reached is smaller.

Even in experiments involving agitated vessels that were done at much lower energy dissipation rates, the breakage of precipitates was found to have time dependent properties (Ayazi Shamlou, Stavrinides, Titchener-Hooker & Hoare, 1994). The time dependency trends in figure 3.11 are consistent with previous observations of stable size distributions reached more rapidly at higher imposed flow stresses for protein precipitates in stirred vessels for protein precipitates (Boychyn et al., 2001; Ayazi Shamlou et al., 1994). The formation of a 'fine' particle population in the sub-micron size range can be observed during precipitate breakage.

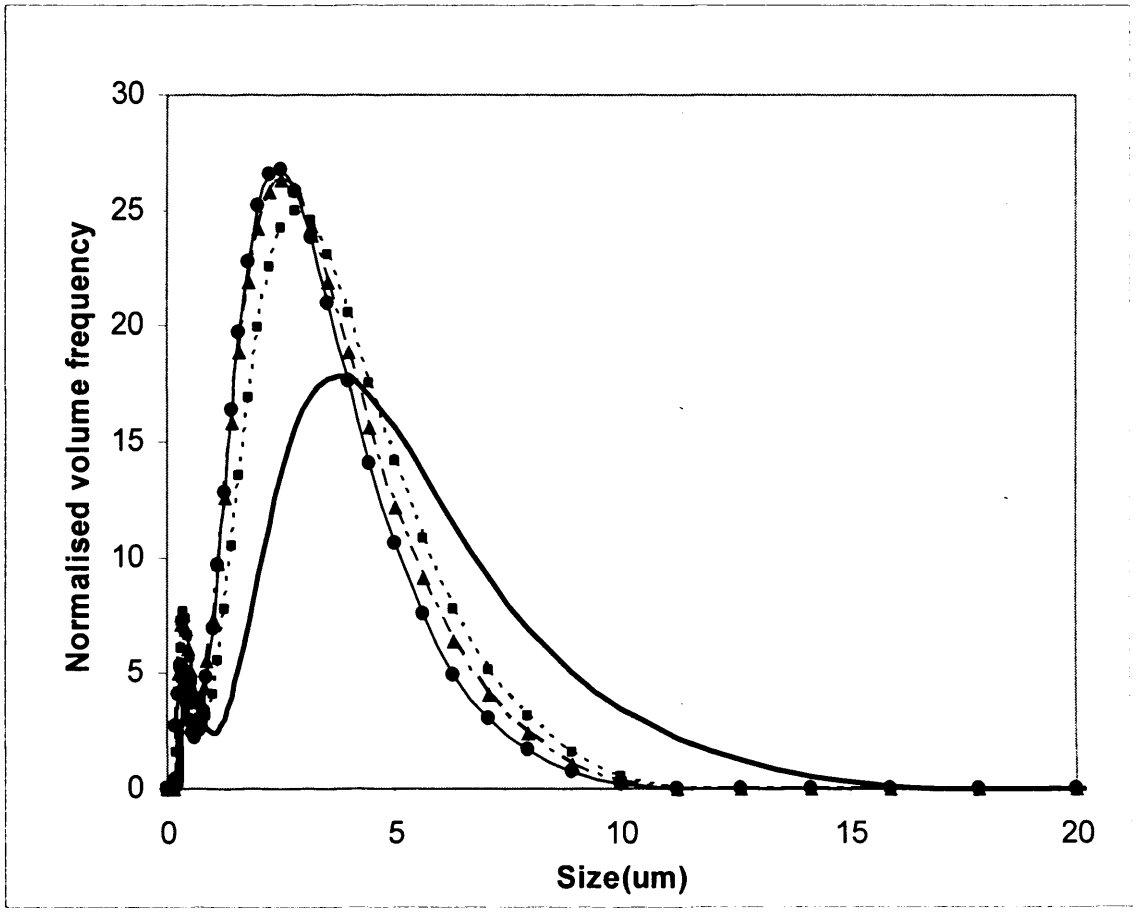

Figure 3.10: Effect of retention time of the protein precipitate in the rotating disc device for a fixed angular speed of 10,000 rpm, on the particle size distribution. The retention time of the material is: 1 min, (■); 8 min, (▲); 15 min, (●). The continuous line is the initial distribution of the material before process. With increasing the retention time within the device, particles move to smaller size distributions.

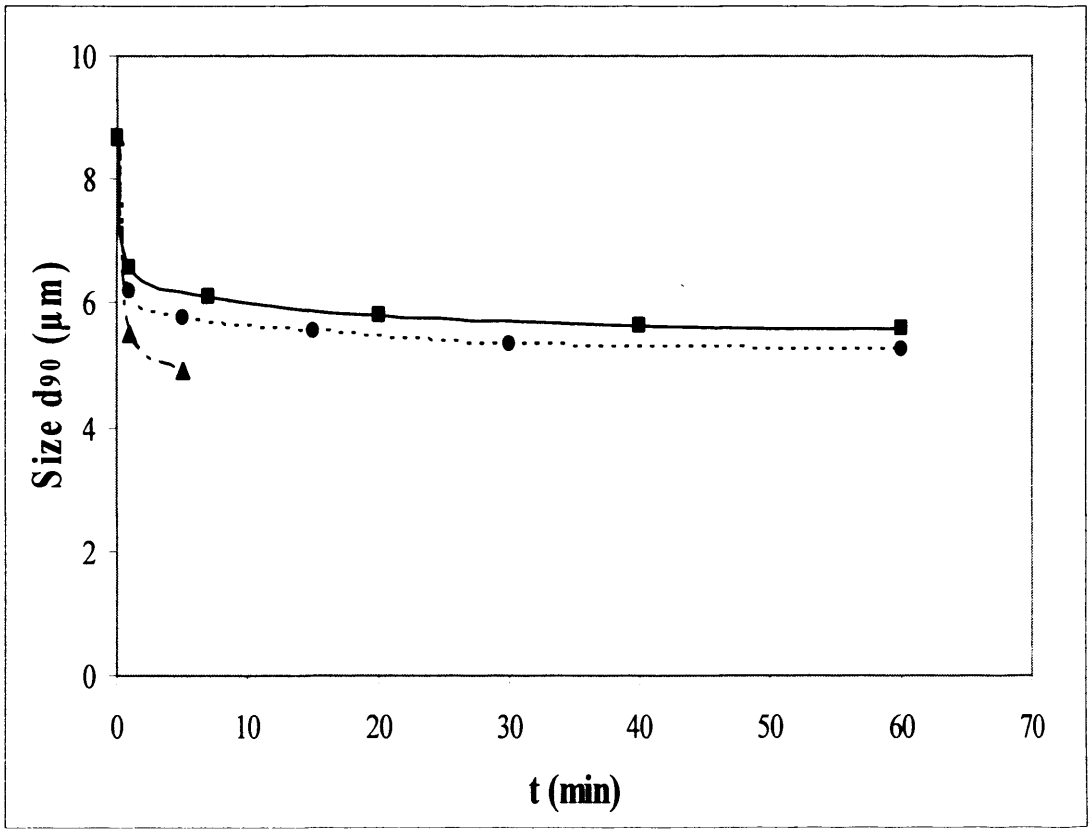

Figure 3.11: Effect of retention time in the rotating disc shear device on the size (d_{90}) of the particle size distribution. The precipitate suspension was processed with three different rotating speeds. The speeds used in the experiment are: 6.500 rpm, (■); 10.000 rpm (●); 15.000 rpm (▲). In the case of the highest rotational speed the experiment had to be stopped due to temperature rise.

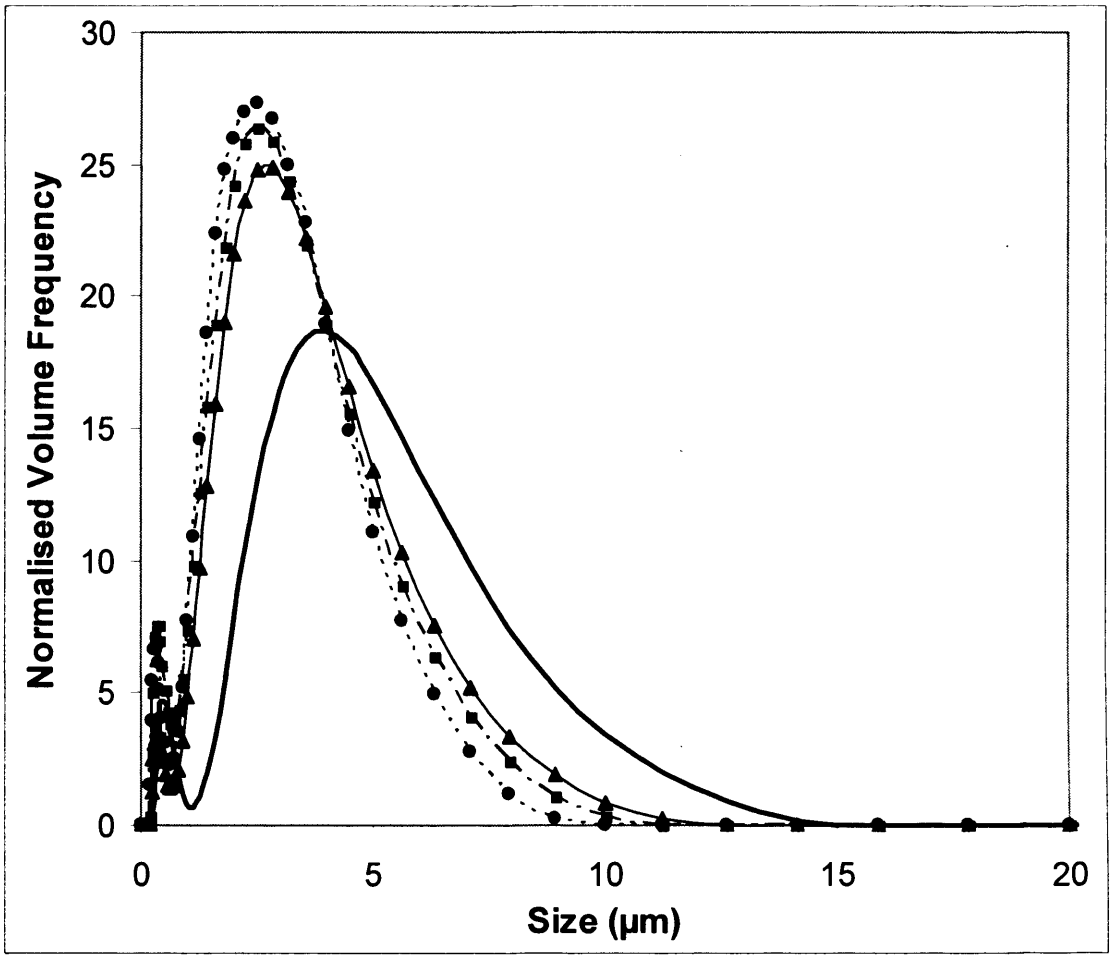

Figure 3.12: Protein precipitate breakage as a function of angular velocity of the rotating disc within the shear device. The angular velocities are: 6,500rpm, (▲); 10,000rpm, (■); 15,000rpm, (●); the continuous line is the initial distribution of the material before the process. For all three experiments the precipitate suspension was processed for 10 minutes.

3.6 Comparison of the two USD devices

The comparison between the results gained up to now in the capillary and the rotating disc devices and an effort towards correlating them will be the focus of this section. Breakage was assumed to happen in both devices within the boundary layer developed in the solid-liquid interface during flow. In figure 3.13 size distributions gained after exposure to shear in the two different devices for different flow conditions are demonstrated. It can be observed that the size distributions gained after exposure to shear in the two devices closely resembled. The conditions for the matching of the particle size distributions shown is random and the issue of concern is if a more holistic approach was possible in order to compare the size distributions of one device with the other. In previous sections of this chapter it was seen that when precipitate particles were exposed sufficiently long to shear conditions a critical size would be reached. This size depended on the intensity of the flow as well ie the velocity with which particles were flown through the capillary and the rotational speed of the disc and the shear rates generated in this processes. For this reason a further experiment was carried out with the use of an even longer capillary. A 90 mm capillary was used in order to further increase the continuous exposure of the precipitate suspension to the shear conditions.

It was assumed that breakage occurred only within the volumes where maximum shear rate was generated. Experimental data of the critical d_{90} sizes gained from all flow conditions of both devices, was correlated with the product of the maximum shear rate and high shear volume as calculated with the CFD simulation (figure 3.14). From this graph it can be observed that by controlling characteristic parameters (ie length) of the capillary device the effect of shear gained with the rotating disc device could be simulated (mimicked). In particular the use of longer capillaries ie 90 mm which provided higher exposure time to shear conditions provides critical d_{90} values resembling the ones gained in the rotating disc device.

A fundamental difference between the two systems was the discrete processing of the capillary device and the continuous processing in the rotating disc device.

As described in the case of experiments with the capillary device the precipitates were left in a stationary face after sample collection and before reprocessing. On the other hand during the continuous processing in the rotating disc device, the material never remained in a static environment due to its recirculation through the high shear zone while flowing in a mixed environment in the meantime. This might have an impact in the nature of the particles processed in each case. In order to mimic (approach) the effect of flow (shear) in the rotating disc device with a capillary one, a sufficiently long capillary that would provide the necessary exposure time and high shear volume in order to reach the minimum critical size for each flow condition.

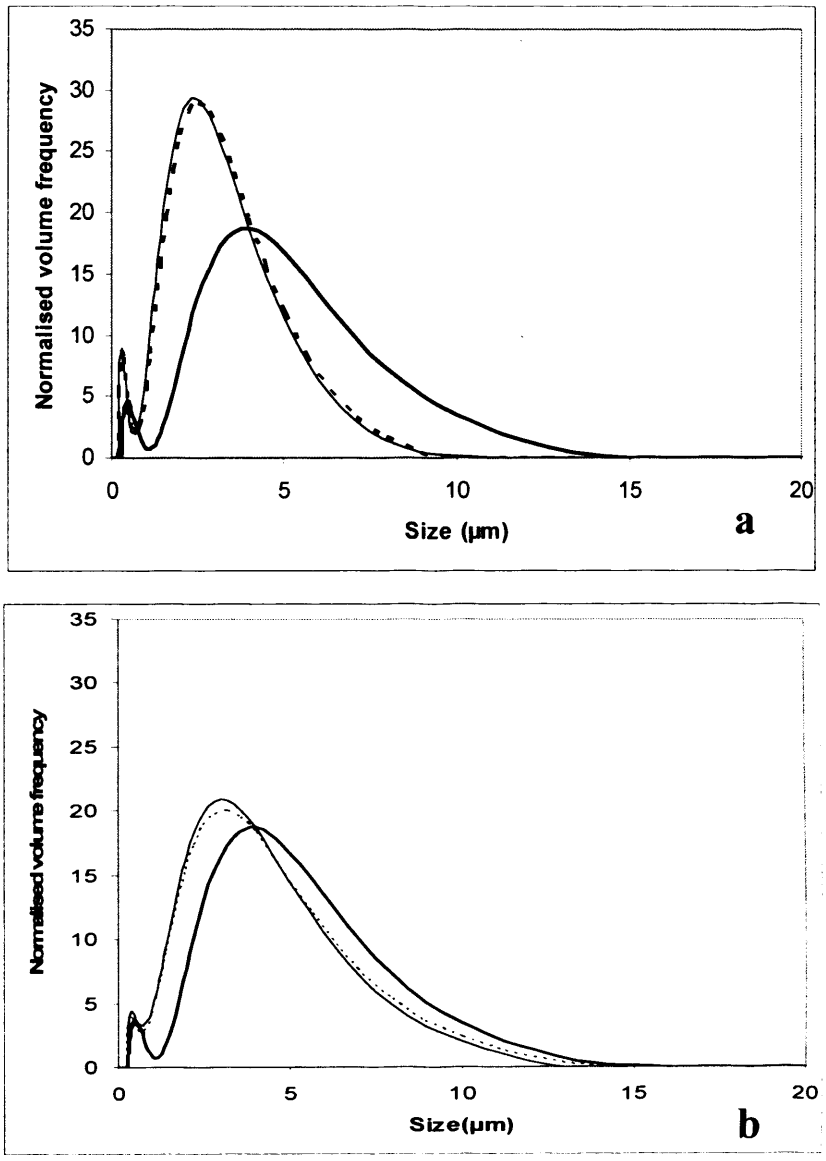

Figure 3.13: Effect of method of application of shear on the initial size distribution for a combination of different processing parameters. The dashed line represents the size distribution of precipitates when processed through a 60 mm long capillary device with a velocity of 36.8 m/s (t=0.0032 s); the continuous line represents results gained in the rotating disc device when the particles were processed with a rotational speed of 10,000 rpm for a retention time of 15 min. The same is represented in figure 3.13b but for different flow conditions. The precipitate suspension was exposed to the following conditions: capillary device l=30 mm for 24 m/s (t=0.005 s) while the processing conditions in the rotating disc were 6500 rpm for a retention time of t=5min.

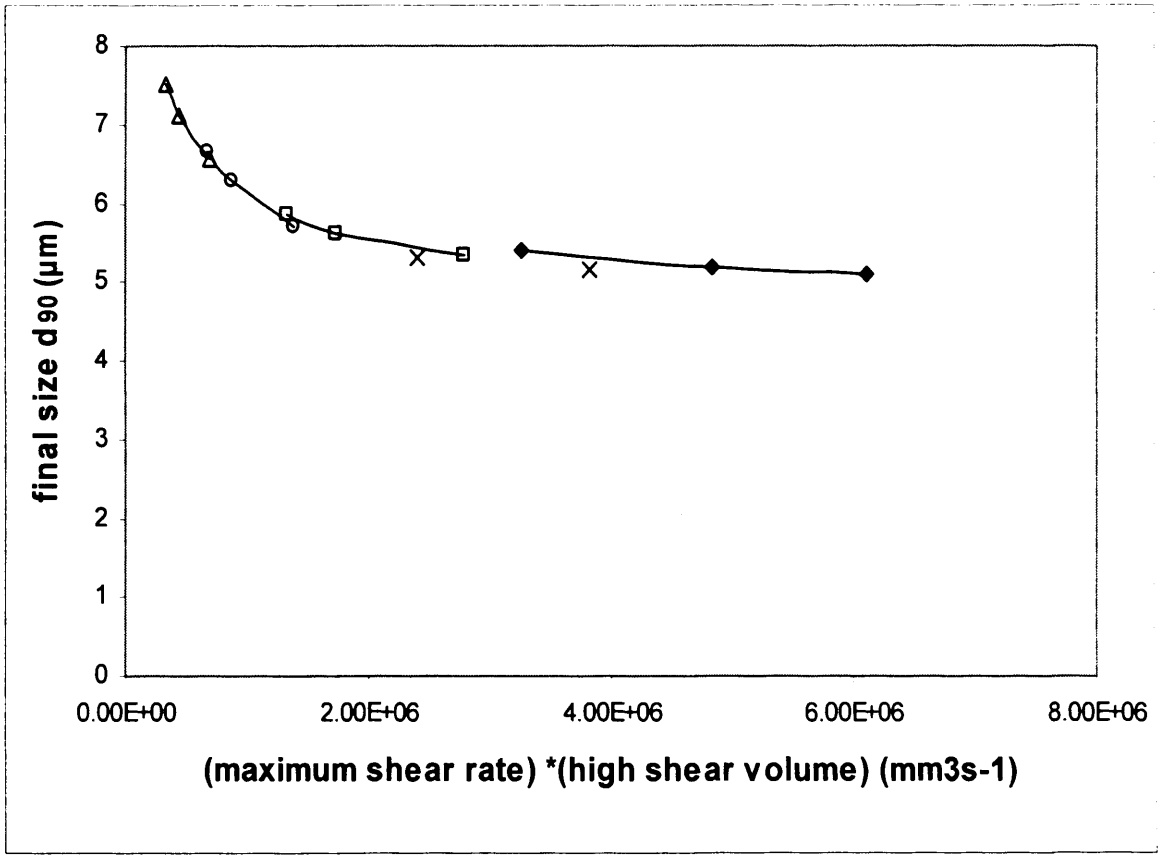

Figure 3.14: Correlation between the final d_{90} size reached for all flow conditions in both devices and the product of the maximum shear rate and the volume of the boundary layer in each device and flow condition. 15 mm (Δ); 30 mm (○); 60 mm (□); 90 mm (x); rotating disc device (♦).

3.7 Discussion

In the analysis of the experimental results that was followed in this work, the parameter for monitoring the breakage of the particles was the d_{90} size value This was done in order to monitor the breakage of the larger particles of the population which we expected that would be more prone to shear-induced breakage.

3.7.1 Mechanism of breakage in both devices importance of continuous exposure time in capillary device

The disruption process of aggregates during flow is not yet clear and well understood. There are different approaches and explanations concerning the mechanism of breakage. One explanation would be that the process of breakage would follow a pattern where very small particles are continuously removed from the parent particle (Ayazi Shamlou et al., 1996; Biscans et al., 1996). In this work a significant change of the particle size distribution in short exposure times was observed. This does not support the explanation of small particles being removed continuously from a large parent-particle. In a related work it was seen that as turbulence in a pipe flow increased, the population of the 'fines' was firstly generated (no generation at low turbulence) and further increased, whereas at low levels of turbulence there was no observation of such population (Zumaeta et al., 2006). The levels of turbulence and energy dissipation in this work were much higher and the diameter of the capillary used was much smaller (250 μm in respect to 3 mm) thus explaining the higher population of fine particles developed. The results gained from the capillary experiments in this work, suggest that the parent particles are disrupted to comparable size (to the unsheared particles) particles and to others of very small diameter (submicron range). There is a possibility that more than one mechanism might take part during the breakage process of flowing particle suspensions. Finally it must be mentioned that the fragments resulting from particle breakage have been shown to be a weak function of shear (Bell & Dunnill, 1982).

3.7.2 Mimics of process unit operations

It has been seen that during many industrial applications short term exposure to intense levels of shear, such as in a centrifugal pump or upon entering the feed zone of a disc stack centrifuge, are primarily responsible for further particle breakage rather than the less intense turbulent flow in pipes or in the centrifuge bowl (Bell & Dunnill, 1982). This has also been demonstrated for a multichamber-bowl centrifuge (Boychyn, Bulmer, More & Hoare, 2000). The mimic of the effect of such flow conditions with the use of different geometry equipment was the target of this work and for this reason in both ultra-scale down process equipment. In order to achieve this, the exposure of particles to flow fields with high shear regions for short time intervals was necessary. Shear rates of the order of 10^5 s^{-1} and times of exposure to between 0.004 and 0.2 s were chosen as being typical of the feed zones of high speed centrifuges (Bell & Dunnill, 1982). It has been seen, that the increase of the number of passes through high shear areas in different configurations has an impact on the size of the resulting particle populations. Such observations agree with the results gained from this work. In both devices the increase of exposure time led to more extensive breakage and eventually a critical value was reached for the particle size.

CHAPTER 4

Embryoid Body Breakage

4.1 Introduction

Research into the breakage of the EBs in a controlled shear environment is described in this chapter. This research consisted in processing the EBs through a capillary system. An experimental model was constructed describing the breakage of the EBs to give a better insight of the breakage process and the engineering properties of the EB. The decrease in size of the embryoid bodies and the resultant viability of the released cells, under a range of flow conditions, were the parameters monitored throughout the experimental procedure. The standard method used for the dissociation of embryoid bodies in cell culture currently consists in their exposure to a concentrated solution of trypsin (an enzyme found in the digestive system used for the break-down of proteins in amino acids) for several (5-10) minutes, followed by a manual trituration process. Trypsin is known to increase the possibility of karyotypic changes and genetic abnormalities on the cells (Maitra et al, 2005; Draper et al., 2004). The capillary shear method provides a means for the dissociation of EBs and single cell release as a first step for an automated procedure which avoids the use of added reagents.

4.3 Brief summary of results

The first objective of the experimental work was to prepare an EB suspension in a repetitive and constant manner. The protocol followed should at the end of the procedure give a constant size distribution of the EB population after every eight day culture. Control experiments were carried out in order to identify which part of the capillary system was responsible for the breakage of the EBs. Normalised size distributions were used so that the area under the line would be fixed for the direct comparison of size changes of the EB population. Linear size scale is

used so that the area under the curve between two sizes is proportional to the volume of particles in that size range.

The suspension of the EBs was pumped through capillaries with different diameters and lengths at varying flow rates. It was seen that the breakage was occurring within the capillary throughout the whole length and was thus correlated with parameters such as the average flow velocity and exposure time to shear conditions. The viability of the released cells was another parameter that was monitored since the release of neuron precursor stem cells was one of the targets in this experimental work. It was seen that the release cells were only 55% viable in contrast to those obtained by trypsin (90%) while the viability of the released cells was not affected by continued high shear in the capillary.

4.3 Control experiments

The first experiments were designed with the aim of standardizing the preparation of the EBs and to define the conditions under which the remaining part of the experimental process should be conducted afterwards. Samples were collected immediately after processing and the size distribution was measured in a laser light-scattering device.

4.3.1 Control I: standardization of initial population

The formation of the EBs took place in a static culture system in 20 mL Petri dishes. EBs were grown for 8 days according to a protocol that induced differentiation in the neuronal pathway under the effect of retinoic acid. Retinoic acid was added on day 4 of the culture (see Material and Methods chapter). The size distribution of the EB population on day 8 was measured for 4 different cultures in order to see whether the size range of the EBs that was obtained on day 8 was consistent and in agreement with other experimental data given in literature. It was observed that during growth the size of the aggregates increased and the structure of the EBs changed from an initial loose cell aggregate to a more structured organisation (figure 4.1).

Figure 4.2 shows the size distributions measured for the EB populations. A satisfactory consistency in the distributions was seen and the average of the four populations was obtained and used in further experiments as the starting EB population (this is the population before processing). In Table 1 the values of the d_{10}, d_{50}, d_{90} of the populations are shown. The d_{90} value is the value of size that is bigger than 90% of the population of the aggregates in the measured population. The same applies for the d_{10} and d_{50} values. The size distribution of the EBs obtained can be considered as a rather wide distribution. This is probably due to the fact that a static culture protocol was followed. It has been seen that in static culture, aggregation between already formed EBs occurs in addition from cells aggregating with each other; this is due to extra cellular matrix (E-cadherin molecules) that adhere EBs together (Dang et al., 2004). As ES cells concentration increases the possibility of EB aggregation also increases. A 'conditioning' and a better control of the size distribution of the EBs could be achieved with the use of shaker flask cultures (Dang et al., 2001) or in stirred tank cultures (Cameron et al., 2006; Fok and Zandstra, 2005). It has been previously reported that murine embryonic stem cell aggregates that have been cultured for 9 days in stirred tanks, may even reach sizes of 1000 μm (Fok and Zandstra, 2005). Due to nutrient and oxygen transfer limitations to the inner part of the EB there is a possibility that a necrotic centre might be formed due to these limitations in large aggregates (diameter>600 μm) (Sen et al., 2001). In this research the biggest EBs formed were smaller than the one required for a necrotic centre to develop.

Sample	d_{10} (μm)	d_{50} (μm)	d_{90} (μm)
1	229	360	532
2	213	372	564
3	202	378	573
4	190	377	524

Table 4.1: *The values of d_{10}, d_{50}, d_{90} parameters, for the population of the EBs on day 8 of their culture. The size distribution was measured with a laser diffraction method. The average value of these measurements was used as the initial size value for the EBs before processing.*

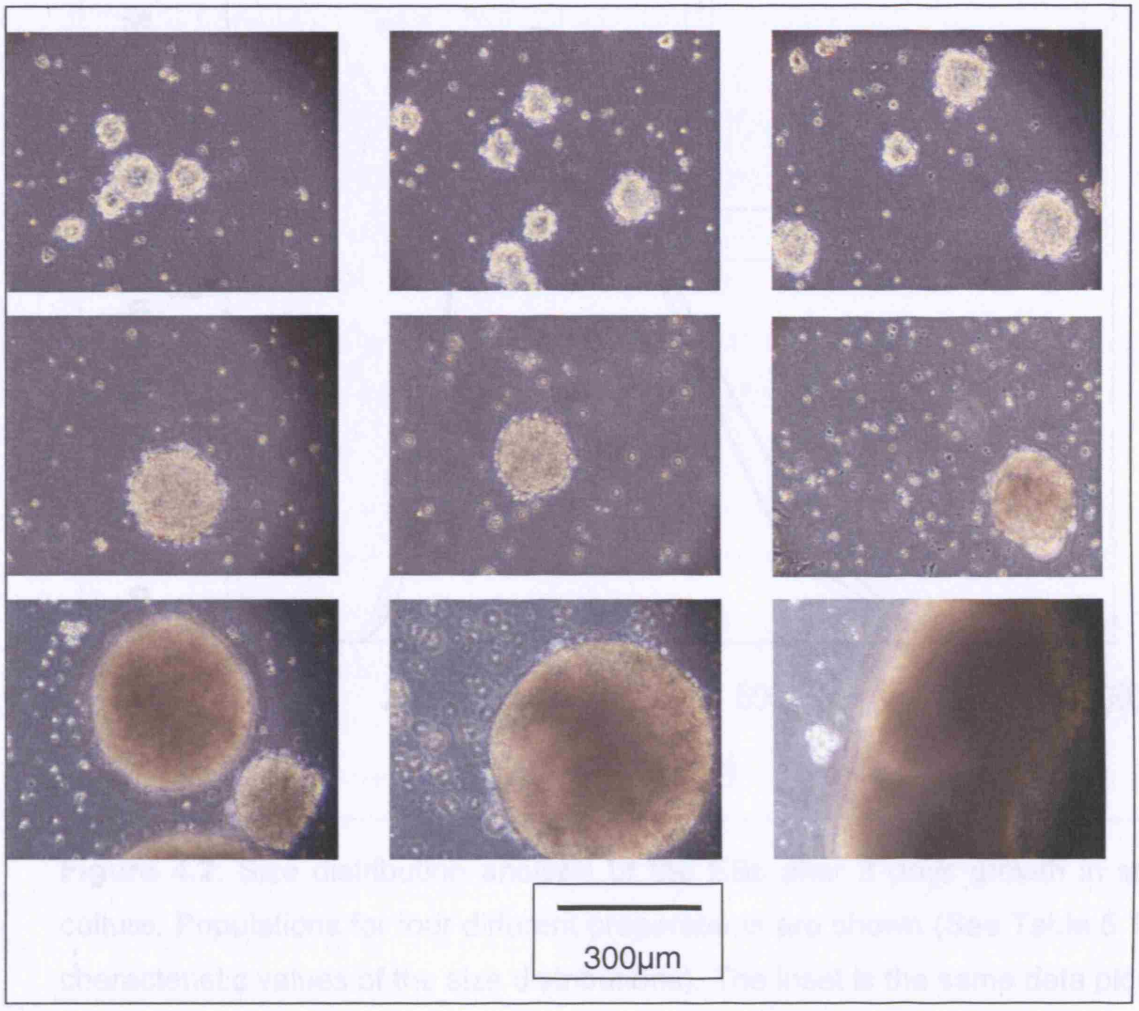

Figure 4.1: Optical observation of the growth of EBs over a time period of 8 days. The first line shows day 2 EBs where tendency for EB – EB aggregation between can be seen. The second line shows day 4 EBs where a more organised structure of the EBs starts developing. The third line shows fully grown EBs on day 8. For each stage of the EB development three representative pictures are shown.

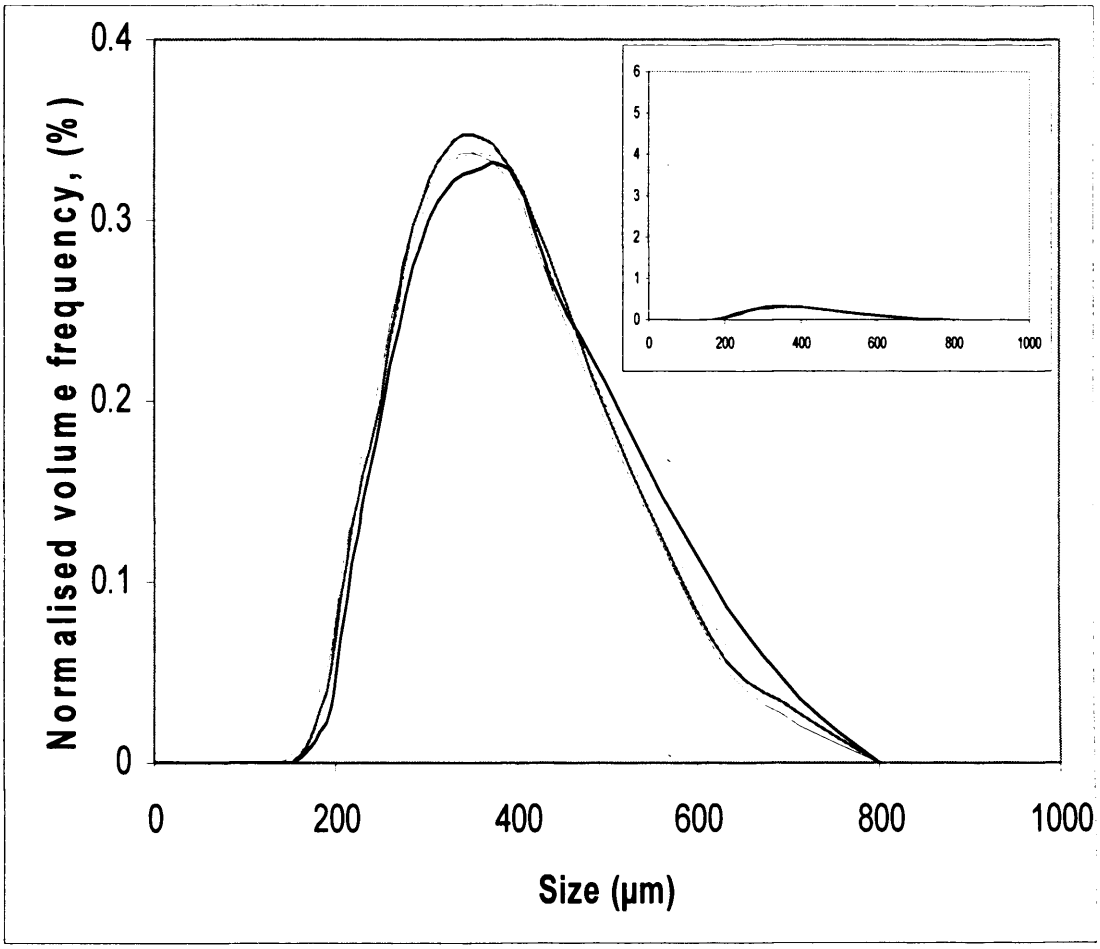

Figure 4.2: Size distribution analysis of the EBs after 8 days growth in static culture. Populations for four different preparations are shown (See Table 5.1 for characteristic values of the size distributions). The inset is the same data plotted with the y-axis on a scale used on figures later-on so as to help comparison.

4.3.2 Control II: Young's modulus

Young's modulus (also known as modulus of elasticity, elastic modulus or tensile modulus) is a measure of the stiffness of a given material. It is defined as the ratio, for small strains, of the rate of change of stress with strain. This can be experimentally determined from the slope of a stress-strain curve created during tensile tests conducted on a sample of the material. AFM was used in order to measure the Young's modulus of the EBs. In the first experiment measurements were made in order to monitor the stiffness of the EB during its growth (figure 4.3b) and it was seen that over the time of culture there was a substantial increase in the Young's modulus. This is in agreement with the belief that over time, the EB develops from a loose aggregate of cells to a more organised, structured and more densely packed cell formation, as was described in the previous chapter, imitating the early embryogenesis stages. A second measurement was made in a population of fully grown, day 8 EBs in order to see whether the size of an EB would affect its inner stiffness. In figure 4.3a the Young's modulus of different size EBs, on day 8 of their growth (representatively chosen out of the total population), was measured. No particular trend was observed. It is most likely that the EBs had similar Young's moduli independent of their size when referring to EBs of the same day of development.

For the experiments following in this chapter, it was assumed that all the day 8 EBs in the population had the same Young's modulus. The behaviour of the EBs under shear conditions and their susceptibility to breakage was considered to be the same for all the EBs of the initial population.

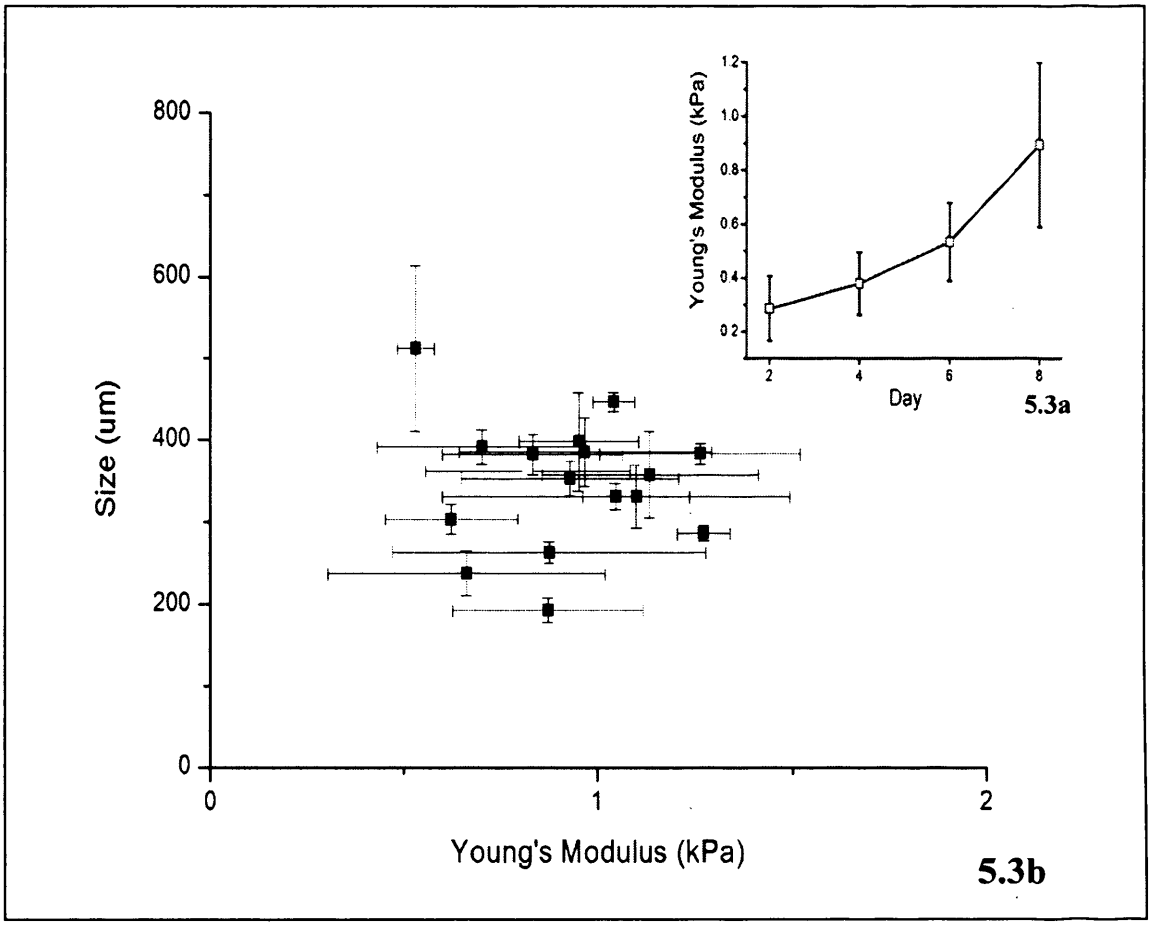

Figure 4.3: The Young's modulus of the EBs on different days of their development is demonstrated in 5.3a. It can be seen that as EBs develop into better organised entities their stiffness increases. In fig5.3b the Young's modulus of different size day 8 EBs is shown. No clear trend is observed and thus the modulus is considered to be the same for all size EBs of the final day of the EB growth. Error bars where calculated for 2 standard deviations for measurements in triplicate. (AFM - Young's modulus measurements for this experiment were carried out by Andrew Pelling)

4.3.3 Control III: High flow rate standardisation

A further experiment was conducted with two capillaries that had the same inner diameter (600 μm) but different lengths. The objective of this experiment was to help define the boundaries for future experimental studies in terms of breakage as affected by exposure time in a sheared environment. Capillaries of 50 and 100 mm were used. EB suspension was forced through the capillaries for 1 pass with the same average flow velocity of 10 m/s in both cases, in order to examine the possible effect of the capillary length on the EB breakage. It was seen that the length of the capillary had a considerable effect on the size of the initial EB population in both cases. Especially in the case of the 100 mm capillary a significant breakage was induced while a substantial release of single cells was seen (4-15 μm). Furthermore it can be seen that for such flow conditions breakage is induced even in smaller cell aggregates (15-120 μm), which were generated from the breakage of the initial EB population. In figure 4.4 the process described is represented graphically; the logarithmic scale in the x-axis was used in order to show more clearly the generation of the single cell population.

In the same capillary system (d=600 μm) EB suspensions were processed for a different range of flow intensities so as to monitor the effect of flow speed on the initial EB population. The length of the capillary used was 100 mm and samples were processed once through the capillary for all flow rates. In figure 4.6 the results of these experiments are shown. It can be seen that the increase of flow speed, for resulted in greater levels of single cell release.

It should be mentioned that in these experiments there might be a possible entrance effect since the capillary diameter used was smaller than many of the initial EBs processed through the capillary. An analysis on the release of single cells during flow in a capillary system due to entrance effects (d = 1mm) will follow later-on.

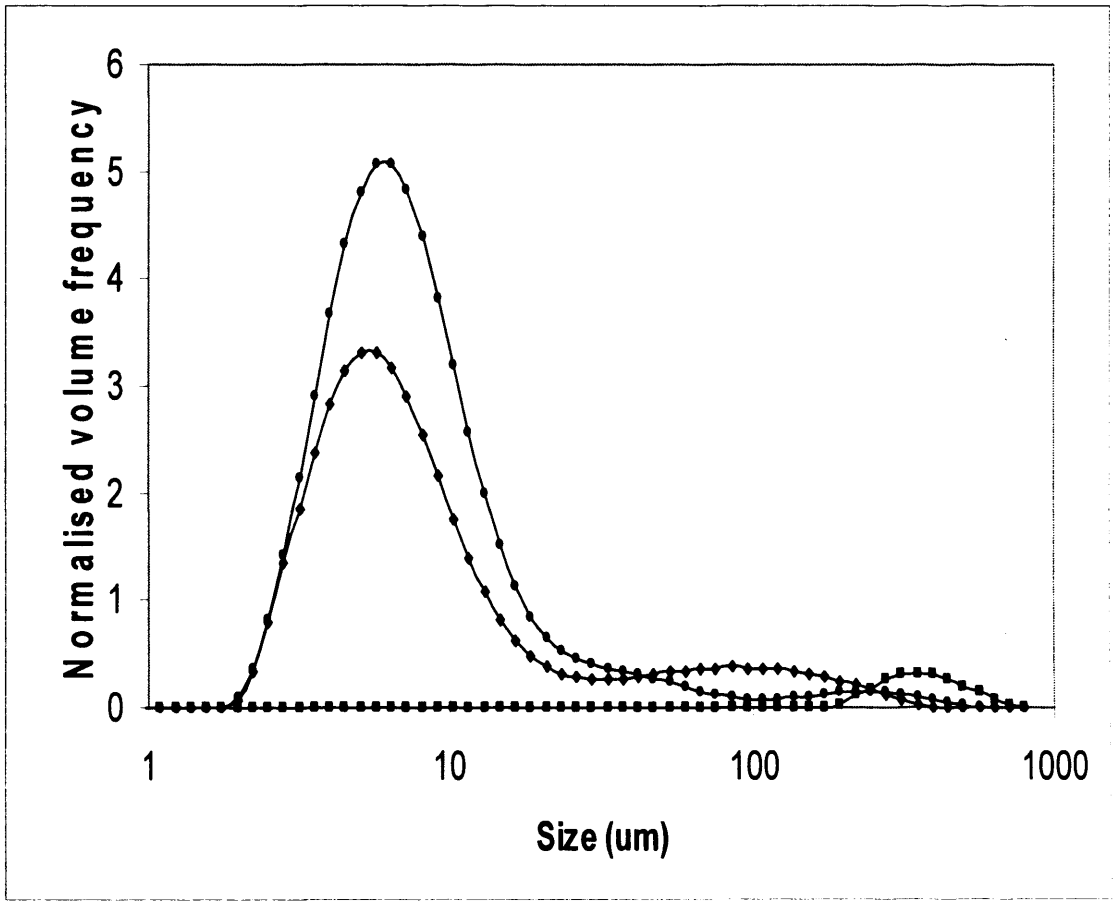

Figure 4.4: Size distribution of the initial population of EBs before shear (■), when processed through a capillary with inner diameter of 600 μm and length of 50 mm (♦); and 100 mm (●) respectively. Each sample was recycled once through each capillary. The volume of the suspension pumped through the capillary was 10 mL. Samples were collected immediately after processing and the particle size distribution analysis was carried out with a laser light scattering method. The results shown are the average values gained from two separate experiments.

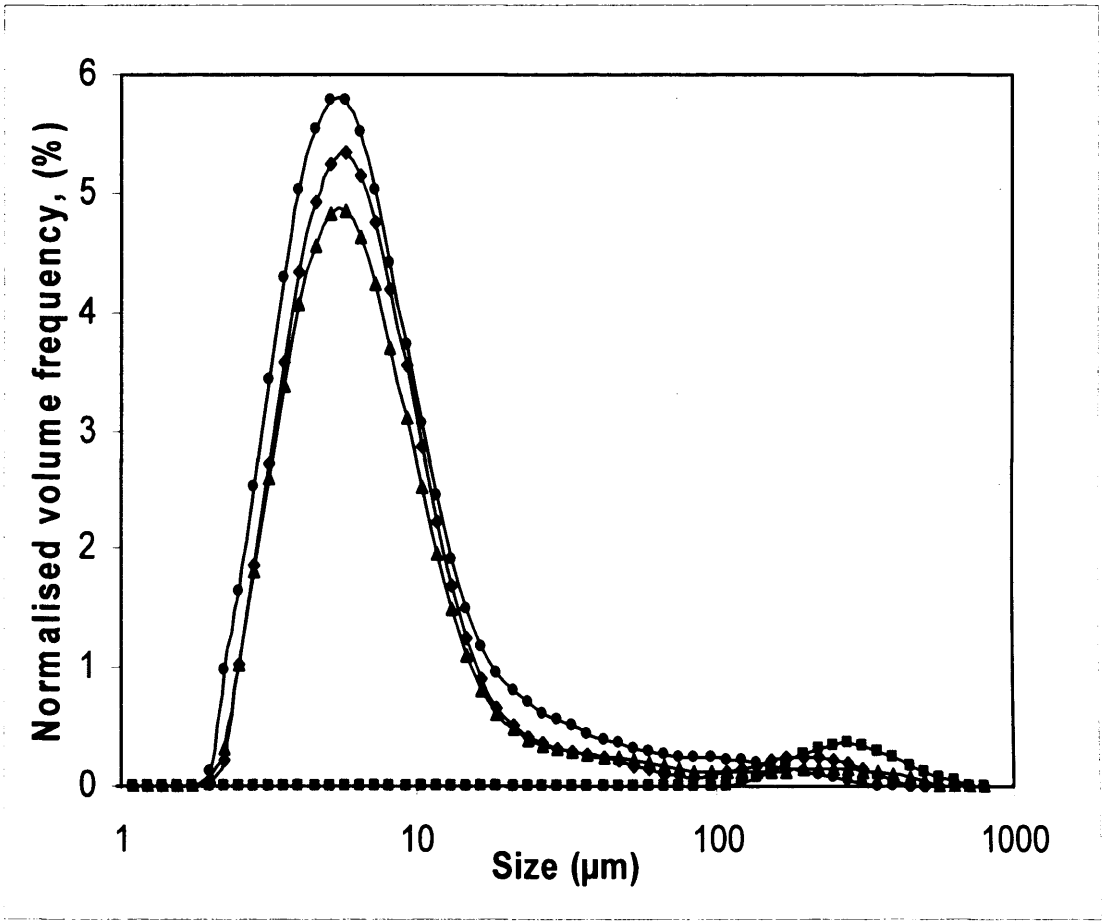

Figure 4.5: Size distribution analysis of the initial population of EBs before shear (■) and when exposed to a flow of 10 m/s (▲); 12 m/s (♦); 14 m/s (●). Each sample was processed once through a capillary. The volume of the solution pumped through the capillary was 10 mL, while the inner diameter was 600 μm. The increase of flow speed, for such high flow intensity, had as a result a small increase of single cell release. Samples were collected immediately after processing and the size distribution was measured in a laser light-scattering device.

4.3.4 Control V: Clarification of final EB solution

During EB culture, a single-cell population was observed to exist in the suspension apart from the EB population. These were cells that probably had not yet been part of the EBs. Such a population would interfere with the measurements of the single-cells released from the EBs. For this reason the suspension including the 8 day EBs and the single cells, was left to settle in a 20 mL Falcon tube for 1 minute in order to separate the EBs. The EBs settled quickly forming a pellet at the bottom of the tube while the single cells remained in the supernatant. The EBs were then re-suspended gently in serum after the removal of the supernatant and were subsequently processed. A wide bore pipette was used so as to avoid any exposure of the EBs to shear conditions. In the measurements of size distribution that followed, there was no observation of a peak in the size range of single cell population (4–15 μm). This method was followed prior to all shear experiments that followed in the analysis. In figure 4.7 the development of the EBs is shown over time from day 2 to day 8 and the increase of their size over the culture period; the pre-mentioned single cell population can be seen as well.

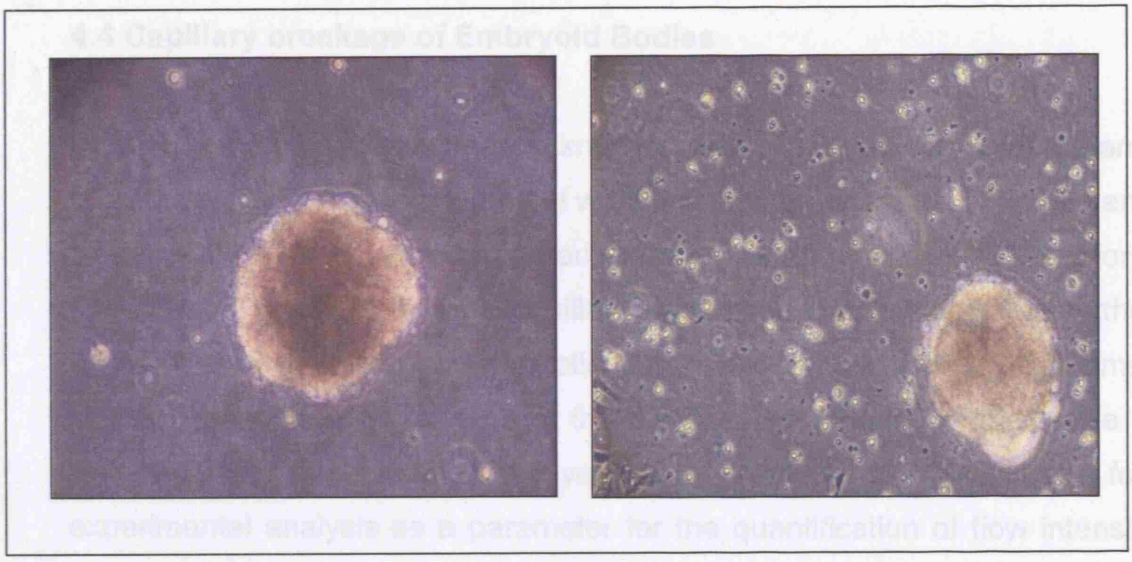

Figure 4.6: Optical observation of EB suspension before (right) and after (left) clarification; the density of single cells in suspension is decreased and is not detectable by the particle sizer (Malvern mastersizer). The image is a representative optical observation.

4.4 Capillary breakage of Embryoid Bodies

From the previous experiments knowledge for the experimental parameter boundaries for further experimental work was gained and a basic understanding of the material (EB) and its characteristics was obtained. In this section the breakage of the EBs through capillary systems will be investigated further in terms of exposure time and controlled flow rate. Furthermore an experimental model describing the breakage of the EBs and the release of the single cells was created. The average flow velocity of the bulk fluid was used for all experimental analysis as a parameter for the quantification of flow intensity. It was preferred to the flow rate due to its broader and more universal meaning.

4.4.1 Experimental process

EB suspensions were fed through the capillary system described over a range of flow rates and exposure times. The suspensions were fed through the capillaries for four different average flow speeds. These were 1.55, 3.1, 6.2 and 8.1 m/s according to the piston speed chosen each time. Suspension was pumped through a capillary with an inner diameter of 1000 μm. This diameter was chosen for two reasons. Firstly it guaranteed that the entrance would be bigger than any of the EBs in the population. Secondly diameters of this size range can be found in the tips of pipettes that are used for handling of cells and EBs during routine lab experimentation and EB growth, thus simulating a flow environment that is encountered very often in manual processes. The exposure time of the EB suspension within shear conditions was increased by recycling the suspension through the capillary for an increasing number of passes. An experiment at 6.2 m/s was also done with an orifice of 1000 μm in order to investigate for entrance effects. The volume of the samples processed was 10 mL. Samples were mixed (shaken) prior to processing so that the EBs would be evenly distributed. After processing, the samples containing the EBs were continuously shaken softly so as to prevent any possibility for EB settling and aggregation. For increasing number of passes the solution was fed again in the barrel and reprocessed. It was made sure that no air was entrapped in the

barrel. In this way any possible mistakes were avoided in the calculation of the flow rate, due to air compressibility.

4.4.2 Entrance effect

During flow in a capillary three high shear areas can be found. The entrance region, the inner wall of the capillary and the exit from the capillary can produce high levels of shear primarily in turbulent flows but also in laminar flows. Various studies have shown that these areas can induce damage to biomaterials when flowing through a capillary system. The characteristics (i.e shape, elasticity) of the material processed as well as the type of stress developed (i.e elongational stress, shear stress) in each area of a capillary are parameters of interest. Studies have shown that super-coiled plasmid DNA was damaged at the capillary entrance due to elongational stress (Meacle et al. 2006). Mammalian cells which have been exposed to different flow fields and shear conditions show a range of results from cell membrane rupture (Born et al., 1992; Al-Rubeai et al., 1995) to altered cell function eg induction of differentiation in the case of stem cells (Yamamoto et al., 2005; Schmelter et al., 2006). So it is of interest to understand and locate the area where the EB breakage will occur in the system used in this research.

An experiment was conducted in order to understand in which areas of the capillary and under which operating conditions the EBs broke into smaller components of cell aggregates and released cells. The EB solution was recycled through a stainless steel orifice (d=1000 μm) for an increasing number of passes. In figure 4.7 the results of this process can be seen. It was seen that for pass1 through the orifice a very small amount of single cells were released from the EBs. There was no further cell release observed for an increased number of passes up to pass 15. It was concluded that the entrance effect for the first pass released cells that were not yet fully incorporated in the actual EB body via extra-cellular matrix (ECM) bonding, but were connected to it in a rather weak way. It is possible to observe these cells in figure 4.1, in the images where day 8 EBs are shown scattered in the medium. However during analysis

for EB breakage later on, an average apparent rate constant was used describing the release of both loosely and tightly bound cells.

4.4.3 Effect of increased velocity and exposure time

The aim of these experiments was to evaluate the effect of exposure time in capillary shear conditions on the size of the EBs for different flow speeds. At the lowest flow speed 1.55 m/s there were low levels of breakage and single cell release. After 6 passes through the capillary no further significant EB breakage was observed (figure 4.8). In order to further increase the release of single cells the flow speed was increased (3.1 m/s) while keeping the same residence time per pass (ie doubling the capillary length) yielding a higher level of EB breakage (figure 4.9). For a high number of passes i.e. passes10 and 15, a new population developed in the submicron size range which probably consisted of extra-cellular matrix and bi-products of the breakage process. At velocities of 6.2 m/s (figure 4.10) again an increased level of EB breakage and single cell release was observed. A fundamental difference was noticed at this flow velocity between the two sets of experiments though. Instead of a maximum level of EB breakage being observed, at 6.2 m/s it appeared that all the EBs would break. This trend was more clearly confirmed at 8.1 m/s.

4.4.4 Effect of flow intensity

Apart from the effect of the retention time on the size distribution of the EBs and the generation of a single cell population, it is expected that the intensity of the flow with which EB suspensions were fed through the capillary device will have an impact on the breakage process. Figure 4.11 illustrates the effect of increasing shear rates on the size of the EB population for the same residence time (t=0.15 s) within the capillary system. It can be seen that the increase of the average flow speed has as a result a more extensive breakage of the EB population and respectively a more intense generation of single cells. As previously seen for lower flow speeds a plateau referring to a critical size was reached after a certain exposure time to shear conditions.

4.4.5 Optical observations

Figure 4.12 shows images of EBs before and after processing through a capillary with an inner diameter of 1000 μm, for increasing exposure times during a flow of v = 6.2 m/s (see figure 4.10). For related size distributions, a number of EBs was seen to lose their spherical shape after increasing residence times, disintegrating into smaller cellular aggregates. There were a number of EBs especially in the first passes, whose shape was not affected and retained their spheroid shape. This probably happened as some of the EBs never came into contact with the capillary walls during the experimental process. At the same time an increasing number of single cells was seen to be released in the suspension following the breakage of the EBs with increasing exposure time. Fragments that probably came from the release of the extra-cellular matrix that held the cells together in the EB were also after 0.45 s residence time.

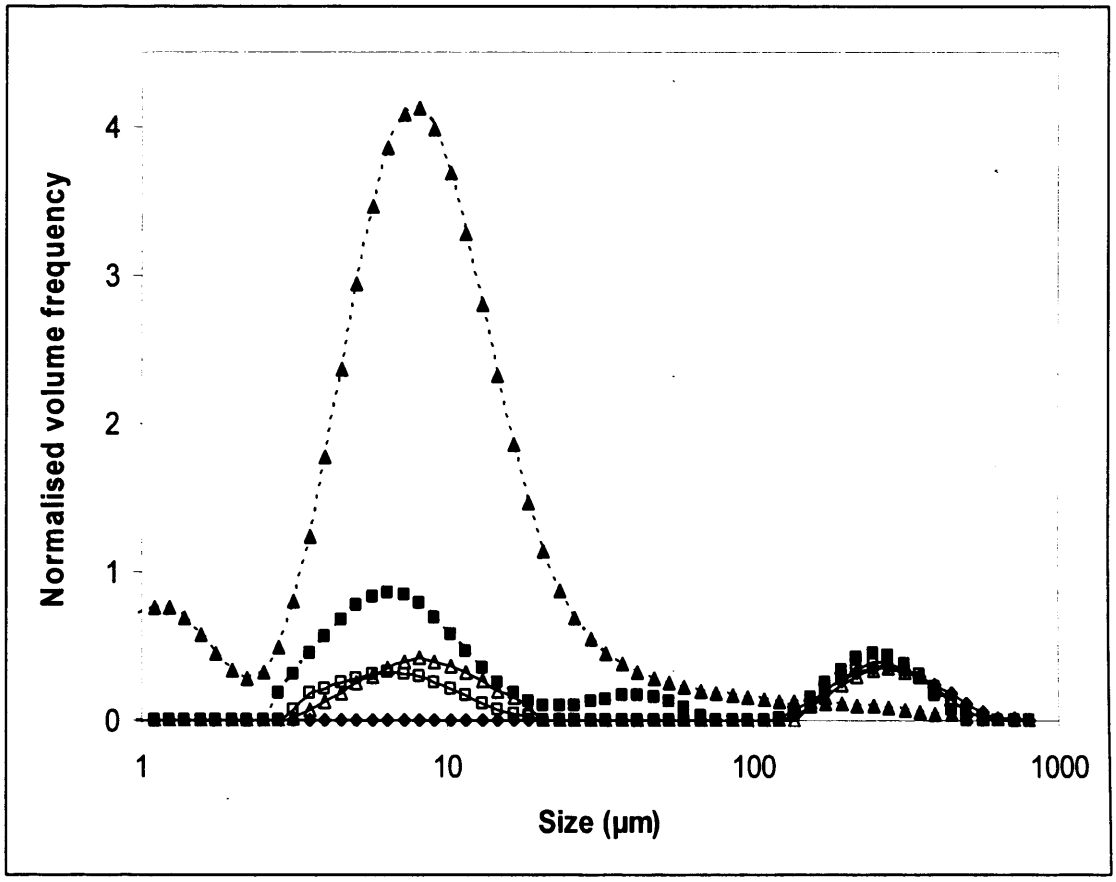

Figure 4.7: Effect of number of passes on single cell release and EB breakage when flown through an orifice with a diameter of 1000 µm for 1 pass (□) and 15 passes (Δ), compared to the effect of flow through a capillary system 200 mm length and of the same diameter for 1 pass (■) and 15 passes (▲). Mean flow velocity through the orifice and the capillary was 6.2 m/s. The volume of the solution pumped through the capillary was 10 mL. Samples were collected immediately after processing and the size distribution was measured with a laser light scattering method (note y-axis reaching maximum value of 4.5 % as opposed to 6 % used for the data in following graphs).

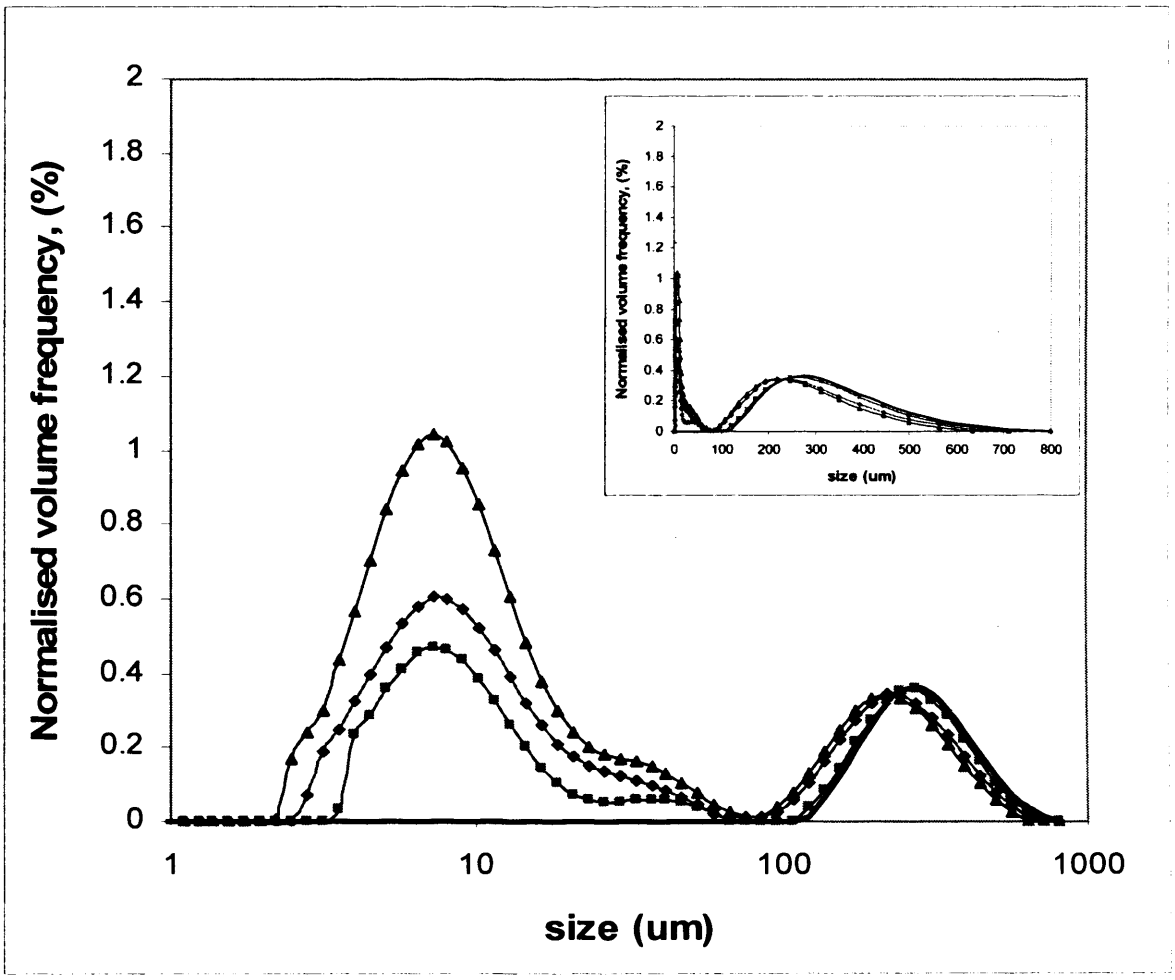

Figure 4.8: Effect of the number of passes through a capillary system of d=1 mm and l = 100 mm on the size distribution of the EB population. The speed of the flow in the capillary was 1.55 m/s. The size distribution was divided into three populations. The lower region peak represents the population of single cells from 4 μm to 16 μm, the population between 16 μm and 120 μm is considered to represent aggregates of cells that came from the breakage of the initial EB population. The final and largest particle population is between 120 μm and 700 μm and indicates the initial EB size distribution before processing and what population remains after each experiment. The bold line shows the size distribution of the initial EB population; pass1 (■); pass 3 (♦); pass 6 (▲).

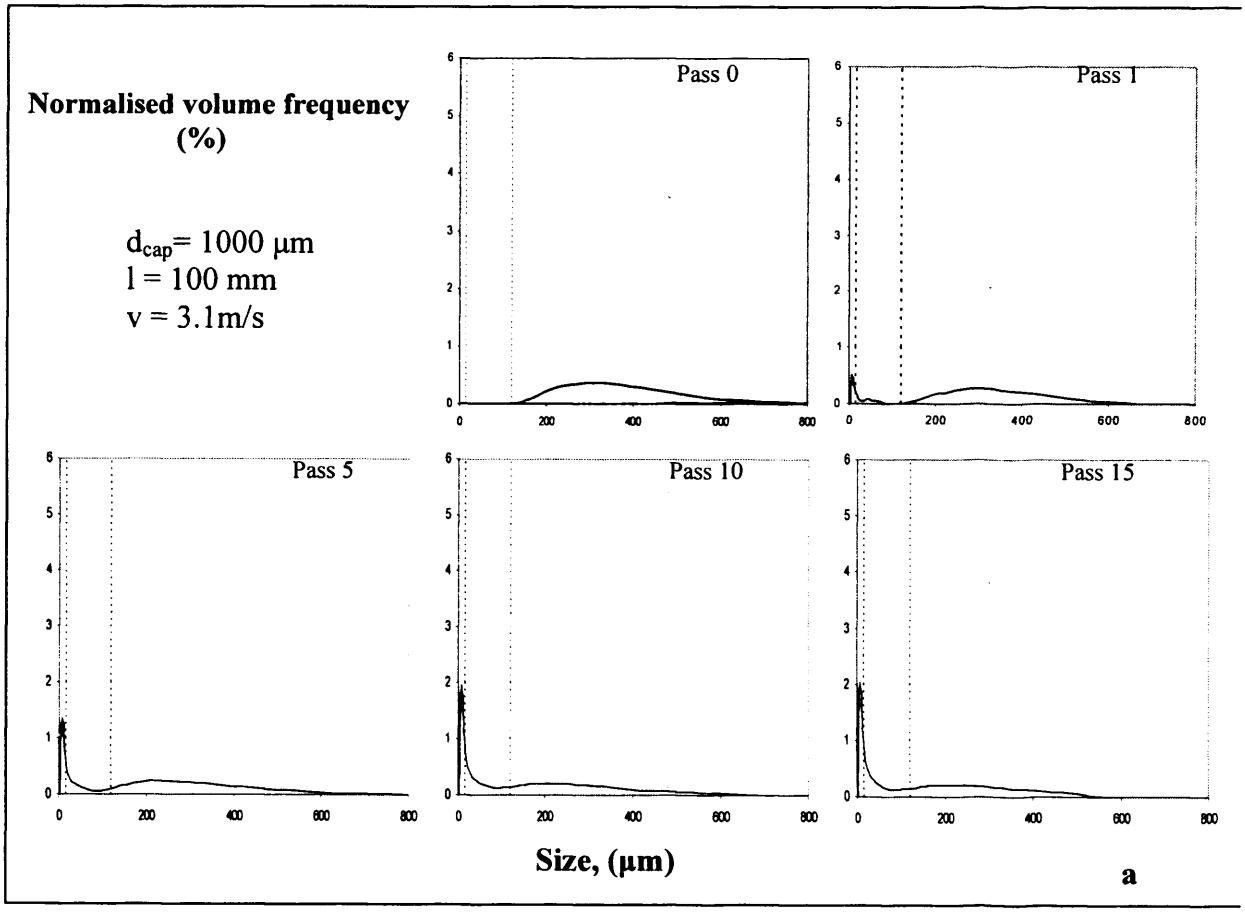
Normalised volume frequency (%)
d_{cap}= 1000 µm
l = 100 mm
v = 3.1m/s
Pass 0
Pass 1
Pass 5
Pass 10
Pass 15
Size, (µm)
a

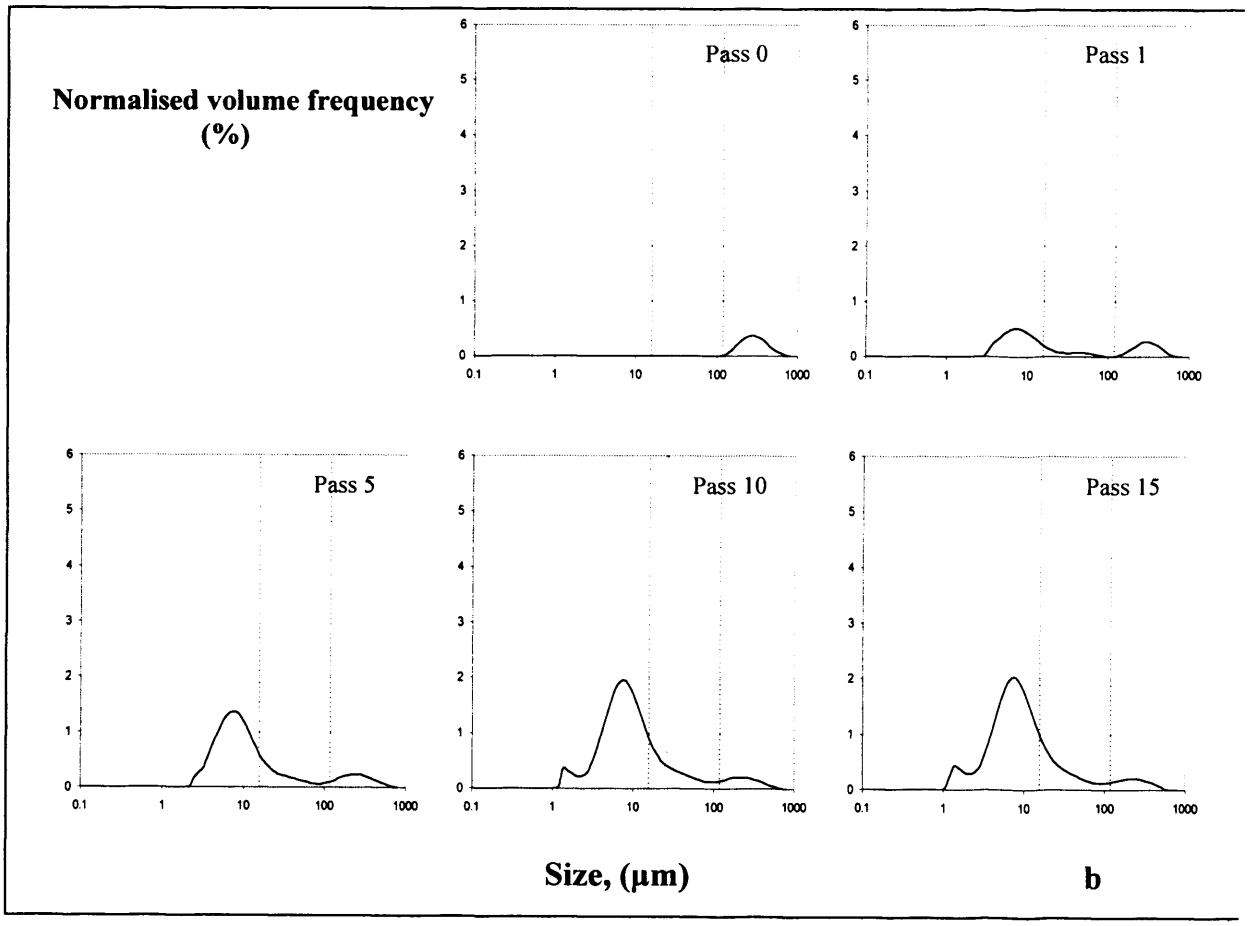
Normalised volume frequency (%)
Pass 0
Pass 1
Pass 5
Pass 10
Pass 15
Size, (µm)
b

Figure 4.9: Effect of number of passes through a capillary system of d=1 mm and l=100 mm on the size distribution of the EB population during laminar flow. The average speed of the flow in the capillary was 3.1 m/s. The size distribution was divided into three populations. The lower size population is between 1 and 4 μm probably due to cell debris formed from total cell rupture and loss of integrity. The next region represents the population of single cells from 4 to 15 μm, the population between 15 and 120 μm is considered to represent aggregates of cells that came from the breakage of the initial EB population. The final and largest particle population is between 120 and 700 μm and indicates the initial EB size distribution before processing and what population remains there after each experiment. (Figure 5.9(a) has linear scale x-axis in order to facilitate observation of EB breakage; Figure 5.9(b) has a logarithmic scale x-axis in order to observe single cell generation).

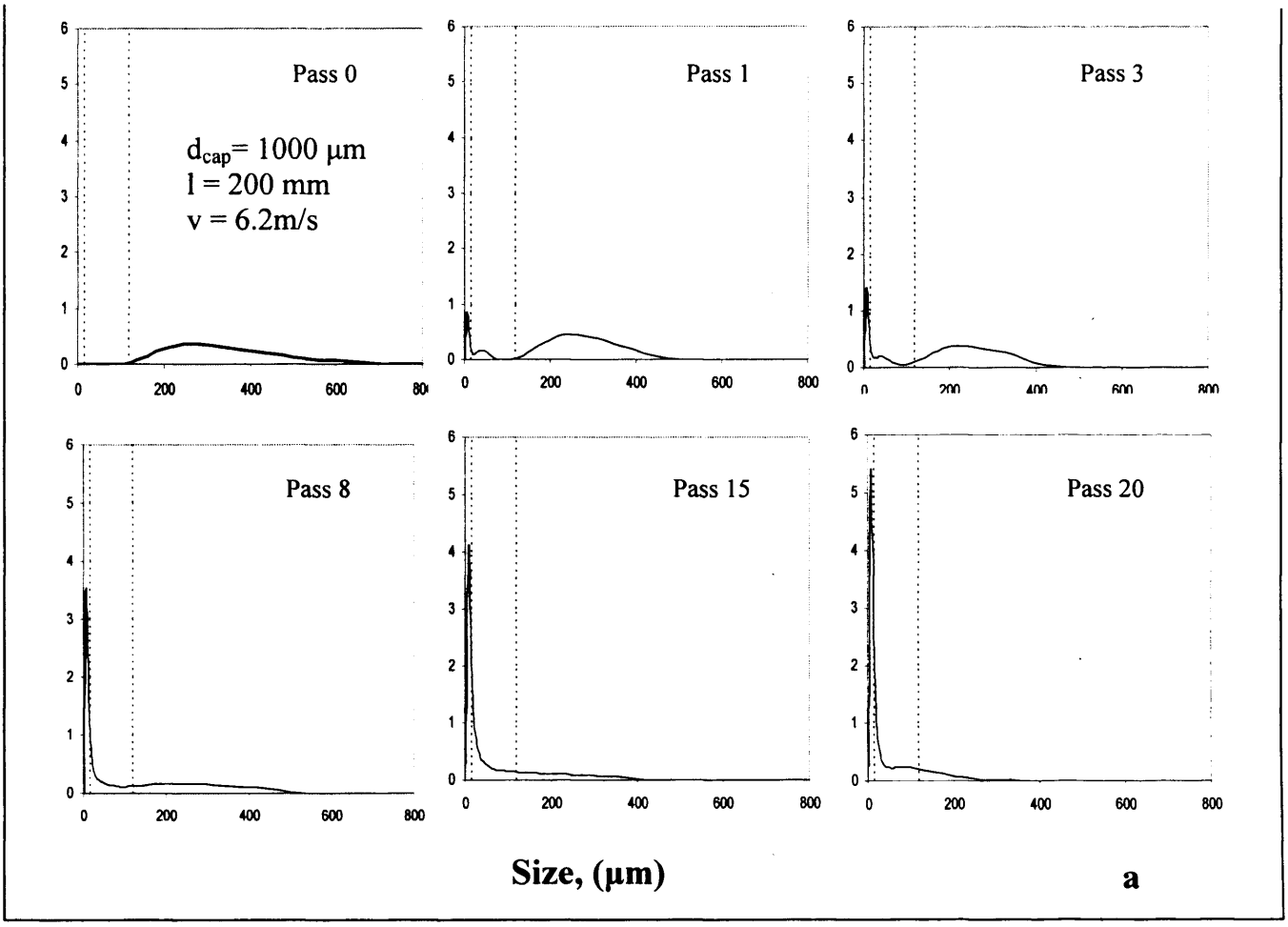
Pass 0
d_{cap}= 1000 µm
l = 200 mm
v = 6.2m/s
Pass 1
Pass 3
Pass 8
Pass 15
Pass 20
Size, (µm)
a

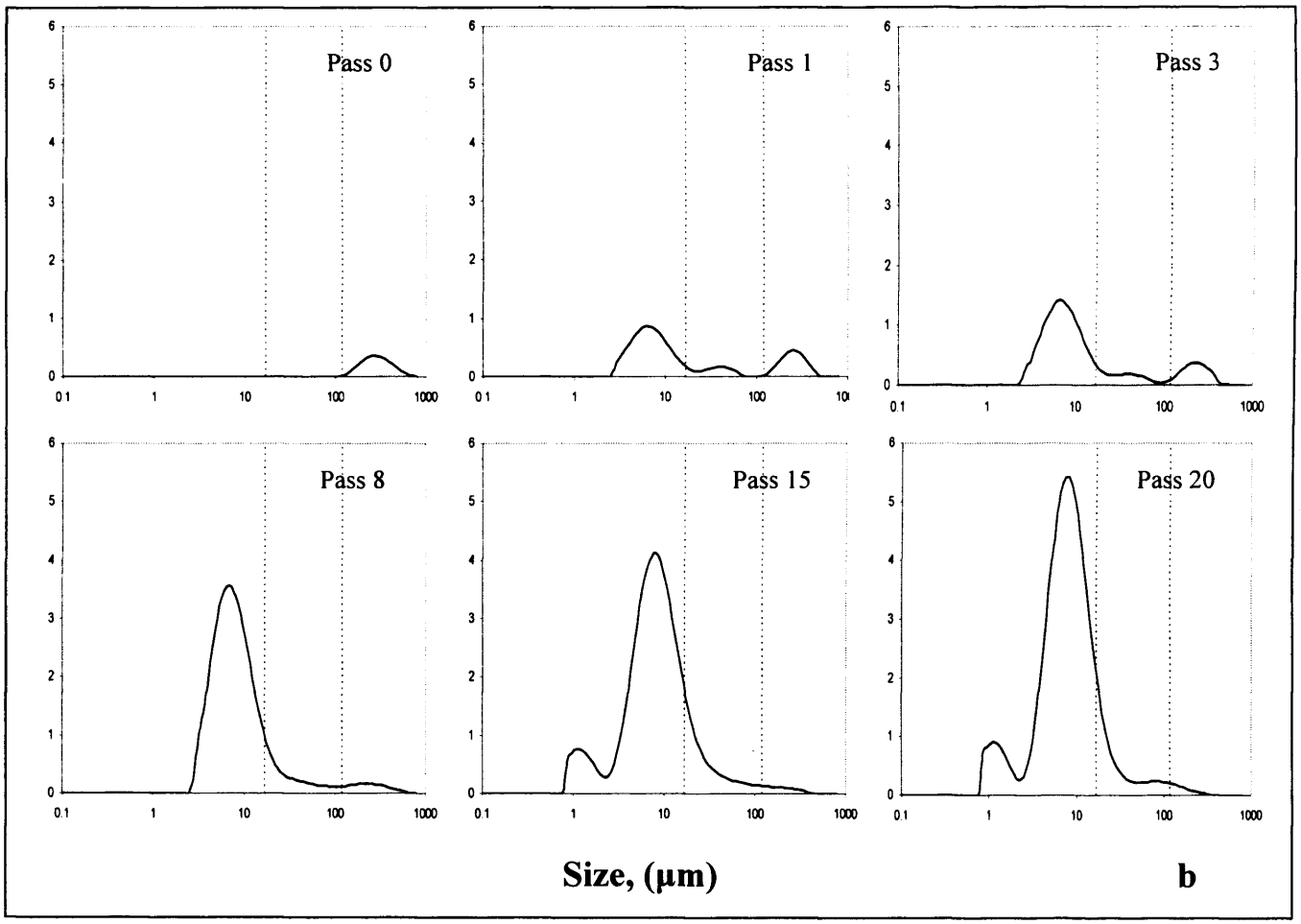
Pass 0
Pass 1
Pass 3
Pass 8
Pass 15
Pass 20
Size, (µm)
b

Figure 4.10: Effect of number of passes through a capillary system of d=1 mm and l=200 mm on the size distribution of the EB population during laminar flow. The average speed of the flow in the capillary was 6.2 m/s. Four populations are examined. The lower size population is between 1 and 4 μm probably due to debris originating from ECM fragments and maybe cell rupture?. The smallest shows the population of single cells ranging from 5 to 15 μm, the population between 15 and 120 μm, is considered to represent aggregates of cells that came from the breakage of the initial EB population. The final and largest particle population is between 120 and 700 μm and represents the initial EB size distribution before processing. (Figure 2a has linear scale x-axis in order to facilitate observation of EB breakage; Figure 2b has a logarithmic scale x-axis in order to observe single cell generation).

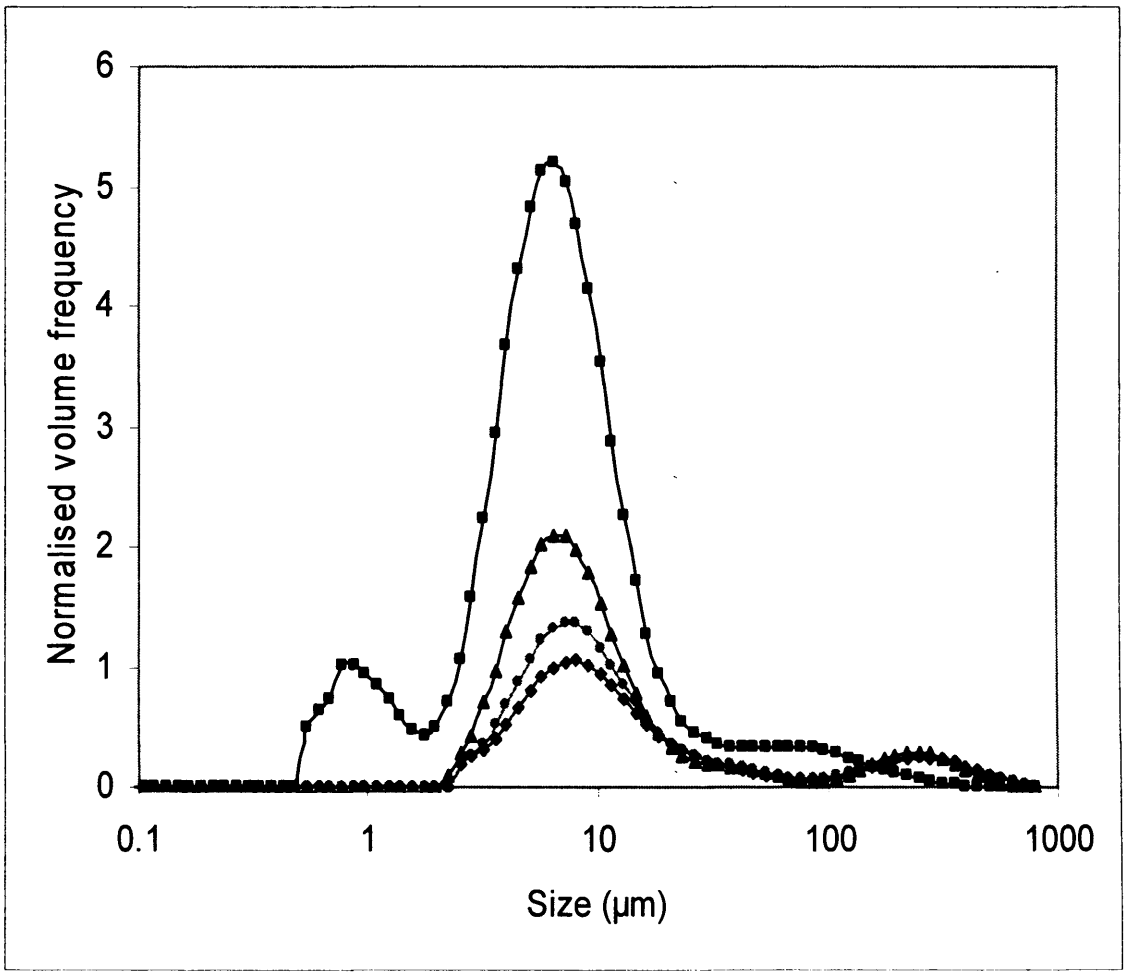

Figure 4.11: Effect of mean flow velocity on the size distribution of the EB population for a fixed residence time of t=0.15 s. The EBs were processed through capillaries of three different lengths 50, 100, 200 mm according to the flow rate used achieving same residence time for all cases. The inner diameter was 1 mm. The material was processed with three different average flow speeds: 1.55m/s (♦); 3.1 m/s (●); 6.2m/s (▲); 8.1 m/s (■).

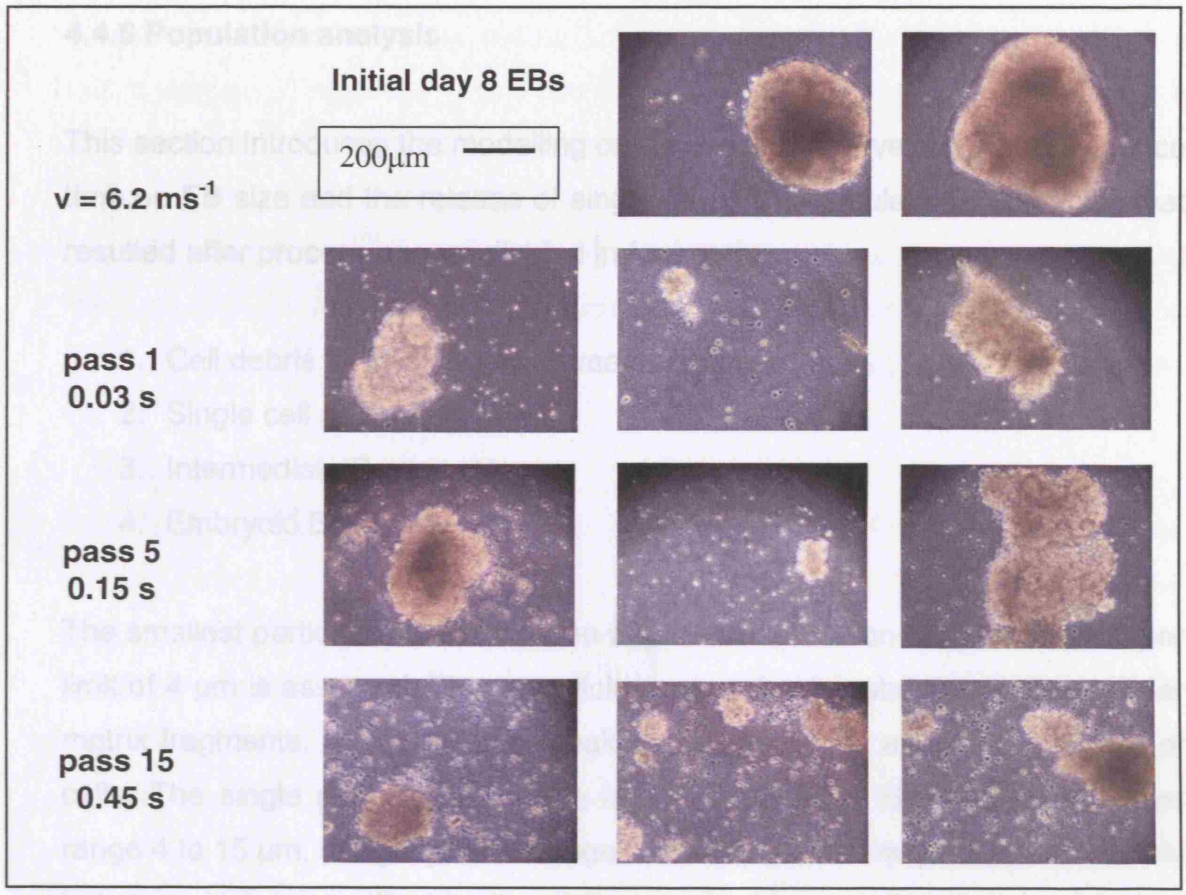

Figure 4.12: Images of the EB before and after exposure to shear conditions. The first row shows EBs on day 8 of their growth prior to processing. The second row shows EBs and released single cells when processed through a 1000 µm capillary and after exposure to shear conditions with an average flow speed of 6.2 m/s, for 1 pass (0.03 s). The third row illustrates further breakage of the EBs and loss of their spheroid shape and subsequent increase on the release of single cells in suspension after flow five times through the capillary. On the final row a big increase in single cell density as well as extra-cellular matrix can observed, whereas the cell aggregates that remain in that form are rather smaller (pass 15 – 0.45 s). Images were taken randomly out of the whole aggregate - single cell suspendion. (Scale bar: 200 µm).

4.4.6 Population analysis

This section introduces the modelling of the effect of flow velocity and residence time on EB size and the release of single cells. The population of particles that resulted after processing was divided in four parts:

1. Cell debris and extra-cellular matrix fragments : V_D
2. Single cell population : V_C
3. Intermediate Bodies : V_{IB}
4. Embryoid Bodies : V_{EB}

The smallest particles, V_D occur in the submicron to micron range and an upper limit of 4 μm is assumed. These particles are probably debris and extra-cellular matrix fragments, a result of the break-up of EBs or the eventual breakage of cells. The single cell population, V_C is assumed to be identified by the size range 4 to 15 μm, a slightly wider range than may be normally assumed for cells but one which is identified by the distinct peak observed. The deconvolution of the light scattering signal will be based on several assumptions could well give this slightly broader shape. The intermediate bodies V_{IB} are identified by bodies which are smaller than the lowest end of the EB size range but larger than the single cells, ie they result from EB breakage and may or may not be further broken down to single cells. This range is assumed to be between 15 and 120 μm. The embryoid bodies, V_{EB} represent the initial feed but after breakage can obviously include the break-up products of the largest bodies. This size range is assumed to be from 120 to the top end of the distribution typically 700 μm.

Figure 4.9 and figure 4.10 show these distributions as volume frequency functions for the range of flow velocities and exposure times studied. The linear form (figure 4.9) allows us to calculate the fraction of particles in each size range (given area under curve). The logarithmic form (figure 4.10) is used to show more clearly what is occurring during breakage.

Figure 4.13 summarises the percentage that remains in the EB population group, V_{EB} for increasing exposure times. The four lines represent the different

velocities the EBs were exposed to during flow through the capillary. It appears that a plateau of breakage is reached in the case of the two lower velocities with approximately 75% and 50 % remaining for flow velocities of 1.55 and 3.1 m/s respectively. At higher flow velocities 6.2 and 8.1 m/s it appears that no EBs will eventually remain. For convenience figure 4.13 shows first order model through the data, based on a best least squares fits to determine the rate constant and the final equilibrium volumes. The reason for the modelling will be discussed later.

A more detailed analysis of the size distributions (figure 4.9 and 4.10) provides further insight on these critical sizes. For the low flow velocities the volume fraction where there is 75% of EBs of smaller diameter is defined by the the size of 400 μm and for 50% is given by the size of 270 μm. At the flow velocity of 6.2 m/s while all EBs are broken the resulting IBs are largely unbroken. A critical size at the lower end of the EB is assumed, ie 120 μm. At the flow velocity of 8.1 m/s it is difficult to determine the size boundary below which IBs remain unbroken. This is evidently near the upper boundary of the single cells and will be discussed later.

Figure 4.14 shows the release of the single cell population; this follows an inverse trend to the breakage of the EBs. With increasing exposure time and increasing shear rate more single cells were released as a consequence of the EB breakage. In the case of the two lower flow rates the volume percentage of single cells released appears to reach maximum values of 16% and 25% of total cell number for flow velocities of 1.55 and 3.1 m/s respectively.

The above analysis of break-up of EBs and formation of single IB and single cells will now be modelled and in particular the critical sizes described earlier will be used to help define the process.

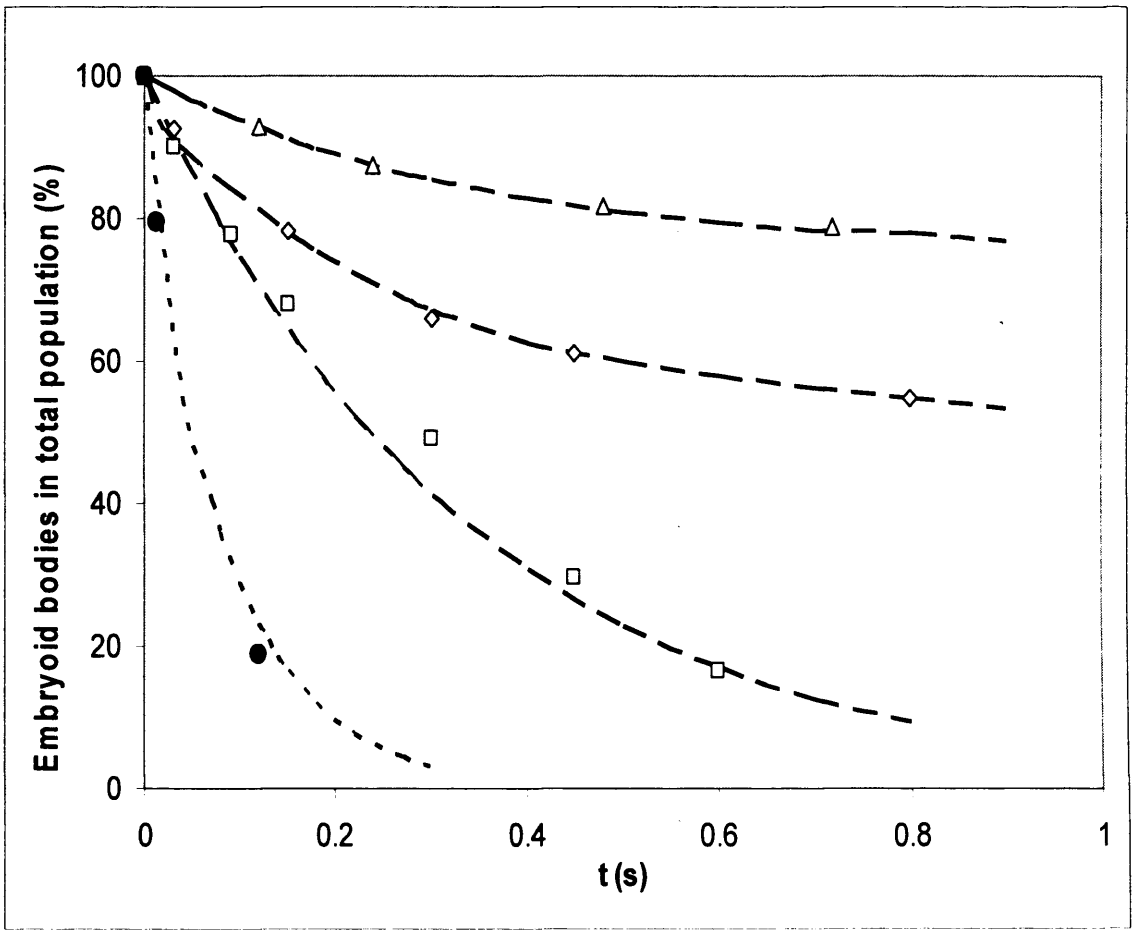

Figure 4.13: Effect of exposure time in a capillary on the % population of Embryoid bodies over total population. The EBs were forced through a 1000 μm of different lengths with four different velocities represented by: 1.55 m/s (Δ); 3.1 m/s (◊); 6.2 m/s (□); 8.1 m/s (●). In the case of the two lower flow rates, a plateau value is reached after which no further breakage of EBs was observed. On the other hand with increasing flow rate such a limit is not reached and full breakage of the EBs is expected to be achieved eventually for increasing exposure times. (----) : model fit used to described data, i.e. best least square fit of 1st order loss to an equilibrium volume : 75% unbroken for 1.55m/s; 50% unbroken for 3.1m/s; 0% unbroken for 6.2 and 8.1 m/s (rate constants will be provided later on section 5.5).

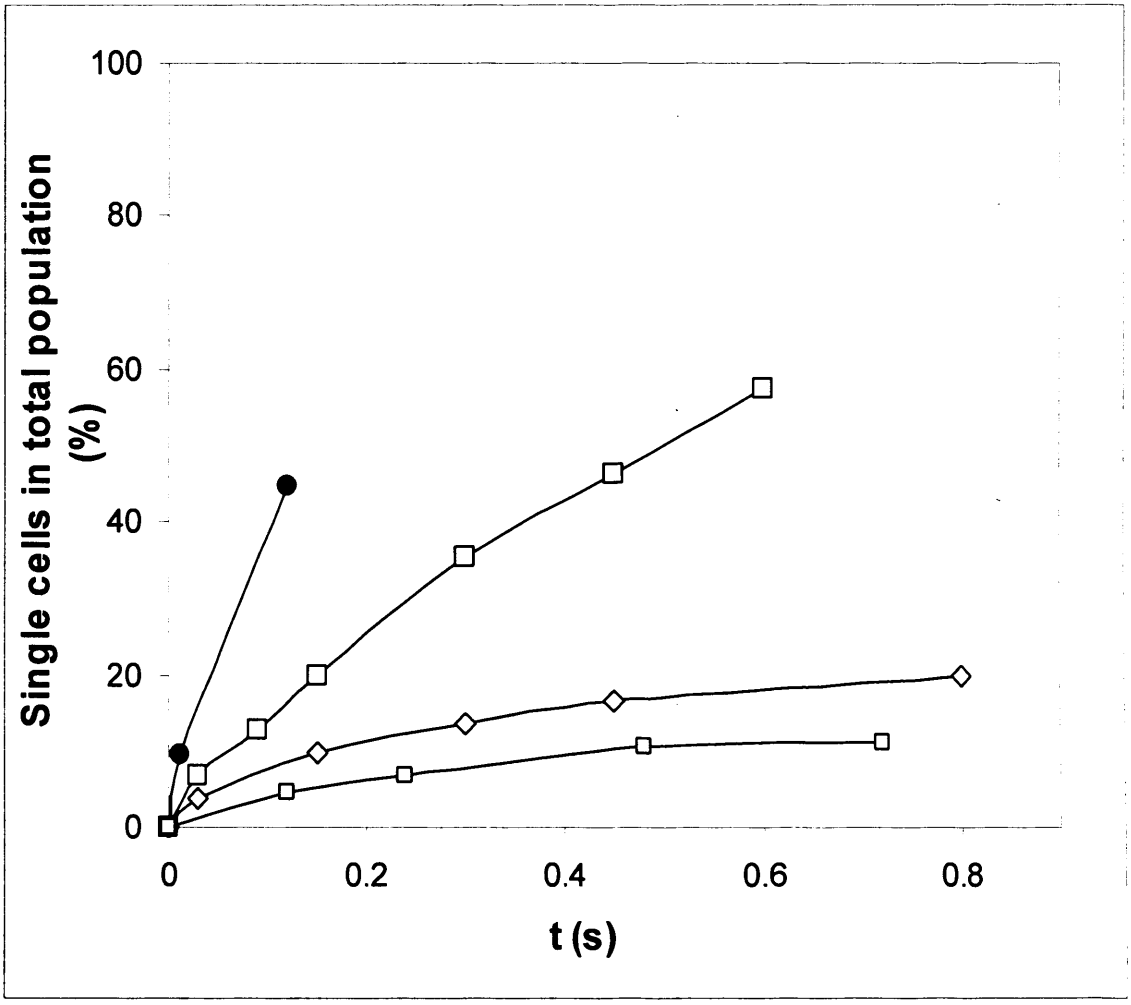

Figure 4.14: Effect of exposure time within the capillary on the % population of single aggregates during processing. The cells were exposed to four different different average shear rates represented by: 1.55 m/s (Δ); 3.1 m/s (◊); 6.2 m/s (□); 8.1 m/s (●). (Lines in this graph are just connecting points they do not represent a model fit)

4.5 Breakage Model

Four populations describe the size distribution resulting from capillary flow (figure 4.15) :

1. Cell debris: V_D
2. Single Cells: V_C
3. Intermediate Bodies: V_{IB}
4. Embryoid Bodies: V_{EB}, [minimum size d_{EBmin} ~ 120 μm]

As the suspension flows through a capillary a range of phenomena are assumed to occur. In this study we focus on the breakage of the EBs. To explore this we will examine three cases in terms of a critical diameter above which breakage occurs :

(i) $d_{cr} \geq d_{EBmin}$
(ii) $d_{cr} \approx d_c$
(iii) $d_c < d_{cr} < d_{EBmin}$

Case (i) $d_{cr} \geq d_{EBmin}$

The key assumptions are:

(a) Embryoid Bodies of size d_{cr} and greater break-up to form Intermediate Bodies and cells. The Embryoid Bodies of size less than d_{cr} are not available for break-up is and they will remain unbroken even after multiple passes. This volume is defined as V_{EBdcr};

(b) the Intermediate Bodies will not break-up;

(c) the breakage of cells to form debris is assumed to be negligible.

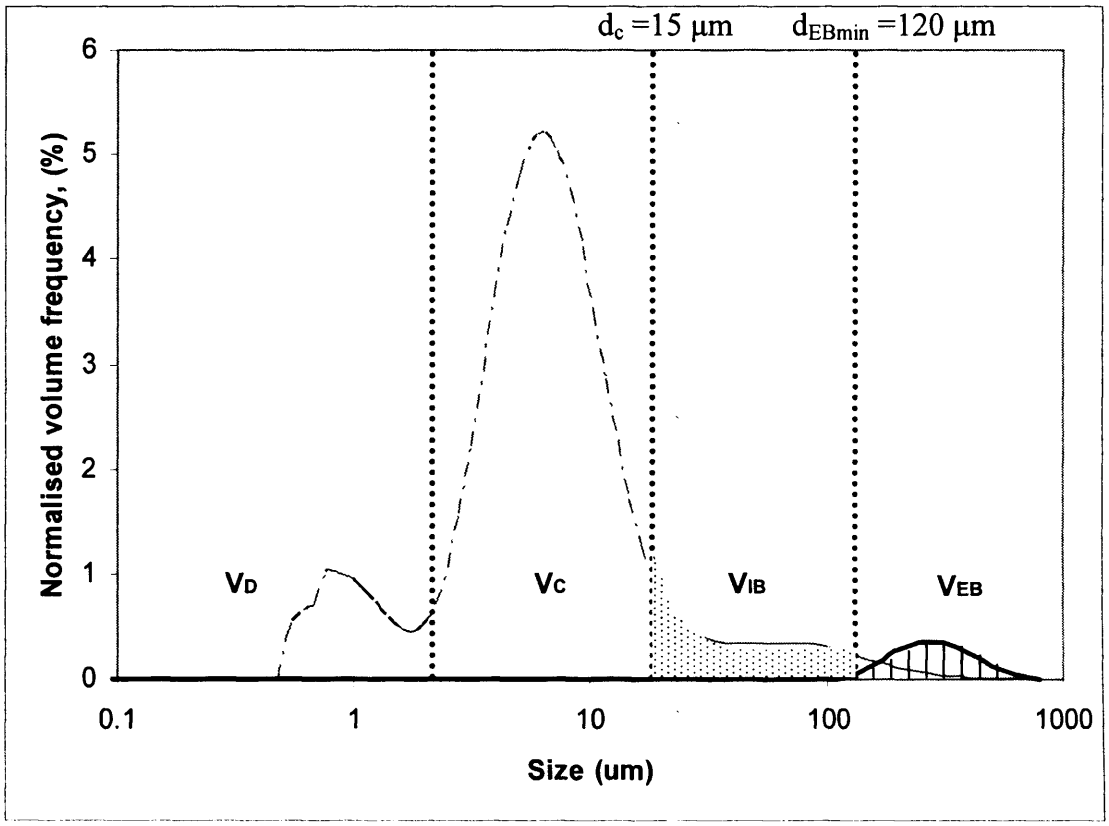

Figure 4.15: Typical size distribution where the distinct populations and critical size values used for modelling EB breakage and single cell formation are shown.

The fraction of Embryoid Bodies susceptible to break-up is given by:

$$\frac{V_{EBo} - V_{EBdcr}}{V_{EBo}}$$

where V_{EBo} is the initial volume of the EB population

A proportion of the EBs which break after processing in the capillary will generate a single cell population (V_c) while the rest will create an intermediate body population (V_{IB}):

$$\Delta V_C = m\, \Delta V_{EB}$$
$$\Delta V_{IB} = (1\text{-}m)\, \Delta V_{EB}$$

where m is the proportion of V_{EB} to form V_C and (1-m) is the proportion of V_{EB} to form V_{IB}. This assumes that the Intermediate Bodies are smaller than dcr and as such they are not susceptible to further break-up.

Figure 4.16 examines the relationship between single cell formation and EB break-up. For the early stages of break-up ($\Delta V_{EB} < 80\%$) there appears to be a linear relationship ie giving a constant value of:

$$m \approx 0.55 \qquad (1)$$

Where single cells are formed only by EB break-up it may be assumed that this linear relationship will continue to $\Delta V_{EB} \approx 100\%$.(to note: where IBs break to form single cells the value of m will increase; this is outside the assumption for this section.

Single cell generation is given by the following equation:

$$\frac{dV_C}{dt} = m \frac{dV_{EB}}{dt} = 0.55 \frac{dV_{EB}}{dt} \qquad (2)$$

We assume that the breakage of the EBs is described by a first order relationship; i.e. the rate of breakage is proportional to the volume of EBs that exists above the critical size:

$$\frac{dV_{EB}}{dt} = k_{EB}(V_{EB\,t} - V_{EBdcr}) \Leftrightarrow$$

$$\int_{V_{EBo}-V_{EBd_{Cr}}}^{V_{EBt}-V_{EBd_{Cr}}} \frac{1}{V_{EBt} - V_{EBd_{Cr}}} dV_{EBt} = k_{EB}\int_{0}^{t} dt \Leftrightarrow$$

$$\ln\left[\frac{V_{EBt} - V_{EBd_{Cr}}}{V_{EBo} - V_{EBd_{Cr}}}\right] = k_{EB}t \qquad (3)$$

where k_{EB} is the average first order rate constant, V_{EBt} is the volume of EBs remaining after time t and V_{EBo} is the initial amount of EBs. The above first order relationships are graphically represented in figure 4.13.

The initial EB population consists of a wide range of different size particles from 120 to 700 μm. It is expected that different sized particles will have a different breakage constant throughout the distribution. Hence k_{EB} must be viewed as an average rate constant.

The average rate constant may be described as follows

$$k_{EB} = \sum_{d_{cr}}^{d_{EB\,max}} k_{EBi}(V_i / V_t) \qquad (4)$$

where d_{cr} to d_{max} represents the full size range susceptible to break-up, subscript *i* refers to the specific rate constant for the defined particle population

V_i , V_t is the total particle size distribution susceptible to break-up ie between d_{cr} and d_{EBmax}.

Effect of increased velocity

Figure 4.17 shows the relation between the breakage constant for increasing exposure times for all flow conditions. As velocity increases from 3.1 to 6.2 m/s the average rate constant remains the same; at the higher velocity the rate constant appears to rise.

An explanation is possible for this behaviour by considering the expression for average rate constant (equation 4). As the velocity is increased for a particular size particle k_{EBi} increases and V_i/V_t decreases (ie d_{cr} decreases, increasing $(d_{EBmax}-d_{cr})$ and hence V_t; hence V_t increases for fixed V_i). Assuming these relationships compensate for each other we may then assume k_{EB} (ie the average values) remains constant. This relationship continues until V_t reaches a limit ie the total value of EBs. Then k_{EBi} increases and V_i/V_t is fixed so that k_{EB} increases.

Case (ii) $d_{cr} \approx d_c$

Key assumptions are:

(a) all EBs and intermediate bodies (IBs) break;

(b) only single cells remain in the end;

(c) breakage to form cell debris is assumed negligible;

(d) IBs break with the same breakage constant as that of the EBs ($k_{IB}=k_{EB}$);

(e) IBs break up to release single cells in the same way as EBs ie $m \approx 0.55$ (equation 1).

$$V_{IB\infty}=0,\ V_{EB\infty}=0,\ V_{C\infty}=100 = V_{EBo}$$

$$\frac{dV_{IB}}{dt} = k_{IB}V_{IB}\ ,\ t=\infty,\ V_{IB}=0,\ (k_{IB}=k_{EB})$$

$$\frac{dV_{IB}}{dt} = 0.45\frac{dV_{EB}}{dt} - 0.55\frac{dV_{IB}}{dt} \qquad (5)$$

$$\frac{dVc}{dt} = 0.55\frac{dV_{EB}}{dt} + \frac{dV_{IB}}{dt} \qquad (6)$$

The graphical representation of the above models is shown in figure 4.18 and compared with the experimental data. The model constructed and described in equation 2 was used for the prediction of single cell release matched closely with the experimental data in the cases of 1.55, 3,1 and 6.2 m/s. When the flow velocity was 8.1 m/s it was seen that when no IB breakage was taken into consideration (equation 2) the model was under-predicting the single cell release. When IB breakage was added as an extra factor (equation 6) of single cell release assuming total IB breakage, it was seen that the model predicted higher values of released cells than our data. This lead to the conclusion that IBs were in fact contributing to single cell generation when the suspension was fed through a capillary at 8.1 m/s. Not all of the IBs though were contributing to this process positioning the d_{cr} between 15 and 120 μm. Figure 4.19 shows a schematic representation of the whole process of EB breakage and single cells release.

Summarising, the bodies (both EBs and intermediate bodies) reach a critical value of final size, under which no further breakage is induced. This final size can be correlated with the shear rate (flow intensity) under which the bodies are being exposed. In figure 4.15 the the critical EB size (d_{cr}) and the flow speed are correlated in a semi-logarithmic way ($d_{cr} = 790e^{-0.4v}$). The final size reached is considered to be the size of a single cell (~15μm).

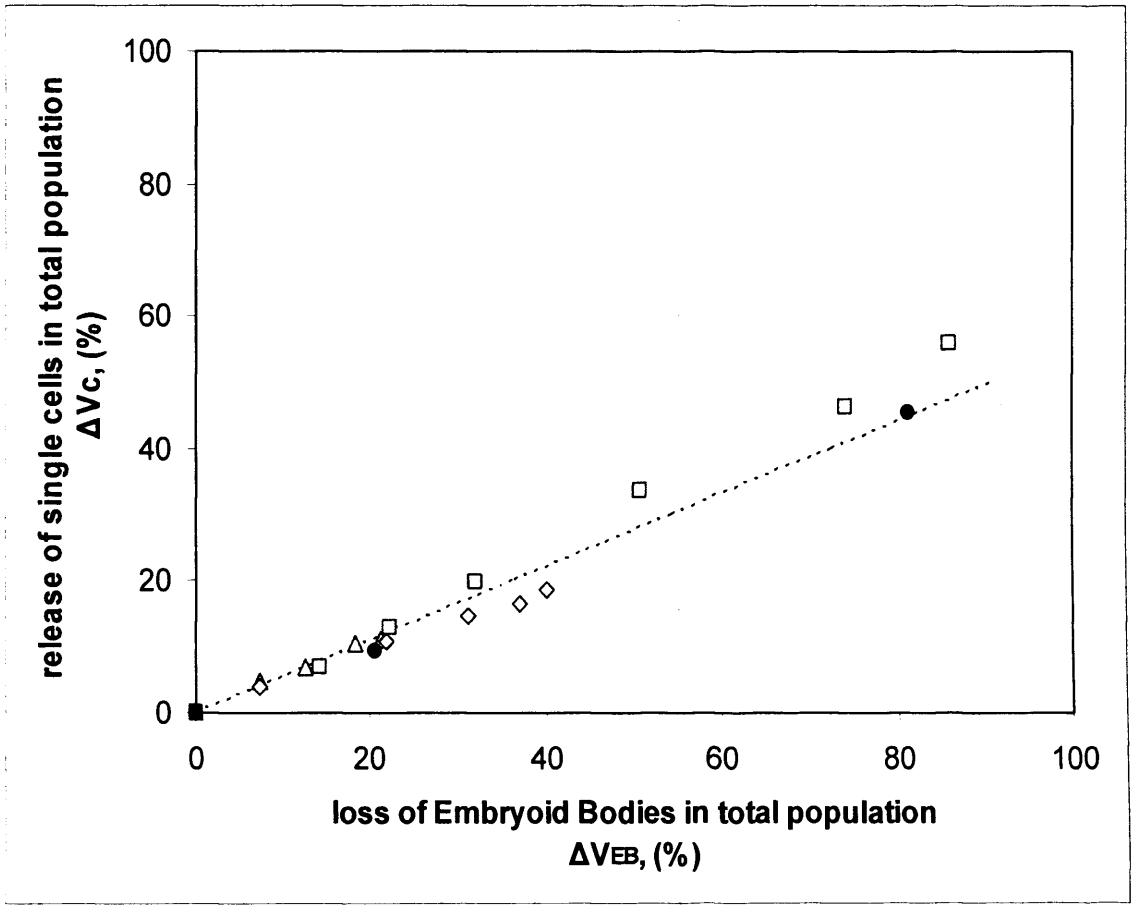

Figure 4.16: Relation between the EB population that breaks-up after flow through the capillary and the released single cell population that results after processing. For all flow conditions it was seen that the proportion of single cells released from the EBs remains constant throughout the range of experimental conditions. The effect of four flow intensities is demonstrated: 1.55 m/s (Δ); 3.1 m/s (◊); 6.2 m/s (□); 8.1 m/s (●).

$\Delta V_C = 0.55 * \Delta V_{EB}$

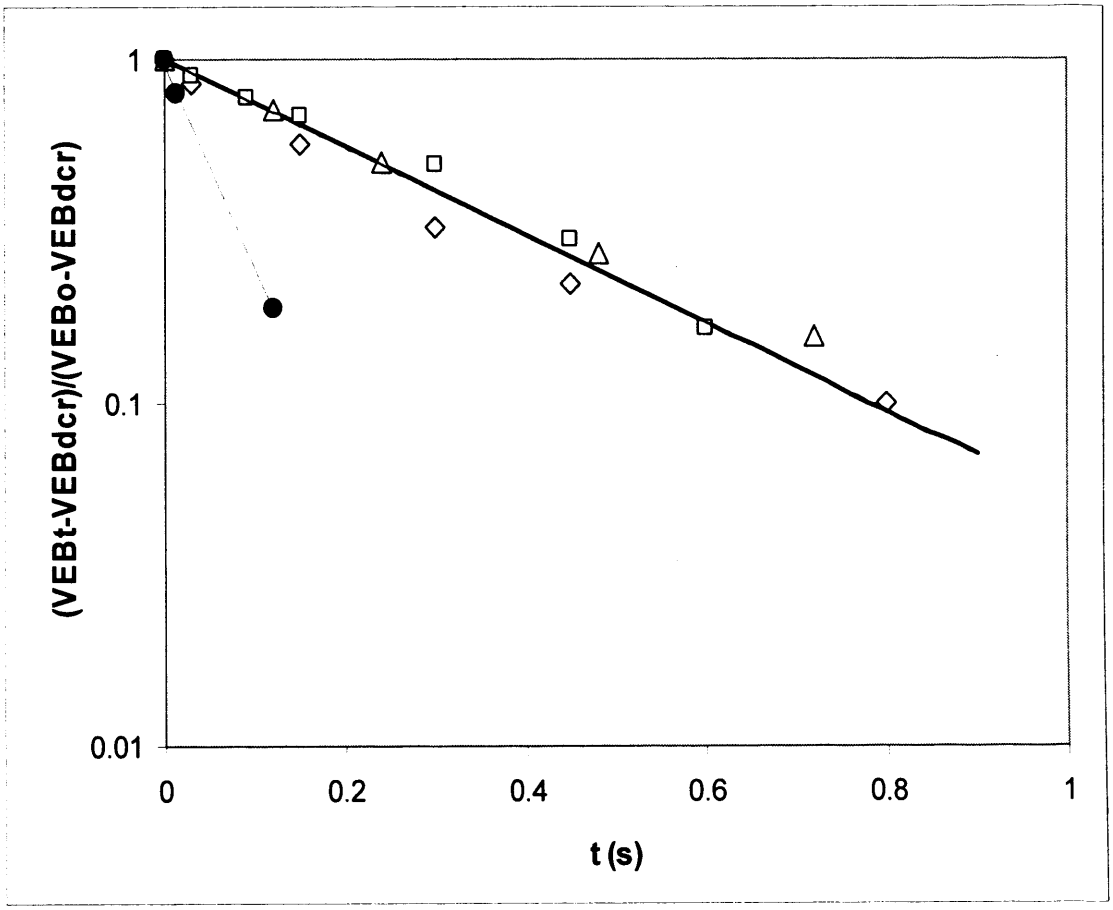

Figure 4.17: First order relation between loss of volume of EBs and exposure time to shear conditions. The EBs were seen to break with an initially constant rate k_{EB} = -2.95 where k_{EB} the (average constant) of the whole EB population in all flow conditions the d_{cr} was seen to be within the size range of the initial EB population. For increasing velocities the d_{cr} is smaller than the smallest EBs of population and the breakage constant was seen to increase to the value of k_{EB}' = -13.72 for a flow with a speed of 8.1 m/s.

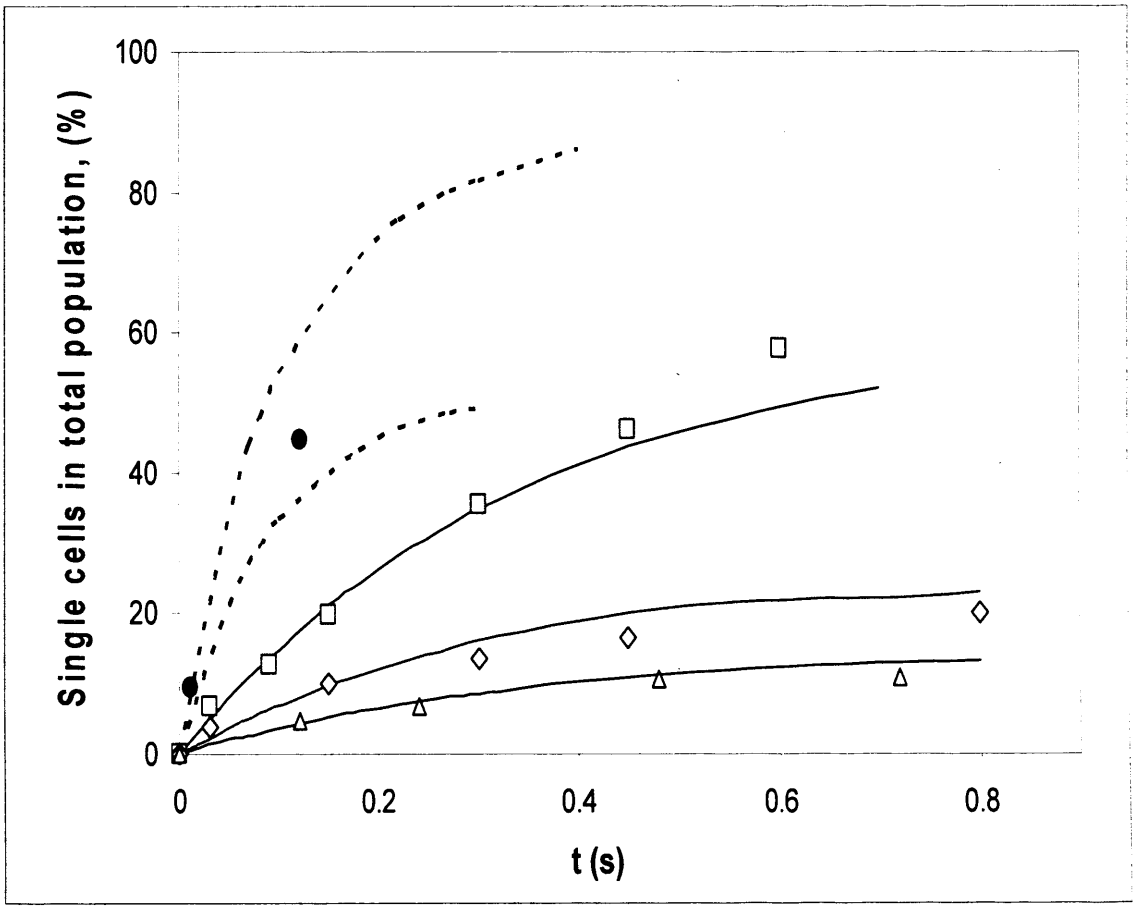

Figure 4.18: Correlation between the predicted single cell release which was calculated by the experimental model (dashed lines) and the experimental values measured for single release. Four different flow intensities are shown. The theoretical values will reach a plateau since only breakage of EBs is considered. Final (plateau reached) single cell values for the experimental model are 16% for 1.55m/s (Δ); 25% for 3.1m/s (◊); 55% for 6.2m/s (□); 55% for 8.1m/s (●). The bold dashed line is an improved model which assumes total EB and Intermediate Body (IB) breakage in the case of the high flow speed (8.1) m.s

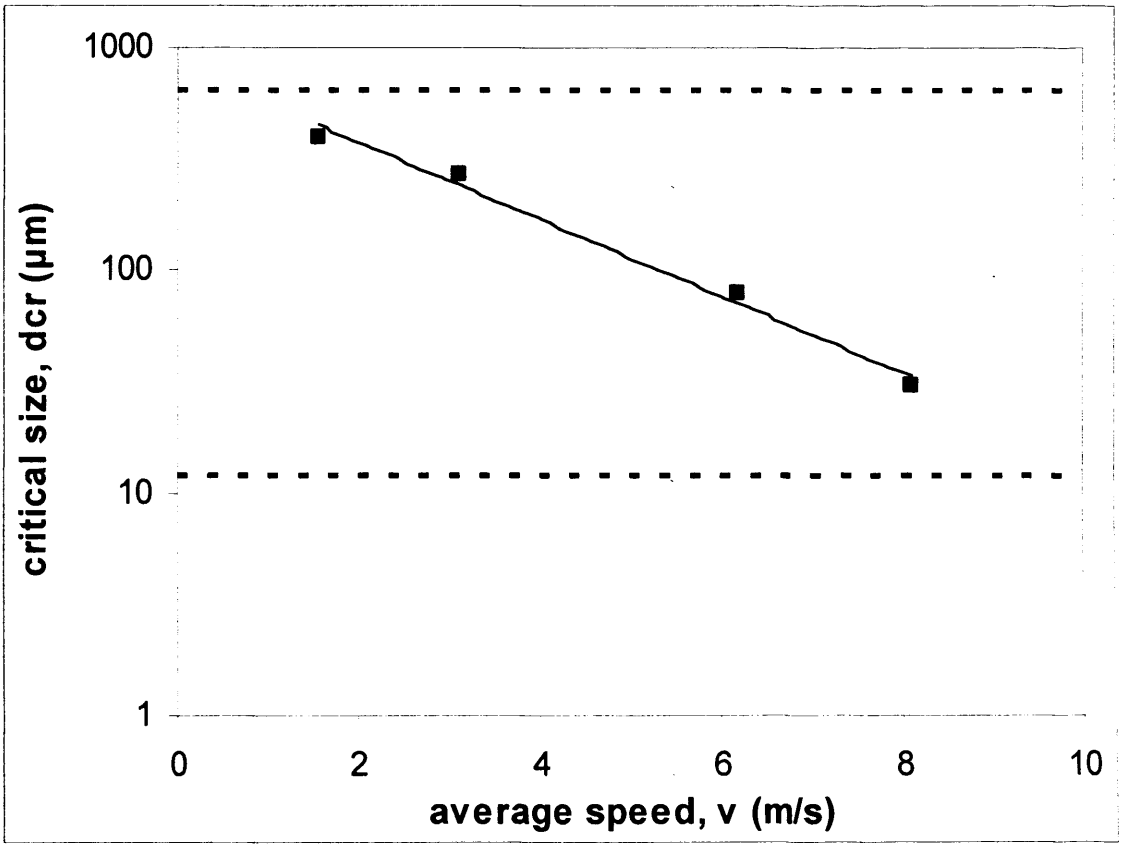

Figure 4.19: The effect of flow intensity on the predicted critical size of the EBs. As critical size we have considered the EB size after which no further breakage is expected to occur for a given flow intensity. The minimum possible value of d_{cr} is when total break-up of EBs and intermediate bodies occurs and is that of a single cell, represented by the lower dashed line. The maximum EB size is represented by the upper dashed line. $d_{cr} = 790e^{-0.4v}$

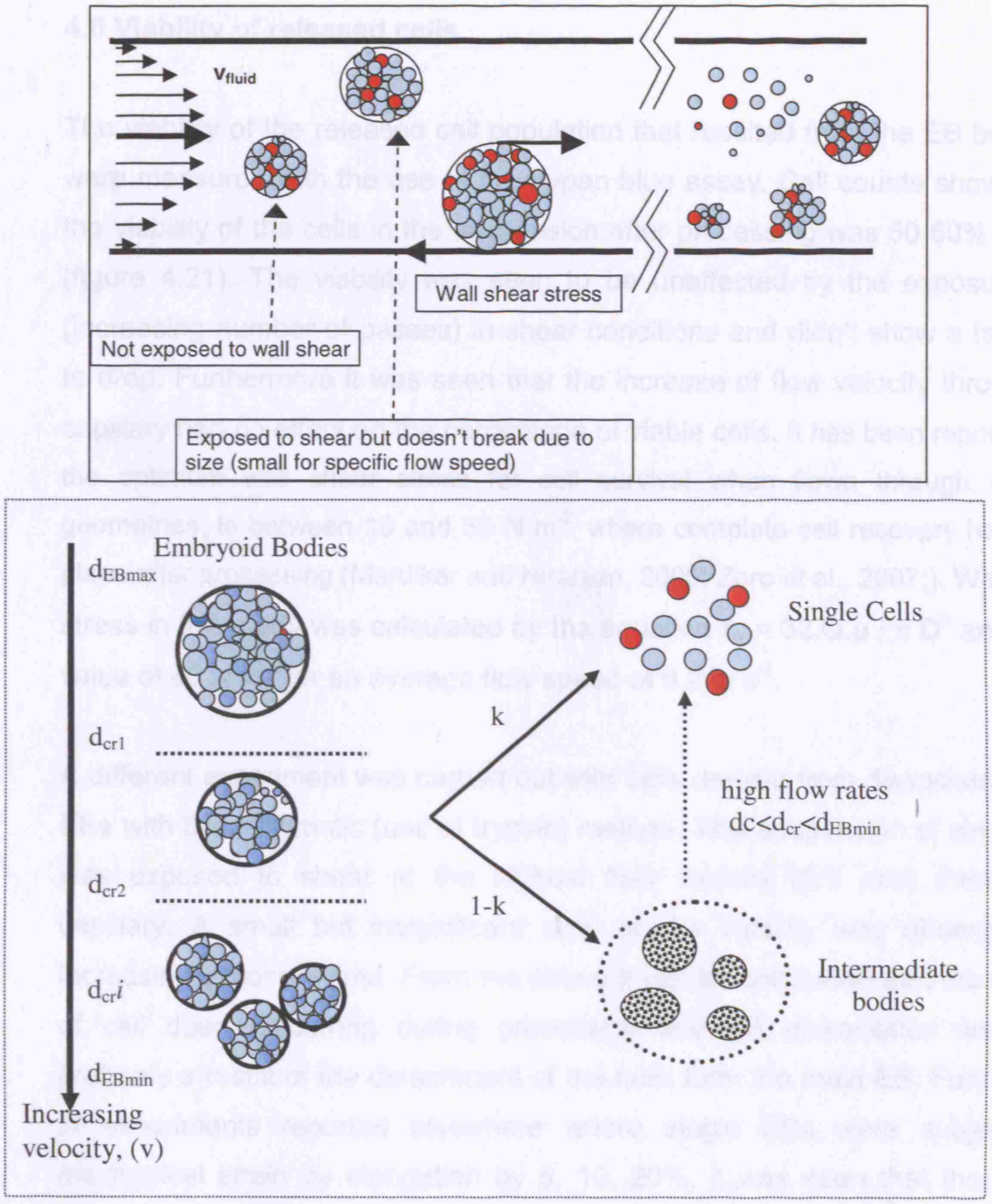

Figure 4.20: Schematic representation of the EB break-up process. The increase of flow rate induces a more extensive breakage of the EB population, moving the critical size (d_{cr}) towards smaller values. The break-up of the EBs generates both single cells and Intermediate bodies. The break-up of the EBs will generate the same proportion of single cells and intermediate bodies for all flow rates. When the flow rate is high enough all of the EB population will eventually be broken-up. Furthermore, provided high enough shear rates can be reached, the intermediate population will further break into single cells as well.

4.6 Viability of released cells

The viability of the released cell population that resulted from the EB breakage were measured with the use of the trypan blue assay. Cell counts showed that the viability of the cells in the suspension after processing was 50-60% (~55%) (figure 4.21). The viability was seen to be unaffected by the exposure time (increasing number of passes) in shear conditions and didn't show a tendency to drop. Furthermore it was seen that the increase of flow velocity through the capillary had no effect on the percentage of viable cells. It has been reported that the optimum wall shear stress for cell survival when flown through capillary geometries, is between 10 and 50 N $m^{-2.}$ where complete cell recovery has taken place after processing (Mardikar and Niranjan, 2000; Zoro et al., 2007;). Wall shear stress in this study was calculated by the equation $\tau_w = 32.Q.\mu / \pi D^3$ and had a value of 43 N m^{-2} for an average flow speed of 6.2 m s^{-1}.

A different experiment was carried out with cells derived from dissociated day 8 EBs with the enzymatic (use of trypsin) method. This suspension of single cells was exposed to shear at the highest flow velocity (8.1 m/s) through the capillary. A small but insignificant drop of cell viability was observed with increasing exposure time. From the above it can be concluded that the majority of cell death occurring during processing and EB dissociation was most probably a result of the detachment of the cells form the main EB. Furthermore in experiments reported elsewhere where single EBs were subjected to mechanical strain by elongation by 5, 10, 20%, it was seen that the applied mechanical strain conditions did not affect the cell viability of ES cells in the EB (Schmelter et al., 2006). This further indicates that the breakage of the cells and the observed loss of viability should be attributed probably to the detachment process of cells from the EB.

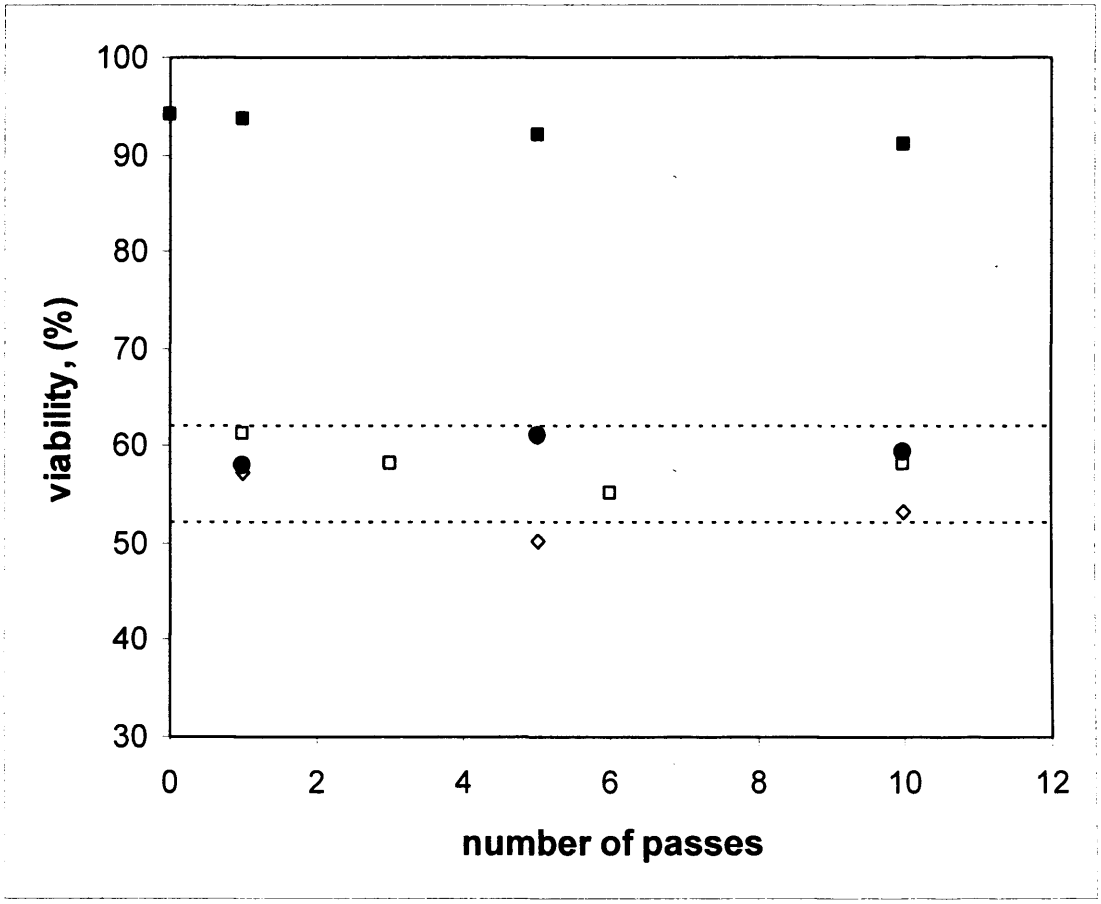

Figure 4.21: Effect of flow intensity and exposure time on the viability of the released single cells after processing. EB's were pumped through a capillary with an inner diameter of 1000 μm. The same exposure time per pass was guaranteed by increasing the length of the capillary when increasing the flow speed. Flow speeds used during the experiment: 3.1m/s (◊); 6.2m/s (□); 8.1m/s (●). In addition EB's were dissociated with an enzymatic method according to which EBs were quenched for 4 minutes in a concentrated trypsin solution (4X) and then pipetted repeatedly until total dissociation of the EBs into single cells. The single cell solution that resulted from this process was then processed in the same capillary system for increasing number of passes with a flow speed of 8.1 m/s (■).

4.5 Discussion

In this chapter the behaviour of EBs exposed to capillary shear conditions was studied. The breakage of the EBs was seen to be a first order relation of the exposure time under standard flow conditions. It has been seen that stem cell exposure to shear stress induces differentiation. There are numerous studies indicating this behaviour. Embryonic stem cells have been seen to differentiate into vascular endothelial cells when exposed to shear conditions (Yamamoto et al., 2005) while endothelial differentiation has been observed be induced on murine embryonic mesenchymal progenitor cell line (Wang et al., 2005) further mechanical-induced cardiovascular differentiation of ESCs has been also observed (Schmelter et al., 2006). In the prementioned studies the exposure time of stem cells was in the order of hours. There is a concern for the effect of shear stress on the differentiation of the neural precursor cells of this study. It must be stressed though that the exposure time of EBs and stem cells to shear conditions didn't exceed 0.45 s which is many orders of magnitude lower than the studies mentioned. In this study stem cells were exposed to shear conditions instantaneously trying to imitate-mimic certain engineering environments that the cells might encounter in lab routine or in future bioprocessing. Taking into consideration the fact that typical cell transfer steps such as aspiration, dispension and pipe flow all involve flows where the cells are exposed for short time periods (sub-second), but may be repeated many times during processing, there is importance for the understanding of such conditions in cell functionality.

CHAPTER 5

Discussion-Future work

5.1 Discussion

This thesis has focused on the study of the effect of shear during bioprocessing using ultra scale-down methods. Ultra scale-down experiments are likely to play an important role in the development of large-scale bioprocesses. Shear studies were carried out using both rotating disc and capillary devices over a range of conditions. Both have important roles in ultra scale-down studies and it is crucial to understand their relationship. In previous chapters the relationship between capillary and rotating disc shear has been discussed (chapter 3) and also the effects of capillary stress on precipitates (chapter 3) and embryoid bodies (chapter 4). This section briefly discusses on the potential for the use of capillary devices in the automated acquisition of experimental bioprocess data.

5.1.1 Use of capillary devices for ultra scale-down studies at the microscale

The ultra scale-down rotating disc device is currently used for the processing of materials in a number of applications. It is a device that is easy to use (fill-process-sample) but has the disadvantage of being suitable for just "one test at a time". Capillary devices could be used similarly for shear processing of biomaterials with the potential of being easily adapted to automated processing. Multi-well plates with working volumes per micro-well ranging from 10 to 1000 μL are being used extensively in biological preparation and research.

The incorporation of capillary micro-devices in automated processes to mimic shear effects of process-scale operations especially in robotic processes where micro-wells are used, could yield a large amount of experimental results. The use of liquid handling systems could lead to highly reproducible techniques something that is of particular importance when dealing with microlitre volumes of material. It could be possible for many process combinations to be studied in

parallel on a single plate when using 96 micro-well plates. A robotic sequence where a capillary could process the material contained in every well can be envisaged. Throughout the plate a range of different experimental conditions could be studied such as the number of passes, the flow rate or the diameter or length of the capillary, could be changed for each plate. A challenge to that end would be to provide pressure drivers capable of producing the desired pressure drops in order to product the high shear rates required. Furthermore the sampling and the way of collecting material in each well after being discharged from the capillary are additional issues to be resolved.

5.1.2 Applications to other biomaterials

In this thesis capillary shear studies were carried out on apparently spheroidal particulate systems such as protein precipitates and embryoid bodies and single cells. It was seen that such a device could be used to study their engineering properties as well as their behaviour under stress conditions during flow. Molecular materials such as DNA have been seen to degrade in the entrance region of the capillary (Meacle et al., 2007 (appendix)). It should be noted that different regions of the capillary might affect materials in diverse ways according to their characteristics. In the case where biomaterials of different geometries should be studied it is possible that in some cases this device might not be suitable. For example filamentous micro organisms have been seen to be affected by turbulent shear (Ayazi Shamlou et al., 1994) but their elongated branched shape might result the blockage of the capillary entrance.

5.1.3 Relation of capillary measurements to full scale processing

A connection between breakage of protein precipitate particles in a capillary and a rotating disc device has been made in this thesis. To date the rotating disc device has been used to predict breakage in process scale equipment. Experiments consisting of direct comparison between ultra scale-down capillaries and pilot scale units could further verify this view. The rotating disc device has been already been used to predict the damage occurring in the feed zone of centrifuges when protein precipitate (Boychyn et al., 2004) and

mammalian cell suspensions (Hutchinson et al., 2006) were processed. So this device is the linking part between the results gained in the capillary and the ones at the process scale. Since in many cases biomaterials can be scarce and expensive and only limited amounts can be used for experimentation, it is of great importance to develop the proper experimentation strategies. This should be done in a way to minimise the necessary experimental procedure while gaining the maximum information. Concerning the capillary an experimental region consisting of a number of different shear rates and a number of passes would describe the large-scale conditions that the biomaterial might experience. The use of extreme conditions of shear could provide the starting point of the sampling process in order to establish the test region of interest (ie maximum shear rate, sufficiently high number of passes) and at the same time save valuable material. Another parameter complicating further such an approach would be to study the effect of the environment on the material (eg pH, ionic strength) that could result in a different reaction to shear. It must be noted that the definition of large scale can vary from one biomaterial to the other. For example for embryoid body production and subsequent processing small volumes (litres) are expected to be needed whereas for protein precipitates large reactors of thousands of litres might be encountered.

Ultra scale-down techniques are required for every unit operation in a process. Once this has been achieved it will be possible to feed material from one scale-down unit to the next making predictions for the behaviour of whole bioprocesses possible. By linking ultra scale-down operations together it will be possible to investigate the complex interactions between processing steps. The ability to run entire bioprocesses at these scales fully representative of the large-scale could be included into process validation protocols during which process control limits are set and tested. The availability of scale-down techniques would allow simultaneous testing of a large combination of process limits to ensure safe and effective operation. Scale-down techniques have been studied concerning upstream and downstream processing. Techniques allowing more rapid process development with small volumes of process materials are required

5.2 Future work

Both the protein precipitate and the EB suspension provided systems of direct relevance to large-scale bioprocess. They are however both complex in nature and in both cases an understanding of the fluid environment and of the material properties is needed to interpret the experimental results. In this chapter some suggestions concerning new directions of research are given.

5.2.1 Exposure of biomaterials in different flow fields

The use a capillary system was predominant and it was possible to compare capillary and rotational devices using protein precipitates. Devices with different geometries could be used to break-up EBs. It is anticipated that exposure of EBs to different flow fields, could induce breakage with different mechanisms. The rotating disc device could be an alternative suggestion where the EBs would be exposed to a more turbulent flow field, while the use of jets and the effect of impact forces could be studied as well. Concerning the protein precipitate suspensions, the use of orifice devices could be used as another way of simulating local high shear areas in bioprocess equipment.

5.2.2 Use of capillary device for 'screening' engineering properties of biomaterials

As seen earlier, capillary devices provide the potential for automated studies of the properties of biomaterials and the effect of exposure to shear stress. Furthermore, the response to shear stress could be affected by the controlling the flow environment of the material the way it is produced etc. An automated system would depend on the design of capillary systems capable of shearing the material in a carefully defined manner. The use of sample processes must match the analytical devices to be used eg for light scattering (particle sizing) measurements –μL quantities are sufficient but for many biological assays large volumes are needed. Considerable attention could be needed to the design of experimentation in order to maximize the use of biological material where only a

few millilitres are available and where analytical methods are difficult to be used.

5.2.3 Controlled growth of EBs

The wide size distribution of the EB population in this study gained in a static culture environment, had as a result a complex behaviour of the population during its flow. A 'conditioning' and a better control of the size distribution of the EBs could be achieved with the use of shaker flask cultures (Dang et al., 2001) or stirred tank cultures (Cameron et al., 2006; Fok and Zandstra, 2005) or in micro-wells with a standard starting inoculation density per well . Processing a narrower particle size distribution would require fewer assumptions during the construction of the model.

5.2.4 Earlier processing of EBs

Capillary shear processing resulted in a 40% loss of cell viability as measure in this study. Youngs modulus measurements and optical observation during the development of the EB over time suggested that the EB obtains a stiffer and more organised structure. Processing of the EB suspension at an earlier stage of the EB growth could allow an understanding of the effect of their "stiffness" or cell-cell bonding on cell death of released cells. This will lead to an understanding of how EB

5.2.5 Combined trypsin and shear method

In the previous section processing of EBs earlier in their development was suggested. A method that could be used way for weakening the bonds between the cells (due to extra-cellular matrix) of the EB prior to shear would the exposure to a trypsin solution. The use of a more dilute trypsin solution, than the one that is currently required, and exposure EBs for less time followed by shear processing could yield a higher viable cell population. In this way the negative effects of both processes could be possibly avoided. Gene expression

analysis should be followed in this case in order to observe the biological effect of this method.

5.2.6 Single EB processing

The study of shear effects on single EBs would give a more clear insight on the mechanisms of breakage. Flow of a single EB through a transparent capillary could reveal more details concerning the EB break-up process. With the use of a high speed camera optical observations of this process could be made. Such a research direction moves away from a bio-processing point of view where suspension of EBs was used and a statistical and average approach was made. This focuses more on the properties of single bodies but this could give a fundamental knowledge on the behaviour of EBs.

5.2.7 Other biological materials to be studied

By standardizing shear studies ie the effect of different parameters on the breakage of biomaterials and by understanding the mechanism of their breakage, it would be valuable to expand to similar studies on a range of other biomaterials. Capillary micro-devices could be used to study in order to broaden the knowledge of shear effects on biomaterials under processing. Due to differences in particle structure it is expected that particle reaction when exposed to shear will be give different for different flow conditions. Examples include biological flocs which are generally weaker than precipitates through to more brittle crystal structures. Alternatively cellular suspension could be further studied where the cells are to be removed eg mammalian cells during antibody production, or in situations where cells are to be used eg stem cell for cell-therapy.

CHAPTER 6

Conclusions

A connection between protein precipitate breakage results gained in a capillary ultra scale-down device and a rotating disc device was made. The length (which controlled the exposure time to shear conditions) and the flow intensity with which protein precipitates were flown through a capillary were correlated to the rotational speed of the rotating disc device. This correlation was obtained with the use of the boundary layer volume and the maximum shear rate as connecting parameters. It was seen that the continuous exposure time and the use of longer capillaries could better mimic the breakage obtained in rotating disc devices even though the maximum shear rates obtained in the capillary device were two orders of magnitude higher. With the use of capillary devices smaller volumes of material are needed to be processed while a range of flow conditions can be developed in order to better simulate what happens in process operations. To predict fluid mixing rates and fluid stress levels within equipment, Computational Fluid Dynamics (CFD) was utilised. The CFD predictions were validated against experimental observations and proved useful in understanding the fluid dynamical behaviour in a model fluid stress device. This demonstrates the effect of CFD as an engineering tool for designing and optimising bioprocesses.

The capillary system was further used for the controlled processing of embryoid bodies (EBs) since only small quantities of this material were available for experimentation. It was seen that the break-up was a function of both the amount of shear as well as of the exposure time of the particle in the sheared environment. Total breakage of the embryoid bodies was observed when material was exposed to sufficiently high flow velocities. An experimental model was constructed predicting EB breakage and single cell release during flow through a capillary device. The breakage of the EBs was seen to be a first order relation of the exposure time under flow conditions. An average apparent rate constant was obtained in order to characterize the breakage rate of the EB

population and was related semi-logarithmically to the average flow velocity with which the EB suspension was flown through the capillary. The viability of the released cells was seen to be unaffected by the exposure time (increasing number of passes) in shear conditions and didn't show a tendency to drop. Furthermore it was seen that the increase of flow speed through the capillary had no effect on the percentage of viable released cells. This indicates that the breakage of the cells and the observed loss of viability should be attributed to the detachment process of cells from the EB.

REFERENCES

Adam, R., Zimm, B. (1977). Shear degradation of DNA. Nucleic Acids Research. 4 (5), 1513-1536.

Al-Rubeai, M., Singh, R.P., Goldman, M.H., & Emery, A.N. (1995). Death mechanisms of animal cells in conditions of intense agitation. Biotechnol. Bioeng. 45, 463-472.

Austin, L., (2002). A treatment of impact breakage of particles, Powder Technology, 126, 85–90.

Ayazi Shamlou, P., Stavrinides, S., Titchener-Hooker, N., Hoare, M. (1994a) Growth-independent breakage frequency of protein precipitates in turbulently agitated bioreactors, Chem. Eng Sci., 49, 2647–2656.

Ayazi Shamlou, A., Stavrinides, S., Titchener-Hooker, N.J., Hoare, M., (1996) Turbulent breakage of protein precipitates in mechanically stirred bioreactors. Bioprocess Engineering 14, 237-243.

Bagutti, C., Wobus, A.M., Fassler, R. & Watt, F.M. (1996). Differentiation of embryonal stem cells into keratinocytes: comparison of wild-type and beta 1 integrin-deficient cells. Dev. Biol., 179: 184-196.

Bain, G., Kitchens, D., Yao, M., Huettner, J.E., Gottlieb, D.I. (1995). Embryonic stem cells express neuronal properties in vitro. *Dev. Biol.* 168,342–57.

Barberi, T., Klivenyi, P., Calingasan, N.Y., Lee, H., Kawamata, H., Loonam, K., Perrier, A.L., Bruses, J., Rubio, M.E., Topf, N., et al (2003) Neural subtype specification of fertilization and nuclear transfer embryonic stem cells and application in Parkinsonian mice. Nat. Biotechnol., 21, 1200-1207.

Bell, D.J. & Dunnill, P., (1982a). Shear disruption of soya protein precipitate particles and the effect of ageing in a stirred tank. Biotechnology and Bioengineering, 24, 1271-1285.

Bell, D.J. & Dunnill, P., (1982b). The influence of precipitation reactor configuration on the centrifugal recovery of isoelectric soya protein precipitate. Biotechnology and Bioengineering, 24, 2319-2336.

Bell, D.J., Hoare, M., & Dunnill, P., (1983). The formation of protein precipitates and their centrifugal recovery. Advances in Biochemical Engineering, 26, 1-72.

Biscans, B., Guiraud, P., Laguérie, C., Massarelli, A., Mazzarotta, B., (1996). Abrasion and breakage phenomena in mechanically stirred crystallizers, The Chemical Engineering Journal, 63, 85-91.

Born, C., Zhang, Z., Al-Rubeai, M., & Thomas, C.R. (1992) Estimation of disruption of animal cells by laminar shear stress. Biotechnol. Bioeng. 40, 1004-1010.

Bowman, R., Davidson, N. (1972). Hydrodynamic shear breakage of DNA. Biopolymers. 11, 2601-2624.

Boychyn, M., Yim, S.S.S., Ayazi Shamlou, P., Bulmer, M., More, J., & Hoare, M. (2001). Characterization of flow intensity in continuous centrifuges for the development of laboratory mimics. Chem eng sci, 56 (16), 4759-4770.

Brown, G., Miles, N., & Jones, T., (1996). A fractal description of the progeny of single impact single particle breakage, Minerals Engineering, 9, 715–726.

Brown L., & Glatz, C.E. Aggregate breakage in protein precipitation, Chem Eng Sci, 42, 1831–1839.

Brustle, O., Jones, K.N., Learish, R.D., Karram, K., Choudhary, K., Wiestler, O.D., et al. (1999). Embryonic stem cell-derived glial precursors: a source of myelinating transplants. Science, 285, 754–756.

Burgi, E., & Hershey, A. (1962). Specificity and concentration limit in self-protection against mechanical breakage of DNA. Journal of Molecular Biology. 4, 313-315.

Buttery, L.D.K., Bourne, S., Xynos, J.D., Wood, H., Hughes, F.J., Hughes, S.P.F., Episkopou, V., & Polak. J.M. (2001). Differentiation of Osteoblasts and *in Vitro* Bone Formation from Murine Embryonic Stem Cells Tissue Engineering, 7(1), 89-99.

Byrne, E.P., Fitzpatrick, J.J., Pampel, L.W., Titchener-Hooker, N.J., (2002) Influence of shear on particle size and fractal dimension of whey protein precipitates: implications for scale-up and centrifugal clarification efficiency. Chemical Engineering Science, 57, 3767-3779.

Cameron, C.M., Hu, W.S., Kaufman, D.S. (2006). Improved development of human embryonic stem cell-derived embryoid bodies by stirred vessel cultivation. Biotechnol Bioeng, 94 (5), 938-48.

Carpenter, M.K., Inokuma, M.S., Denham, J., (2001) Enrichment of neurons and neural precursors from human embryonic stem cells. Exp Neurol, 172,383-397.

Chan, M.Y.Y., Hoare, M., Dunnill. P., (1986) The kinetics of protein precipitation by different reagents, Biotechnol. Bioeng, 28, 387-393.

Cherry, R.S., Papoutsakis, E.T. (1989) Growth and death rates of bovine embryonic kidney cells in turbulent microcarrier bioreactor, Bioprocess Eng., 4 81–89.

Chisti, Y., (2000). Animal-cell damage in sparged bioreactors. Trends Biotechnol. 18, 420-432.

Chisti, Y., (2001). Hydrodynamic damage to animal cells, Crit Rev Biotech. 21(2), 67-110.

Dang, S.M., Gerecht-Nir, S., Chen, J., Itskovitz-Eldor J. & Zandstra, P.W. (2004). Controlled, scalable embryonic stem cell differentiation culture, Stem Cells, 22, 275–282.

Dang, S.M., Kyba, M., Perlingeiro, R., Daley, G.Q., Zandstra, P.W. (2002). Efficiency of embryoid body formation and hematopoietic development from embryonic stem cells in different culture systems. Biotechnol. Bioeng., 78(4), 442–453.

Dani, C,. (1999) Embryonic Stem Cell-Derived Adipogenesis. Cells Tissues Organs, 165, 173-180.

Datar, R. (1986). Economics of primary separation steps in relation to fermentation and genetic engineering, *Process Biochemistry*, 21, 19-26.

Devereux, N., Hoare, M., Dunnill, P. (1984). The development of improved methods for the initial recovery of protein precipitates in "Solid – Liquid separation" Gregory, J., Society of Chem. Ind., Ellis Horwood (Pub.), 143-160.

Doetschmann, T.C., Eistetter, H., Katz, M., Schmidt, W., & Kemler, R. (1985) The in-vitro development of blastocyst-derived embryonic stem cell lines: formation of visceral yolk sac, blood islands and myocardium. J. Embryol. Exp. Morphol., 87, 27-45.

Draper, J.S., Moore, H.D., Ruban, L.N., Gokhale, P.J., & Andrews, P.W. (2004). Culture and characterization of Human Embryonic stem cells. Stem cells and development. 13, 325–336.

Evans M.J., Kauffman M.H. (1981) Establishment in culture of pluripotent cells from mouse embryos. Nature, 292, 154-156.

Fairchild, P., Brook, F., Gardner, R., Graça, L., Strong, V., Tone, Y., Nolan, K., Waldmann, H. (2000). Directed differentiation of dendritic cells from mouse embryonic stem cells. Current Biology, 10 (23), 1515-1518.

Fahrner, R. (1993). New role for pilot plants in product development, *Biopharm*, April, 34-37.

Firth, B.A., & Hunter R.J., J. Colloid Interface Sci., (1976) 33,1631.

Fisher, R.R., & Glatz, C.E. (1988a) Polyelectrolyte precipitation of proteins: I. The effect of reactor conditions, Biotechnol. Bioeng., 32, 777-785.

Fisher, R.R., & Glatz, C.E. (1988b) Polyelectrolyte precipitation of proteins: II. Models of the particle size distributions, Biotechnol. Bioeng., 32, 786-796.

Fisher, R.R., Glatz, C.E., & Murphy, P.A. (1986) Effects of mixing during acid addition on fractionally precipitated protein . Biotechnol. Bioeng. 28, 1056-1063.

Fleischmann, M., Bloch, W., Kolossov, E., Andressen, C., Muller, M. (1998). Cardiac specific expression of the green fluorescent protein during early murine embryonic development. FEBS Lett. 440, 370–76.

Fok, E.Y.L., Zandstra, P.W. (2005). Shear controlled single step mouse embryonic stem cell expansion and embryoid body based differentiation. Stem Cells, 23, 1333-1342.

Foster, P. R., Dunnill, P., & Lilly, M.D., (1976) The Kinetics of Protein Salting-out: Precipitation of Yeast Enzymes by Ammonium Sulphate. *Biotechnol. Bioeng.* , 18, 545.

Fraichard, A., Chassande, O., Bilbaut, G., Dehay, C., Savatier, P., and Samarut, J. (1995). In vitro differentiation of embryonic stem cells into glial cells and functional neurons. J.Cell Sci., 108, 3181–3188.

Galinat, S., Masbernat, O., Guiraud, P., Dalmazzone, C., & Noik, C., (2005) Drop break-up in turbulent pipe flow downstream of a restriction, Chemical Engineering Science, 60, 6511–6528.

Gerecht-Nir, S., Cohen. S., Itskovitz-Eldor, J., (2003), Bioreactor cultivation enhances the efficiency of human embryoid body (hEB) formation and differentiation, 86 (5), 493-502.

Gilbertson, J.A., Sen, A., Behie, L.A., &. Kallos, M.S. (2006). Scaled-up production of mammalian neural precursor cell aggregates in computer-controlled suspension bioreactors, Biotechnol. Bioeng. 94 (4), 783–792.

Glatz C.E., Hoare, M., Landa-Vertiz, J. (1986) The formation and growth of protein precipitates in a continuous stirred tank reactor. AIChE J., 32, 1196-1204.

Guan, K., Chang, H., Rolletschek, A., and Wobus, A. M. (2001). Embryonic stem cell-derived neurogenesis. Retionic acid induction and lineage selection of neuronal cells. Cell Tissue Res., 305, 171–176.

Hagesaether, L., Jakobsen, H.A., & Svendsen, H.F. (2002) Modeling of the dispersed-phase size distribution in bubble columns, Industrial Engineering Chemistry Research 41, 2560–2570.

Hershey, A., & Burgi, E. (1960). Molecular homogeneity of the deoxyribonucleic acid of phage T2. Journal of Molecular Biology. 2, 143-152.

Hoare, M. (1982a) Protein precipitation and precipitate ageing, Part I: Salting out and ageing of casein precipitates, Trans. IChemE, 60, 79-87.

Hoare, M. (1982b) Growth of protein precipitates during hindered settling or exposure to shear, Trans IChemE, 60, 157–163.

Hoare, M., Bell, D.J., & Dunnill, P. (1984) Process design for the recovery of food proteins by precipitation and centrifugation, Engng and Food, 2, 691–700.

Hoare, M., & Dunnill, P., (1986a). Protein processing-the immediate challenge. The Chemical Engineer, December, 23-25.

Hoare, M., & Dunnill, P., (1989). Biochemcial engineering challenges of purifying useful proteins. Phil. Trans. R. Soc. Lond. B324, 497-507.

Hutchinson, N., Bingham, N., Murrell, N., Farid, S., & Hoare, M. (2006). Shear stress analysis of mammalian cell suspensions for prediction of industrial centrifugation and its verification. Biotech Bioeng., 95 (3), 483-491.

Kallos, M.S., et al., (1998) High cell density growth of mammalian neural stem cells as aggregates in bioreactors, in Fluidization IX, Engineering Foundation: New York., 653-660.

Kallos, M.S., Behie, L.A., Vescovi, A.L. (1999). Extended serial passaging of mammalian neural stem cells in suspension bioreactors. Biotechnol Bioeng. 65(5), 589-99.

Kawasaki, H., Mizuseki, K., Nishikawa, S., Kaneko, S., Kuwama, Y., Nakanishi, S., Nishikawa, S.I., & Sasai, Y. (2000). Induction of midbrain dopaminergic neurons from ES cells by stromal cell-derived inducing activity. Neuron, 28, 31-40.

Keller, G.M. (1995). In vitro differentiation of embryonic stem cells. Curr Opinion Cell Bio, 7, 862-869.

Keller, G. (2005) Embryonic stem cell differentiation: emergence of a new era in biology and medicine. Genes Dev, 19, 1129 –1155.

Kim, J.H, Auerbach, J.M., Rodríguez-Gómez, J.A., Velasco, I., Gavin, D., Lumelsky, N., Lee, S.H., Nguyen, J., Sánchez-Pernaute, R., Bankiewicz, K., & McKay, R. (2002). Dopamine neurons derived from embryonic stem cells function in an animal model of Parkinson's disease. Nature, 418, 50-56.

Kobayashi, M. (2004). Breakup and strength of polystyrene latex flocs subjected to a converging flow. Colloids and Surfaces A: Physicochemical and EngineeringAspects, 235 (1-3), 73-78.

Kramer, J., Hegert, C., Guan, K., Wobus, A. M., Müller, P. K. & Rohwedel, J. (2000). Embryonic stem cell-derived chondrogenic differentiation in vitro: activation by BMP-2 and BMP-4. Mech. Dev., 92,193-205.

Kunz, I.D., Kauzmann, W., (1974). Hydration of proteins and polypeptides. Adv. Protein Chem., 28, 239–345.

Lakhotia, S., Bauer, K.D., & Papoutsakis, E.T. (1992), Damaging agitation intensities increase DNA-synthesis rate and alter cell-cycle phase distributions of CHO cells, Biotechnol. Bioeng. 40, 978-990.

Lee, S-H., Lumelsky, N., Studer, L., Auerbach, J. M., and McKay, R. D. (2000). Efficient generation of midbrain and hindbrain neurons from mouse embryonic stem cells. Nat. Biotechnol., 18, 675–679.

Levy, M., Collins, I., Yim, S., Ward, J., Titchener-Hooker, N., Ayazi Shamlou, P., Dunnill, P. (1999). Effect of shear on plasmid DNA in solution. Bioprocess Engineering. 20, 7-13.

Li, M., Pevny, L., Lovell-Badge, R., & Smith, A. (1998) Generation of purified neural precursors from embryonic stem cells by lineage selection. Curr. Biol., 8, 971-974.

Liu, S., Qu, Y., Stewart, T.J., Howard, M.J., Chakrabortty, S., Holekamp, T.F., & McDonald J.W. (2000). Embryonic stem cells differentiate into oligodendrocytes and myelinate in culture and after spinal cord transplantation, PNAS, 97 (11), 6126-6131.

Luo & Svendsen, H.F. (1996) Theoretical model for drop and bubble breakup in turbulent dispersions, *A.I.Ch.E. Journal,* 42, 1225–1233.

Lysaght, M.J., & Hazlehurst, A.L. (2004). Tissue engineering: the end of the beginning. Tissue Eng., 10 (1-2), 309-20.

Maitra, A., Arking, D.E., Shivapurkar, N., Ikeda, M., Stastny, V., Kassauei, K., Sui, G., Cutler, D.J. et al (2005) Genomic alterations in cultured human embryonic stem cells, Nature Genetics, 37, 1099-1103.

Maltsev VA, Rohwedel J, Hescheler J, Wobus AM. (1993). Embryonic stem cells differentiate in vitro into cardiomyocytes representing sinusnodal, atrial, and ventricular cell types. Mech Dev 44(1), 41–50.

Manweiler, K., & Hoare, M. (1992). The scale-down of an industrial disc stack centrifuge. Bioprocess engineering, 8, 19-25.

Mardikar, S.H., & Niranjan, K., (2000). Observations on the shear damage to different animal cells in a concentric cylinder viscometer. Biotechnol Bioeng., 68(6), 697-704.

Martin, G. R. (1981). Isolation of a pluripotent cell line from early mouse embryos cultured in medium conditioned by teratocarcinoma stem cells. Proc. Natl. Acad. Sci. USA, 78, 7634–7638.

Mason, C., Hoare, M., (2006). Regenerative Medicine Bioprocessing: Building a Conceptual Framework Based on Early Studies. Tissue Engineering, 13(2): 301-311.

McQueen, A., Meilhoc, E., & Bailey, J.E., (1987). Flow effects on the viability and lysis of suspended mammalian cells. Biotechnol. Lett., 9, 831-836.

Meacle, F.J., Zhang, H., Papantoniou, I., Ward, J.M., Titchener-Hooker, N.J., Hoare, M. (2007). Degradation of supercoiled plasmid DNA within a capillary device, Biotechnol Bioeng, 97 (5), 1148-1157.

Mendez, I., Sanchez-Pernaute, R., Cooper, O., Vinuela, A., Ferrari, D., Bjorklund, L., Dagher, A., Isacson, O. (2005). Cell type analysis of functional fetal dopamine cell suspension transplants in the striatum and substantia nigra of patients with Parkinson's disease. Brain Advance Access. published on May 4.

Menter, F.R., (1996). A comparison of some recent eddy-viscosity turbulence models, Journal of Fluids Engineering, 118 (3), 514 – 519.

Moreira, J.L., Santana, P.C., Feliciano, A.S., Cruz, P.E., Racher, A.J., Griffiths, J.B., Carrondo, M.J. (1995). Effect of viscosity upon hydrodynamically controlled natural aggregates of animal cells grown in stirred vessels. Biotechnol Prog, 11 (5), 575-83.

Nakano T. (1996). In vitro development of hematopoietic system from mouse embryonic stem cells: a new approach for embryonic hematopoiesis. Int J Hematol., 65 (1), 1-8.

Nishikawa, S.I., Nishikawa, S., Hirashima, M., Matsuyoshi, N., Kodama, H. (1998). Progressive lineage analysis by cell sorting and culture identifies FLK1+VE-cadherin+ cells at a diverging point of endothelial and hemopoietic lineages, Development , 125 (9), 1747-1757.

North, P., Champion, J. (1974). Hydrodynamic Degradation of DNA. Journal De Chimie Physique.71(10), 1284.

Odell, J., Taylor, M. (1994). Dynamics and thermomechanical stability of DNA in solution. Biopolymers. 34, 1483-1493.

Okabe, S.,Forsberg-Nilsson, K.,Spiro, A.C., Segal, M., & McKay, R.D., (1996) Development of Neuronal Precursor Cells and Functional Postmitotic Neurons from Embryonic Stem Cells *in vitro*, *Mech. Dev.*, 59, 89-102.

Palacios, R., Golunski, E., Samaridis, J. (1995) In vitro generation of hematopoietic stem cells from an embryonic stem cellline. Proc. Natl. Acad. Sci. *USA,* 92, 7530–7534

Petenate, A., Glatz, C. (1983a) Isoelectric precipitation of soy protein: I. Factors affecting particle size distribution. Biotechnol. Bioeng., 25, 3049-3058.

Petenate, A., Glatz, C. (1983a) Isoelectric precipitation of soy protein: II. Kinetics of protein aggregate growth and breakage. Biotechnol. Bioeng. 25, 3059-3078.

Potocnik, A.J., Nielsen, P.J., & Eichmann, K. (1994). In vitro generation of lymphoid precursors from embryonic stem cells. EMBO J., 13(22), 5274–5283.

Redber, S., (1990) Statistical Models for the Fracture of Disorder Media, Elsevier Science, The Netherlands.

Reubinoff, B.E., Itsykson, P., Turetsky, T., Pera, M.F., Reinhartz, E., Itzik, A., Ben-Hur, T. (2001) Neural progenitors from human embryonic stem cells. *Nat Biotechnol.* 19, 1134-1140.

Reynolds, B.A., & Weiss, S. (1992) Generation of neurons and astrocytes from isolated cells of the adult mammalian central nervous system. Science, 255, 1707-1710.

Reynolds B.A., & Weiss, S. (1996) Clonal and population analyses demonstrate that an EGF-responsive mammalian embryonic CNS precursor is a stem cell. Dev Biol, 175, 1-13.

Risau, W., Sariola, H., Zerwes, H.G., Sasse, J., Ekblom, P., Kemler, R., & Doetschman, T. (1988). Vasculogenesis and angiogenesis in embryonic-stem-cell-derived embryoid bodies Development, 102 (3), 471-478.

Rohwedel, J., Maltsev, V., Bober, E., Arnold, H.H., Hescheler, J., Wobus, A.M. (1994). Muscle cell differentiation of embryonic stem cells reflects myogenesis in vivo: developmentally regulated expression of myogenic determination genes and functional expression of ionic currents. Dev. Biol.164, 87–101.

Rothstein, F. (1994). Differential precipitation of proteins: science and technology. In: Protein process engineering. New York: Marcel Dekker.115–208.

Schmelter, M., Ateghang B., Helmig, S., Wartenberg, M., & Sauer, S. (2006). Embryonic stem cells utilize reactive oxygen species as transducers of mechanical strain-induced cardiovascular differentiation, The FASEB Journal. 20 (1), 182-1184.

Schuldiner, M., Yanuka, O., Itskovitz-Eldor, J., Melton, D. A., and Benvenisty, N. (2000). Effects of eight growth factors on the differentiation of cells derived from human embryonic stem cells. Proc. Natl. Acad. Sci. USA, 97, 11307–11312.

Selomulya, C., Bushell, G., Amal, R., & Waite, T. (2003). Understanding the role of restructuring in flocculation: the application of a population balance model, Chem Eng Sci, 58, 327–338.

Sen, A., Kallos, M.S., Behie, L.A. (2001). Effects of hydrodynamics on culture of mammalian neural stem cell aggregates in suspension bioreactors. Ind Eng Chem Res., 40, 5350-5357.

Sen, A., Kallos, M.A., &. Behie, L.A. (2002) Expansion of mammalian neural stem cells in bioreactors: effect of power input and medium viscosity. Brain Res Dev Brain Res, 134 (1-2), 103-13.

Sen, A., Kallos, M.S., Behie, L.A. (2004). New tissue dissociation protocol for scaled-up production of neural stem cells in suspension bioreactors. Tissue Engineering,2004,10(5-6),904-913.

Serra, T., Colomer, J., Casmitjana, X., (1997) Aggregation and break-up of particles in a shear flow. Journal of Colloid and Interface Science 187, 466-473.

Smith, A.G., Heath, J.K., Donaldson, D.D., Wong, G.G., Moreau, J., Stahl M. & D. Rogers, D. (1988). Inhibition of pluripotential embryonic stem cell differentiation by purified polypeptides, *Nature,* 336, 688–690.

Smith, A.G. (1991) Culture and differentiation of embryonic stem cells, Methods in cell science, 13(2), 89-94.

Smith, A.G. (2001). Embryo-derived stem cells: of mice and men, Annu Rev Cell Dev Biol, 17, 435–462.

Spiegel, T. (1999) Whey protein aggregation under shear conditions –effects of lactose and heating temperature on aggregate size and structure. International journal of Food Science and Technology, 34, 523-531.

Stavrinides, S., Ayazi-Shamlou, P., Hoare, M. (1993). Effects of engineering parameters on the precipitation, recovery and purification of proteins, in "Processing of Solid - Liquid Suspensions", Butterworth Heinmann, 118-158.

Stewart, C.L., Kaspar, P., Brunet, L.J., Bhatt, H., Gadi, J., Kontgen, F., & Abbondanzo, S.J., (1992). Blastocyst implantation depends on maternal expression of leukemia inhibitory factor. *Nature* 359, 76–79

Stone, A. (2003). FDA Issues Felled Advanced Tissue Sciences. Genetic Engineering News, 23, (11), 25-28.

Strubing C, Ahnert-Hilger G, ShanJ, WiedenmannB, Hescheler J, Wobus AM. (1995) Differentiation of pluripotent embryonic embryonic stem cells into the neuronal lineage in vitro gives rise to mature inhibitory and excitatory neurons. Mech. Dev., 53, 275-287.

Svendsen, C.N., & Smith, A.G., (1999). New prospects for human stem-cell therapy in the nervous system, Trends Neurosc., 22, 357-364.

Titchener-Hooker, N.J., Hoare, M., Dunnill, P., (1990) New approaches to the more efficient purification of proteins, enzymes, Biochem. Engng 6, Annals NY Acad. Sci., 589, 157-171.

Titchener-Hooker, N.J., Hoare, M., McIntosh, R.V., Foster P.R. (1992) The effect of fluid-jet mixing on protein precipitate growth during low-frequency conditioning. Chemical Engineering Science, 47, 75-86.

Titchener-Hooker, N.J., & McIntosh,I.V., (1992). A study of the effect of low-frequency conditioning on the size distribution properties and centrifugal recovery of human albumin precipitate, Bioprocess and Biosystems engineering, 8, num 1-2.

Tropepe, V., Hitoshi, S., Sirard, C. (2001) Direct neural fate specification from embryonic stem cells: a primitive mammalian neural stem cell stage required through a default mechanism. Neuron, 30, 65-78.

Tsai, M., Takeishi, T., Thompson, H., Langley, K.E., Zsebo, K.M., Metcalfe, D.D., Geissler, E.N., & Galli, S.J., (2000). Induction of Mast Cell Proliferation, Maturation, and Heparin Synthesis by the Rat c-Kit Ligand, Stem Cell Factor Proceedings of the National Academy of Sciences, 88, 6382-6386.

Versteeg H.K., & W. Malalasekera, W. (1995). An Introduction to Computational Fluid Dynamics the Finite Volume Method, Pearson Prentice Hall,England.

Virkar, P.D., Hoare, M., Chan, M.Y.Y, Dunnill, P., (1982) Kinetics of the acid precipitation of Soya protein in a continuous-flow tubular reactor, Biotech. Bioengng. 24, 871-887.

Vold, M., (1963). Computer Simulation of Floc Formation in a Colloidal Suspension, *J. Colloid Interface Sci.,* 18, 684.

Wang, H., Riha, G.M., Yan, S., Li, M., Chai, H., Yang, H., Yao, Q., Chen, C. (2005). Shear stress induces endothelial differentiation from a murine embryonic mesenchymal progenitor cell line. Arteriosclerosis, Thrombosis, and Vascular Biology. 25, 1817.

Wang R, Clark R, Bautch VL. (1992). Embryonic stem cell-derived cystic embryoid bodies form vascular channels: an in vitro model of blood vessel development. Development, 114, 303–16.

Weiss, S. (2000) Pathways for Neural Stem Cell Biology and Repair. Nat. Biotechnol. 17, 850-851.

Weissman, I.L., Anderson, D.J., Gage, F. (2001). Stem and progenitor cells : origins, phenotypes, lineage commitments and transdifferentiations, Ann. Rev. Cell Dev. Biol., 17,387-403.

Wiles, M.V., & Keller, G. (1991). Multiple hematopoietic lineages develop from embryonic stem (ES) cells in culture. Development., 111 (2), 259-267.

Williams, R.L., Hilton, D.J., Pease, S., Willson, T.A., Stewart, C.L., Gearing, D.P., Wagner, E.F., Metcalf, D., Nicola N.A., & Gough, N.M. (1988). Myeloid leukemia inhibitory factor maintains the developmental potential of embryonic stem cells. *Nature* 336, 684–687.

Wichterle, H., Lieberam, I., Porter, J.A., & Jessell, T.M. (2002). Directed differentiation of embryonic stem cells into motor neurons. Cell, 110, 385-397.

Wobus, A.M., Kaomei, G., Shan, J., Wellner, M.C., Rohwedel, J., Ji, G., Fleischmann, B., Katus, H.A., Hescheler, J., Franz, W.M. (1997). Retinoic acid accelerates embryonic stem cell-derived cardiac differentiation and enhances development of ventricular cardiomyocytes. J. Mol. Cell. Cardiol., 29(6), 1525–1539.

Yamamoto, K., Sokabe, T., Watabe, T., Miyazono, K., Yamashita, J. K., Obi, S., Ohura, N., Matsushita, A., Kamiya, A., Ando, J. (2005). Fluid shear stress induces differentiation of Flk-1-positive embryonic stem cells into vascular endothelial cells in vitro. Am. J. Physiol. Heart Circ. Physiol. 288, 1915-1924.

Yamashita, J., Itoh, H., Hirashima, M., Ogawa, M., Nishikawa, S., Yurugi, T., Naito, M., Nakao, K., Nishikawa, S. (2000). Flk1-positive cells derived from embryonic stem cells serve as vascular progenitors. Nature, 408 (6808), 92-96.

Ying, Q.L., Stavridis, M., Griffiths, D., Li, M., & Smith, A. (2003). Conversion of embryonic stem cells into neuroectodermal precursors in adherent monoculture, Nature Biotechnology, 21, 183-186.

Ying, Q.L., Stavridis, M., Griffiths, D., Li, M., & Smith, A. (2003b) Conversion of embryonic stem cells into neuroectodermal precursors in adherent monoculture. Nat. Biotechnol., 21, 183-186.

Zandstra, P.W., Bauwens, C,Yin T, Liu, Q., Schiller, H., Zweigerdt, R., Pasumarthi, K.B., Field, L.J., (2003). Scalable production of embryonic stem cell-derived cardiomyocytes. Tissue Eng., 9(4), 767–778.

Zhang, Z., Ferenczi, M.A., & Thomas, C.R., (1992). A micromanipulation technique with a theoretical cell model for determining mechanical properties of single mammalian cells Chem. Eng. Sci.47, 1347–1354.

Zhang, Z., Chisti, Y., & Moo-Young, M. (1995). Effects of the hydrodynamic environment and shear protectants on survival of erythrocytes in suspension. J. Biotechnol. 43, 33-40.

Zhang, S-C., Wernig, M., Duncan, I. D., Brüstle, O., and Thomson, J. A. (2001). In vitro differentiation of transplantable neural precursors from human embryonic stem cells. Nat. Biotechnol., 19, 1129–1133.

Zumaeta, N., Cartland-Glover, G, Heffernan, S., Byrne, E., & Fitzpatrick, J., (2005). Breakage model development and application with CFD for predicting breakage of whey protein precipitate particles, Chemical Engineering Science, 30, 3443–3452.

Zumaeta, N., Byrne, E.P., Fitzpatrick, J.J., (2006) Predicting precipitate particle breakage in a pipeline: Effect of agitation intensity during precipitate formation. Chemical Engineering Science, 61, 7991-8003.

Zweigerdt, R., Burg, M., Willbold, E., Abts, H., Ruediger, M. (2003)Generation of confluent cardiomyocyte monolayers derived from embryonic stem cells in suspension: a cell source for new therapies and screening strategies. Cytotherapy, 5,399–413.

APPENDIX